

Quadrupolar Nuclei in Solid-state Nuclear Magnetic Resonance

Dieter Freude

in

Encyclopedia of Analytical Chemistry

R.A. Meyers (Ed.)

pp. 12188–12224

© John Wiley & Sons Ltd, Chichester, 2000

Quadrupolar Nuclei in Solid-state Nuclear Magnetic Resonance

Dieter Freude

Universität Leipzig, Leipzig, Germany

the most important experimental techniques for the study of quadrupolar nuclei with half-integer spins such as DOR, dynamic-angle spinning (DAS), MQMAS, echo and nutation techniques, and some recent developments in deuterium NMR. Electric field gradient and chemical shift data for the most commonly studied quadrupolar nuclei with half-integer spins, ^{27}Al , ^{23}Na , and ^{17}O , and a few references to recent solid-state NMR studies of some other quadrupolar nuclei are given.

1 Introduction	1
2 Basic Theory	2
3 Excitation	5
4 Line Shape of Static and Magic-angle Spinning Nuclear Magnetic Resonance Spectra	7
5 Double-rotation and Dynamic-angle Spinning	10
6 Multiple-quantum Magic-angle Spinning Technique	12
7 Nutation Technique	15
8 Echo Techniques	16
9 ^2H Nuclear Magnetic Resonance Spectroscopy	17
10 Survey of Nuclear Magnetic Resonance Parameters for Selected Compounds	25
Acknowledgments	25
Abbreviations and Acronyms	25
Related Articles	26
References	26

1 INTRODUCTION

The applicability of the NMR technique continues to expand in physics, chemistry, materials science, geology, biology, and medicine for either spectroscopic studies or imaging purposes. The majority of the recent applications can be found in the field of analytical chemistry. In 1998, *Current Contents (Physical, Chemical and Earth Sciences)* referred to about 8500 NMR studies, including 1800 studies of solids. Solid-state NMR, for which some special techniques must be used in order to obtain highly resolved spectra, is mostly applied to ^1H or ^{13}C nuclei with spin $I = \frac{1}{2}$. About 100 of 130 NMR isotopes have $I > \frac{1}{2}$, and the electric quadrupole interaction strongly broadens the NMR signal in the solid-state powder spectra. However, more than 400 references to solid-state NMR studies of quadrupolar nuclei in *Current Contents* in 1998 demonstrate that this problem could be overcome.

The demand for the characterization of inorganic materials and some recently developed experimental techniques have led to growing interest in high-resolution solid-state NMR spectroscopy of quadrupolar nuclei in powder samples. In addition, the perturbing effect of the electric quadrupole interaction is reduced at higher magnetic fields, which are now commercially available up to 21 T also for solid-state NMR spectrometers. In addition, approaches of the solid-state NMR traditionally used in the study of spin- $\frac{1}{2}$ nuclei have been adapted for use with quadrupolar nuclei, e.g. echo methods, sample spinning about the magic angle (MAS), multiple-dimensional spectroscopy, double resonance and adiabatic transfer. Some techniques, e.g. DOR and multiple-quantum transition in combination with fast spinning (MQMAS), were developed for quadrupolar nuclei with half-integer spins.

This article describes the basic theory, the line shape for first- and second-order quadrupole broadened spectra with and without MAS of the powder, the most important experimental techniques for the study of quadrupolar nuclei with half-integer spins such as DOR, DAS, MQMAS, echo and nutation techniques, and finally some recent developments of the deuterium NMR. Since single-crystal studies are not considered in this article,

Solid-state nuclear magnetic resonance (NMR) spectroscopy is mostly applied to ^1H or ^{13}C nuclei with the nuclear spin $I = \frac{1}{2}$, but about 100 of 130 NMR isotopes have $I > \frac{1}{2}$, and the electric quadrupole interaction strongly broadens the NMR signal in the solid-state powder spectra. The perturbing effect of the electric quadrupole interaction is reduced at the higher magnetic fields which are available at present. In addition, approaches of the solid-state NMR traditionally used in the study of spin- $\frac{1}{2}$ nuclei have been adapted for use with quadrupolar nuclei, and some techniques, e.g. double-rotation (DOR) and multiple-quantum transition in combination with fast spinning [multiple-quantum magic-angle spinning (MQMAS)], were recently developed for quadrupolar nuclei with half-integer spins.

This article describes the basic theory, the line shape for first- and second-order quadrupole broadened spectra with and without magic-angle spinning (MAS) of the powder,

we refer to recent papers by Vosegaard et al.,^(1,2) which describe the up-to-date experimental techniques, and the review by Kanert and Mehring, ‘Static Quadrupole Effects in Disordered Cubic Solids’.⁽³⁾ The classical papers of Volkoff et al., ‘Nuclear Electric Quadrupole Interaction in Single Crystals’,^(4,5) of Das and Saha, ‘Electric Quadrupole Interaction and Spin Echoes in Crystals’,⁽⁶⁾ and the classical review by Cohen and Reif, ‘Quadrupole Effects in NMR Studies of Solids’,⁽⁷⁾ should also be mentioned.

Some other reviews on solid-state NMR of quadrupolar nuclei include mainly powder studies. They are, in chronological order, Spiess, ‘Deuteron NMR – A New Tool for Studying Chain Mobility and Orientation in Polymers’,⁽⁸⁾ Freude and Haase, ‘Quadrupole Effects in Solid-state NMR’,⁽⁹⁾ Jäger, ‘Satellite Transition Spectroscopy of Quadrupolar Nuclei’,⁽¹⁰⁾ Hoatson and Vold, ‘²H-NMR Spectroscopy of Solids and Liquid Crystals’,⁽¹¹⁾ Chmelka and Zwanziger, ‘Solid-state NMR Line Narrowing Methods for Quadrupolar Nuclei – Double Rotation and Dynamic-angle Spinning’,⁽¹²⁾ Chandrakumar, ‘Spin-1 NMR’,⁽¹³⁾ Ulrich and Grage, ‘H-2 NMR (Solid-state NMR of Polymers)’,⁽¹⁴⁾ and Smith and van Eck, ‘Recent Advances in Experimental Solid-state NMR Methodology for Half-integer Spin Quadrupolar Nuclei’.⁽¹⁵⁾

For the spin–lattice relaxation of quadrupole spins, which is not considered in the present article, we refer to Chapter 7 in Freude and Haase.⁽⁹⁾ A survey of nuclear quadrupole frequency data published before the end of 1982 is given by Chihara and Nakamura in *Landolt-Börnstein*, Vol. 20.⁽¹⁶⁾ Values of the chemical shift of quadrupolar nuclei in solids can be found in books such as *Multinuclear NMR* edited by Mason.⁽¹⁷⁾ For ²H NMR we refer to other publications.^(11,13,14,18) In section 10 we present as a continuation of Freude and Haase⁽⁹⁾ some electric field gradient and chemical shift data for the most commonly studied quadrupolar nuclei with half-integer spins ²⁷Al, ²³Na and ¹⁷O. A few references to recent solid-state NMR studies of some other quadrupolar nuclei are also given.

2 BASIC THEORY

At least three Cartesian coordinate systems were used for the description of the NMR interactions: the external magnetic field in the z -direction and the radiofrequency (RF) coil in the x -direction determine the laboratory axis system (LAB) with the coordinates (x, y, z) . The interaction representation is based on the coordinates $x_i = x \cos \omega t$, $y_i = \pm y \cos \omega t$, $z_i = z$. This system rotates around the direction of the external magnetic field with

the applied RF $\omega = 2\pi\nu$. The microscopic properties of the complex under study such as the dipolar interactions, the anisotropy of the chemical shift or the electric field gradient are described in the principal axis system (PAS). The principal axes (X, Y, Z) are related to the structure of the complex, e.g. for the dipolar interaction the Z -direction is parallel to the internuclear vector.

The various interactions of the nuclear spin \mathbf{I} can be described by the corresponding Hamiltonians. In the following we use I for the spin number and \mathbf{I} for the spin angular momentum vector and also for the corresponding vector operator (Hamiltonian). The interaction of a nuclear spin with an external magnetic field \mathbf{B} gives the Hamiltonian (Equation 1)

$$\mathcal{H} = \mathbf{I}Z\mathbf{B} \quad (1)$$

$Z = -\gamma\hbar\mathbf{I}$ includes the unity matrix \mathbf{I} , the gyromagnetic ratio γ of the nuclear spins and Planck’s constant, $h = 2\pi\hbar$.⁽¹⁹⁾ For the case of a static external magnetic field B_0 pointing in the z -direction and the application of an RF field $B_x(t) = 2B_{\text{rf}} \cos(\omega t)$ in the x -direction, we have for the external interactions Equation (2):

$$\mathcal{H}_0 + \mathcal{H}_{\text{rf}} = \hbar\omega_L I_z + 2\hbar\omega_{\text{rf}} \cos(\omega t) I_x \quad (2)$$

where $\omega_L = 2\pi\nu_L = -\gamma B_0$ denotes the Larmor frequency and the nutation frequency ω_{rf} is defined as $\omega_{\text{rf}} = -\gamma B_{\text{rf}}$. The transformation from the laboratory frame to the rotating frame gives, by neglecting the part which oscillates with twice the RF, Equation (3):

$$\mathcal{H}_{0,i} + \mathcal{H}_{\text{rf},i} = \hbar\Delta\omega I_z + \hbar\omega_{\text{rf}} I_x \quad (3)$$

where $\Delta\omega = \omega_L - \omega$ denotes the resonance offset.

In addition to the external interactions there exist internal interactions of a nuclear spin, which can be efficiently expressed in the notation of irreducible tensor operators.⁽²⁰⁾ The definition and the most important feature (coordinate rotation) of an irreducible tensor operator of rank k with $(2k + 1)$ components is given by Equation (4):

$$P_R T_q^{(k)} P_R^{-1} = \sum_{q'=-k}^{+k} T_{q'}^{(k)} D_{q'q}^{(k)}(R) \quad (4)$$

where $D_{q'q}^{(k)}(R)$ denote the matrix elements of the irreducible representation of the group $O^+(3)$ of the ordinary three-dimensional rotations. The transformation operator P_R is defined as $P_R = \exp[i\Omega\mathbf{e}_r\mathbf{J}]$, where \mathbf{J} is the total angular momentum operator, \mathbf{e}_r is the unit vector pointing in the direction of rotation and Ω represents the angle of rotation. The rotation transforms the eigenfunctions, $|lm\rangle$, of the angular momentum operator

I_z as Equation (5):

$$P_R|Im\rangle = \sum_{m'} |Im'\rangle D_{m'm}^{(k)}(R) \quad (5)$$

The matrix elements $D_{q'q}^{(k)}(R)$ (Wigner matrices) can be written as Equation (6):

$$D_{m'm}^{(k)}(\alpha, \beta, \gamma) = \exp\{i\alpha m'\} d_{m'm}^{(k)}(\beta) \exp\{i\gamma m\} \quad (6)$$

with the Euler angles α , β and γ . The elements $d_{m'm}^{(k)}(\beta)$ of the reduced Wigner matrices depend on the angle β only. They are given in Table 1 for rank 2; values for rank 4 can be found in Zheng et al.⁽²¹⁾ As presented in Figure 1, a positive rotation to a frame (x, y, z) about the Euler angles includes the rotation α about the original z axis, the rotation β about the obtained y' axis and the rotation γ about the final z'' axis [cf. Rose⁽²²⁾].

Table 1 Reduced Wigner matrix $d_{qq'}^{(k)}(\beta)$ for rank 2^a

q'/q	-2	-1	0	1	2
-2	a^4	$-\sqrt{2}a^2c$	$\sqrt{\frac{3}{2}}c^2$	$-\sqrt{2}b^2c$	b^4
-1	$\sqrt{2}a^2c$	$a^2(2d-1)$	$-\sqrt{3}cd$	$b^2(2d+1)$	$-\sqrt{2}b^2c$
0	$\sqrt{\frac{3}{2}}c^2$	$\sqrt{3}cd$	$\frac{1}{2}(3d^2-1)$	$-\sqrt{3}cd$	$\sqrt{\frac{3}{2}}c^2$
1	$\sqrt{2}b^2c$	$b^2(2d+1)$	$\sqrt{3}cd$	$a^2(2d-1)$	$-\sqrt{2}a^2c$
2	b^4	$\sqrt{2}b^2c$	$\sqrt{\frac{3}{2}}c^2$	$\sqrt{2}a^2c$	a^4

^a The following abbreviations are used: $a = \cos \frac{\beta}{2}$, $b = \sin \frac{\beta}{2}$, $c = \sqrt{2}ab = \frac{1}{\sqrt{2}} \sin \beta$ and $d = a^2 - b^2 = \cos \beta$.

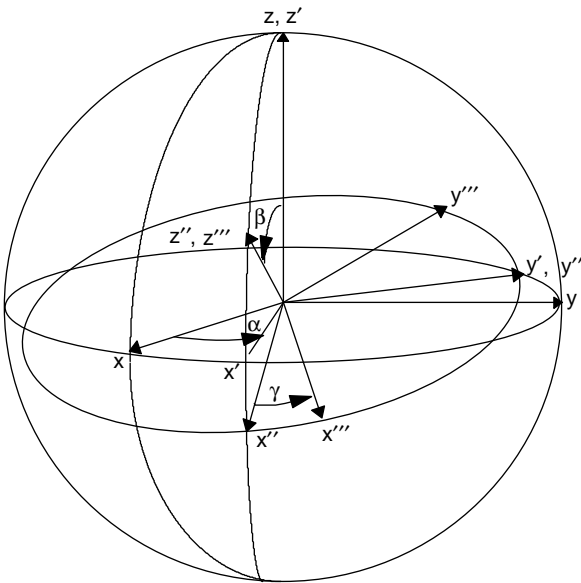


Figure 1 Euler angles.

The commutator shows another important feature of an irreducible tensor operator (Equations 7–9):⁽²⁰⁾

$$[I_z, T_q^{(k)}] = qT_q^{(k)} \quad (7)$$

and

$$[I_{\pm 1}, T_q^{(k)}] = \mp \sqrt{\frac{1}{2}\{k(k+1) - q(q \pm 1)\}} T_{q \pm 1}^{(k)} \quad (8)$$

with

$$I_{\pm 1} = \mp \frac{1}{\sqrt{2}}(I_x \pm iI_y) \quad (9)$$

The tensor product $U_Q^{(K)}$ of two operators $T_q^{(k)}$ and $V_{q'}^{(k')}$ is defined according to Equation (10):⁽²⁰⁾

$$U_Q^{(K)} = \sum_{qq'} T_q^{(k)} V_{q'}^{(k')} \langle kk'qq' | kk'KQ \rangle \quad (10)$$

where $\langle kk'qq' | kk'KQ \rangle$ are Clebsch–Gordan coefficients.⁽²⁰⁾ The scalar product of the operators $T_q^{(k)}$ and $V_{q'}^{(k')}$ is simpler (Equation 11):

$$T_q^{(k)} \cdot V_{q'}^{(k')} = \sum_{q=-k}^{+k} (-1)^q T_q^{(k)} V_{-q}^{(k')} \quad (11)$$

Fortunately, most internal interactions in the NMR can be written in this form.⁽²³⁾ In the following the operators $T_q^{(k)}$ and $V_{q'}^{(k')}$ act on two noninteracting systems, the nuclear spin coordinates and the spatial coordinates (lattice parameters), respectively.

In the strong external magnetic field it holds for the internal interactions by neglecting the nonsecular part of the corresponding Hamiltonian that (Equation 12)

$$[\mathcal{H}_0, \mathcal{H}_{\text{internal}}] = 0 \quad (12)$$

Comparison of Equation (12) with Equation (7) shows that only tensor elements with $q = 0$ contribute to the secular part of the internal Hamiltonians in a strong external magnetic field, if the system is described in the laboratory frame (LAB). However, the microscopic properties of the system are described in the PAS and a rotation of the coordinates from the PAS to the LAB by means of the Wigner matrix elements $D_{q'0}^{(k)}(R)$ must be performed. For example, the element $q = 0$ of the tensor $V^{(k)}$ is obtained by Equation (13):

$$V_0^{(k)}(\text{LAB}) = \sum_{q'=-k}^k V_{q'}^{(k)}(\text{PAS}) D_{q'0}^{(k)}(R) \quad (13)$$

Operators of rank 0 are invariant with respect to rotations. For the chemical shift we have (Equations 14–16)

$$T_0^{(0)} = \frac{-1}{\sqrt{3}} I_z B_0 \quad (14)$$

$$V_0^{(0)} = \sqrt{3} \sigma_{\text{iso}} \quad (15)$$

and

$$\mathcal{H}_{\text{chemical shift}}^{\text{isotropic}} = -\gamma\hbar\sigma_{\text{iso}}I_zB_0 \quad (16)$$

where σ_{iso} is the isotropic part of the shielding tensor (Equation 17):

$$\sigma_{\text{iso}} = \frac{\sigma_{XX} + \sigma_{YY} + \sigma_{ZZ}}{3} \quad (17)$$

Rank 0 operators do not contribute to dipolar interactions or quadrupolar interaction in first order. The contribution of the rank 1 operators can be neglected for all considered interactions. Therefore, anisotropy of the chemical shift, dipolar interactions and quadrupolar interactions in first order can be described by rank 2 operators in the form of Equation (18):

$$\mathcal{H} = C \sum_{q=-2}^{+2} (-1)^q T_q^{(2)} V_{-q}^{(2)} \quad (18)$$

Several contributions as described in Table 2 can be superimposed. The elements of the shielding tensor σ (trace $3\sigma_{\text{iso}}$) and of the traceless tensor of the electric field gradient V [which must not be confused with the operator $V^{(k)}$] are given in the PAS. Parameters of the anisotropy are $\delta = \sigma_{ZZ} - \sigma_{\text{iso}}$ for the chemical shift and $V_{ZZ} = eq$ for the electric field gradient, where e denotes the elementary charge and the value q alone has no physical meaning in SI units. Q is the quadrupolar moment and eQ is called the electric quadrupolar moment. The asymmetry parameter η is in the range $0 \leq \eta \leq 1$. With the convention $|V_{ZZ}| \geq |V_{YY}| \geq |V_{XX}|$ or $|\sigma_{ZZ} - \sigma_{\text{iso}}| \geq |\sigma_{YY} - \sigma_{\text{iso}}| \geq |\sigma_{XX} - \sigma_{\text{iso}}|$, we obtain

(Equations 19 and 20)

$$\eta = \frac{V_{XX} - V_{YY}}{V_{ZZ}} \quad (19)$$

or

$$\eta = \frac{\sigma_{XX} - \sigma_{YY}}{\sigma_{ZZ} - \sigma_{\text{iso}}} \quad (20)$$

Equation (21):

$$I_{\pm 1} = \mp \frac{1}{\sqrt{2}}(I_x \pm iI_y) \quad (21)$$

and Equation (22):

$$F(\alpha, \beta, \eta) = \left(\frac{3 \cos^2 \beta - 1}{2} + \frac{\eta}{2} \sin^2 \beta \cos 2\alpha \right) \quad (22)$$

are used in Table 2. The last row in Table 2 gives components which were transformed from the PAS into the LAB by the Euler angles α and β using Equation (13) for rank 2. With Equation (18) we obtain for the secular part of the Hamiltonian in the LAB for quadrupolar interaction in the first order (Equation 23)

$$\mathcal{H}_Q = \frac{eQV_{ZZ}}{4I(2I-1)} [3I_z^2 - I(I+1)] \times \left(\frac{3 \cos^2 \beta - 1}{2} + \frac{\eta}{2} \sin^2 \beta \cos 2\alpha \right) \quad (23)$$

The quadrupolar coupling constant C_{qcc} is commonly defined according to Equation (24):

$$C_{\text{qcc}} = \frac{e^2 q Q}{h} \quad (24)$$

Table 2 Some contributions to the Hamiltonian^a

Parameter	Chemical shift	Dipolar interaction between I_i and I_k	Quadrupole interaction
C	$\hbar\gamma$	$-2\gamma_i\gamma_k\hbar^2 \frac{\mu_0}{4\pi}$	$\frac{eQ}{2I(2I-1)}$
$T_0^{(2)}$	$\sqrt{\frac{2}{3}}I_zB_0$	$\sqrt{\frac{1}{6}}(3I_{zi}I_{zk} - I_iI_k)$	$\sqrt{\frac{1}{6}}[3I_z^2 - I(I+1)]$
$T_{\pm 1}^{(2)}$	$\sqrt{\frac{1}{2}}I_{\pm 1}B_0$	$\sqrt{\frac{1}{2}}(I_{\pm 1i}I_{zk} + I_{zi}I_{\pm 1k})$	$\sqrt{\frac{1}{2}}(I_{\pm 1i}I_z + I_{-z}I_{\pm 1})$
$T_{\pm 2}^{(2)}$	0	$I_{\pm 1i}I_{\pm 1k}$	$I_{\pm 1}^2$
$V_0^{(2)\text{PAS}}$	$\sqrt{\frac{3}{2}}(\sigma_{ZZ} - \sigma_{\text{iso}}) = \sqrt{\frac{3}{2}}\delta$	$\sqrt{\frac{3}{2}}I_{ik}^{-3}$	$\sqrt{\frac{3}{2}}V_{ZZ} = \sqrt{\frac{3}{2}}eq$
$V_{\pm 1}^{(2)\text{PAS}}$	0	0	0
$V_{\pm 2}^{(2)\text{PAS}}$	$\frac{1}{2}(\sigma_{XX} - \sigma_{YY}) = \frac{1}{2}\eta\delta$	0	$\frac{1}{2}(V_{XX} - V_{YY}) = \frac{1}{2}\eta eq$
$V_0^{(2)\text{LAB}}$	$\sqrt{\frac{3}{2}}\delta F(\alpha, \beta, \eta)$	$\sqrt{\frac{3}{2}} \frac{1}{I_{ik}^3} \left(\frac{3 \cos^2 \theta_{ik} - 1}{2} \right)$	$\sqrt{\frac{3}{2}}eq F(\alpha, \beta, \eta)$

^a The dipolar interaction is the homonuclear one. For heteronuclear dipolar interactions $T_0^{(2)}$ must be substituted by $\sqrt{1/6}I_{zi}I_{zk}$.

However, for the quadrupolar frequency, ν_Q or ω_Q , different definitions exist in the literature. We use the values according to Equation (25):

$$\nu_Q = \frac{3e^2qQ}{2I(2I-1)\hbar} = \frac{3C_{qcc}}{2I(2I-1)} \quad (25)$$

or Equation (26):

$$\omega_Q = \frac{3e^2qQ}{2I(2I-1)\hbar} \quad (26)$$

which were introduced for half-integer spin nuclei in the field of nuclear quadrupolar resonance (NQR) by Das and Hahn,⁽²⁴⁾ and established by Abragam⁽¹⁹⁾ also for NMR. For different definitions in the case of half-integer spin nuclei, see Freude and Haase⁽⁹⁾ (p. 33) and some papers following Frydman and Harwood.⁽²⁵⁾ For integer spins even less notational consistency exists, cf. Hoatson and Vold⁽¹¹⁾ (pp. 5 and 8). Equation (24) is still valid, but the definition of the quadrupolar frequency after Equation (26) is seldom used for spin-1 nuclei.

By substituting $V_{ZZ} = eq$ and using the angular dependent quadrupole frequency (Equation 27)

$$\nu'_Q = \nu_Q \left(\frac{3 \cos^2 \beta - 1}{2} + \frac{\eta}{2} \sin^2 \beta \cos 2\alpha \right) \quad (27)$$

one can write (Equation 28)

$$\mathcal{H}_Q^{\text{first-order}} = \frac{\hbar \nu'_Q}{6} [3I_z^2 - I(I+1)] \quad (28)$$

Equation (28) represents the first-order contribution of the quadrupolar interaction in the strong external magnetic field. From the second-order contribution the secular part with respect to I_z is given by Equation (29):

$$\begin{aligned} \mathcal{H}_Q^{\text{second-order}} = \frac{\hbar \nu_Q^2}{9\nu_L} \left\{ 2I_Z \left[2I_Z^2 - I(I+1) + \frac{1}{4} \right] V_{-1}V_1 \right. \\ \left. + I_Z \left[I_Z^2 - I(I+1) + \frac{1}{2} \right] V_{-2}V_2 \right\} \quad (29) \end{aligned}$$

The components $V_{p,p'}$ in Equation (29) correspond to the LAB. They can be obtained from the components in the PAS by means of Equation (13).

The homonuclear dipolar interaction of a pair (i, k) of spins with the distance r_{ik} and an angle θ between the internuclear vector and the direction of the external magnetic field is described by the Hamiltonian (Equation 30)

$$\mathcal{H}_D = \frac{\mu_0}{4\pi} \gamma_i \gamma_k \hbar^2 \left(\frac{3 \cos^2 \theta_{ik} - 1}{2r_{ik}^3} \right) (3I_{z,i}I_{z,k} - \mathbf{I}_i \mathbf{I}_k) \quad (30)$$

and it holds that $\gamma_i = \gamma_k$. For heteronuclear dipolar interactions we have $\gamma_i \neq \gamma_k$ and $(3I_{z,i}I_{z,k} - \mathbf{I}_i \mathbf{I}_k)$ in Equation (30) must be substituted by $(I_{z,i}I_{z,k})$.

The Hamiltonian of the chemical shift is the sum of the isotropic and the anisotropic contributions (Equation 31):

$$\mathcal{H}_{CS} = \gamma \hbar B_0 I_z \left[\sigma_{\text{iso}} + \delta \left(\frac{3 \cos^2 \beta - 1}{2} + \frac{\eta}{2} \sin^2 \beta \cos 2\alpha \right) \right] \quad (31)$$

3 EXCITATION

The energy of a spin interaction can be described by the size of the corresponding Hamiltonian $\|\mathcal{H}\|$. For NMR the usual sequence is $\|\mathcal{H}_0\| \gg \|\mathcal{H}_{\text{rf}}\| \gg \|\mathcal{H}_Q\|$, $\|\mathcal{H}_D\|$, $\|\mathcal{H}_{\text{CSA}}\|$. Expressed in frequencies: the Larmor frequency ($\|\mathcal{H}_0\|$), cf. Equation (2), is of the order of magnitude of 10–1000 MHz, the nutation frequency ($\|\mathcal{H}_{\text{rf}}\|$), cf. Equation (2), is of the order of magnitude of 1–400 kHz and the internal interactions are smaller than the RF field strength. However, the latter is sometimes not correct for quadrupolar nuclei in solids. We can assume the relation $\|\mathcal{H}_0\| \gg \|\mathcal{H}_Q\| \gg \|\mathcal{H}_D\|$, $\|\mathcal{H}_{\text{CSA}}\|$ and have to distinguish the well-defined cases $\|\mathcal{H}_{\text{rf}}\| \gg \|\mathcal{H}_Q\|$ (*) or $\|\mathcal{H}_{\text{rf}}\| \ll \|\mathcal{H}_Q\|$ (**) and the ill-defined intermediate case (***). A so-called hard pulse can perform a nonselective excitation of the whole quadrupolar broadened spectrum, if the RF field strength meets (*). The soft pulse (**) excitation is limited to any single transition ($m = -I, -I+1, \dots, I-1$) in a single crystal or to the central transition ($m = -\frac{1}{2}$) for powdered materials. Here the transition m denotes the transition between the magnetic quantum numbers $m \longleftrightarrow m+1$.

The excitation of quadrupolar nuclei with half-integer spins is discussed in detail by Freude and Haase.⁽⁹⁾ For a short description of the problem of excitation of any NMR transition, we start from the basic equation for the frequency spectrum of a rectangular pulse with the duration τ and the carrier frequency ν_0 with $\delta\nu = \nu - \nu_0$ (Equation 32):

$$f(\delta\nu) = \frac{1}{\tau} \int_{-\tau/2}^{+\tau/2} \cos(2\pi\delta\nu t) dt = \frac{\sin(\pi\delta\nu\tau)}{\pi\delta\nu\tau} \quad (32)$$

It has its maximum $f(\delta\nu) = 1$ for $\nu = \nu_0$ and the first nodes in the frequency spectrum occur at $\delta\nu = \pm 1/\tau$. The spectral energy density E is proportional to the square of the RF field strength which includes the offset dependence of Equation (32). If we define the usable bandwidth of excitation $\delta\nu_{1/2}$ in analogy to electronics by Equation (33):

$$E(\nu = \pm\delta\nu_{1/2}) = \frac{1}{2}E(\nu = \nu_0) \quad (33)$$

or Equation (34):

$$f^2(\nu = \pm\delta\nu_{1/2}) = \frac{1}{2}f^2(\nu = \nu_0) \quad (34)$$

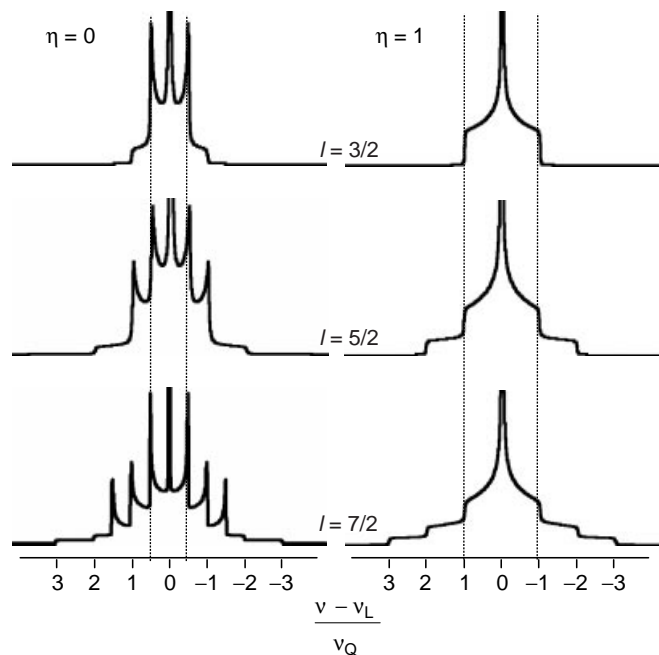


Figure 2 Examples of the static line shape (without MAS) of first-order quadrupolar broadened powder spectra for nonselective excitation. The central line is not fully represented (cut off). The theoretical line shapes are slightly Gaussian broadened.

the bandwidth of excitation $\delta\nu_{1/2} \approx 0.886/\tau$ follows from Equation (32). It should be noted that also the quality factor of the probe, $Q = \nu/\delta\nu_{\text{probe}}$, limits the bandwidth of excitation independently of the applied RF field strength or pulse duration. A superposition of the free induction decay (FID) of the NMR signals (liquid sample excited by a very short pulse) for some equidistant values of the resonance offset (without retuning the probe) shows easily the bandwidth $\delta\nu_{\text{probe}}$ of the probe. The spectral range of resonances for first-order quadrupolar shifts, which should be excited, amounts to $\nu_Q(2I - 1)$ or $3C_{\text{qcc}}/2I$ (cf. Figure 2). The superposition of both limitations gives the conditions in Equation (35):

$$\frac{1}{\tau} > 1.13\nu_Q(2I - 1) \approx \frac{1.4C_{\text{qcc}}}{2I} \quad (35)$$

and Equation (36):

$$\delta\nu_{\text{probe}} > \nu_Q(2I - 1) = \frac{3C_{\text{qcc}}}{2I} \quad (36)$$

for a “nonselective” excitation of the spectrum. For increasing pulse width τ or decreasing bandwidth $\delta\nu_{\text{probe}}$ of the probe, a “partly selective”, i.e. nonuniform, excitation of the transitions or a “selective” excitation of one transition only takes place.

If the single pulse is substituted by a composite pulse, a designed broadband or narrowband excitation can be achieved.⁽²⁶⁾

The intensity of the FID $G(t=0)$ after the pulse with the RF field strength w_{rf} and the duration τ is, for nonselective excitation of all transitions $m \leftrightarrow m+1$, given by Equation (37):⁽⁹⁾

$$G_{m,m+1}^{\text{nonselective}}(0) = \frac{3[I(I+1) - m(m+1)]}{2I(I+1)(2I+1)} \sin w_{\text{rf}}\tau \quad (37)$$

Equation (37) gives also the relative intensities of all transitions, e.g. 12/30, 9/35 and 4/21 for the central lines in the case of nonselective excitation of the $I = \frac{3}{2}$, $\frac{5}{2}$ and $\frac{7}{2}$ nuclei, respectively. The selective excitation of a single transition can be described by Equation (38):⁽⁹⁾

$$G_{m,m+1}^{\text{selective}}(0) = \frac{3\sqrt{I(I+1) - m(m+1)}}{2I(I+1)(2I+1)} \times \sin\left(\sqrt{I(I+1) - m(m+1)}w_{\text{rf}}\tau\right) \quad (38)$$

Comparison with Equation (37) reveals that the maximum observed intensity is reduced by $\sqrt{I(I+1) - m(m+1)}$, but the effective nutation frequency is enhanced by the same value. For the central transition, $m = -\frac{1}{2}$, we obtain Equation (39):

$$\nu_{\text{rf}}^{\text{eff}} = (I + \frac{1}{2})\nu_{\text{rf}} \quad (39)$$

Thus, for the selective excitation of the central transition, the optimum pulse duration is equal to the duration of a nonselective $\pi/2$ pulse divided by $I + \frac{1}{2}$. The RF power should be as low as possible. Second-order quadrupolar broadening, the chemical shift anisotropy and dipole broadening give the lower limit for the RF power which should be applied, in order to excite the full central transition in powder spectra. Then, only a small portion of the satellite powder spectra is also excited. The partly selective excitation of more than one transition can be treated only numerically.⁽⁹⁾

The problem of ill-defined excitation in cases of strong quadrupolar interaction can be overcome by adiabatic frequency sweeps. Adiabatic passages are well known in NMR.⁽¹⁹⁾ Kentgens⁽²⁷⁾ established in 1991 the quantitative excitation of a half-integer spin system by a frequency-stepped adiabatic half-passage (FSAHP) on the basis of an approach of Sindorf and Bartuska⁽²⁸⁾ and introduced in 1999 double-frequency sweeps (DFS) in static, MAS and MQMAS NMR experiments on the basis of an appropriate time-dependent amplitude modulation to the carrier frequency, which was applied before by Fu et al.⁽²⁹⁾ to integer spin systems in single crystals.

In the FSAHP, the spin system is far off-resonance at the beginning of the irradiation. The frequency is then

stepped through the region of resonances slowly enough that the density operator can follow the Hamiltonian. Switching off the RF power at the resonance position of the central transition creates a single-quantum coherence like a $\pi/2$ pulse applied to a spin- $\frac{1}{2}$ system. A full passage would be comparable to a nonselective π pulse. A frequency sweep that adiabatically inverts the satellite transitions, in order to transfer magnetization to the central levels and increase the intensity of the corresponding signal, was introduced by Haase and Conradi.⁽³⁰⁾ The combination of this population enhancement with cross-polarization (CP) from ^{27}Al to ^{17}O was demonstrated.⁽³¹⁾ A DFS can be generated by an amplitude modulation of the RF which causes two sidebands that are swept from a start frequency to a final frequency during the pulsing.⁽³²⁾ The authors claim that the DFS technique enhances the signal intensity also in MQMAS experiments.

The exclusive detection of the $\pm\frac{1}{2} \leftrightarrow \pm\frac{3}{2}$ transitions, which is based on a central-transition signal enhancement by means of an adiabatic RF sweep was introduced by McDowell et al.⁽³³⁾ in order to simplify the spectra and increase the sensitivity. Another approach to resolution enhancement by population transfer between Zeeman levels of the quadrupolar spin system with selective pulses and adiabatic frequency sweeps was first applied to ^{63}Cu in superconductors by Haase et al.⁽³⁴⁾

Another NMR technique that uses adiabatic passage in combination with rotational echo and double resonance was introduced by Gullion.⁽³⁵⁾ He combined the principles of rotational-echo double resonance (REDOR),⁽³⁶⁾ with the transfer-of-populations double-resonance (TRAPDOR) developed by Grey et al.⁽³⁷⁾ The so-called REAPDOR NMR technique allows first, like TRAPDOR, the indirect detection of signals which are too broad to be directly observable for the single-resonance observation of the quadrupolar nucleus and second, like REDOR, the measurement of distances between spin pairs.⁽³⁵⁾

CP excites a spin system by polarization transfer from another spin system. CP was introduced by Hartmann and Hahn⁽³⁸⁾ and is described in detail in the textbook by Slichter.⁽³⁹⁾ S. Vega⁽⁴⁰⁾ first applied static CP to half-integer nuclei and A.J. Vega^(41,42) considered the spin dynamics of cross-polarization magic-angle spinning (CPMAS) NMR as a function of the ratio $v_{\text{rf}}^2/v_{\text{Q}}v_{\text{rot}}$. Applications until 1992 are reviewed in Chapter 6.2 of Freude and Haase.⁽⁹⁾ Recent discussions about the spin-locking efficiency of the CPMAS NMR of half-integer quadrupolar nuclei were presented by Hayashi,^(43,44) Ding and McDowell^(45,46) and Sun et al.⁽⁴⁷⁾ The combination of CP with other NMR techniques will be considered in sections 5–7.

4 LINE SHAPE OF STATIC AND MAGIC-ANGLE SPINNING NUCLEAR MAGNETIC RESONANCE SPECTRA

The following considerations concern the angular dependent quadrupolar shift. Assuming the resonance offset to be zero, the quadrupolar shift should be given as $\nu - \nu_{\text{L}}$. For simplicity, we omit $-\nu_{\text{L}}$, the subtraction of the Larmor frequency. The conventions $\nu_{m,m+1}$ and $\nu_{m,-m}$ for single-quantum transitions and symmetric transitions, respectively, are used here in agreement with the majority of the literature. For the central transition $\nu_{-1/2,+1/2}$ we have $m = -\frac{1}{2}$. Then, the first-order quadrupolar shift becomes, with ν'_{Q} from Equation (27), Equation (40):

$$\nu_{m,m+1} = \nu'_{\text{Q}}(m + \frac{1}{2}) \quad (40)$$

for single-quantum transitions, which means zero for the central transition $m = -\frac{1}{2}$. The first-order quadrupolar contribution is zero for all symmetric transitions $m \leftrightarrow -m$. See Equation (28) and note that $I_z \equiv m$ is a number in this case.

The second-order quadrupolar shift can be obtained by means of Equation (29) as Equation (41):

$$\begin{aligned} \nu_{m,m+1} = & -\frac{v_{\text{Q}}^2}{18\nu_{\text{L}}} \{ [24m(m+1) - 4I(I+1) + 9]V_1V_{-1} \\ & + [6m(m+1) - 2I(I+1) + 3]V_2V_{-2} \} \quad (41) \end{aligned}$$

or Equation (42):

$$\begin{aligned} \nu_{m,-m} = & -\frac{mv_{\text{Q}}^2}{18\nu_{\text{L}}} \{ [4I(I+1) - 8m^2 - 1]V_1V_{-1} \\ & + [2I(I+1) - 2m^2 - 1]V_2V_{-2} \} \quad (42) \end{aligned}$$

for single or symmetric quantum transitions, respectively. The components V_j are given in the LAB and can be described, with the Wigner matrices of rank 2, as functions of corresponding values in the PAS, which are given in Table 2. The V_jV_{-j} terms in Equations (41) and (42), therefore, can be written also as Wigner matrices for which the rank goes up to 4. Amoureux⁽⁴⁸⁾ gave a corresponding equation with the coefficients for the transformation of Equation (42) from the LAB into the PAS.

The second-order quadrupolar shift of the central transition can also be obtained with $m = -\frac{1}{2}$ from Equations (41) and (42) (Equation 43):

$$\begin{aligned} \nu_{-1/2,+1/2} = & -\frac{v_{\text{Q}}^2}{6\nu_{\text{L}}} \left[I(I+1) - \frac{3}{4} \right] \\ & \times (A \cos^4 \beta + B \cos^2 \beta + C) \quad (43) \end{aligned}$$

Table 3 Functions A , B and C for the second-order static and MAS line shapes of the central transition (cf. Equation 43)

Function	Static	MAS
A	$-\frac{27}{8} - \frac{9}{4}\eta \cos 2\alpha - \frac{3}{8}\eta^2 \cos^2 2\alpha$	$+\frac{21}{16} - \frac{7}{8}\eta \cos 2\alpha - \frac{7}{48}\eta^2 \cos^2 2\alpha$
B	$+\frac{15}{4} - \frac{1}{2}\eta^2 + 2\eta \cos 2\alpha + \frac{3}{4}\eta^2 \cos^2 2\alpha$	$-\frac{9}{8} - \frac{1}{12}\eta^2 + \eta \cos 2\alpha - \frac{7}{24}\eta^2 \cos^2 2\alpha$
C	$-\frac{3}{8} + \frac{1}{3}\eta^2 + \frac{1}{4}\eta \cos 2\alpha - \frac{3}{8}\eta^2 \cos^2 2\alpha$	$+\frac{5}{16} - \frac{1}{8}\eta \cos 2\alpha + \frac{7}{48}\eta^2 \cos^2 2\alpha$

The components $V_p V_{-p}$ are substituted now by functions depending on the Euler angles α and β and the asymmetry parameter η . The functions A , B , C (Table 3, static) were first used by Narita et al.⁽⁴⁹⁾ in order to calculate the second-order powder pattern of the central transition for a static (nonrotating) sample. Müller⁽⁵⁰⁾ showed that in the case of very fast MAS of the samples Equation (43) holds with other functions A , B , C (Table 3, MAS).

In order to deduce quadrupole parameters from experimentally obtained spectra, it is usual to fit the experimental spectrum with calculated spectra using a utility program of the spectrometer software. Figures 2 and 3 show spectra, which were obtained with the program WINFIT from Bruker. If the spinning speed is not large compared with the second-order shift, the average Hamiltonian can be used for numerical calculations.

Equation (43) allows an analytical determination of the center of gravity $\nu_{cg} \equiv \nu_{iso}$ for the powder pattern, which is called the isotropic quadrupolar shift of the signal of the central transition. This shift is not influenced by a rotation of the sample. We denote it as $\nu_{iso Q}$ (Equation 44):

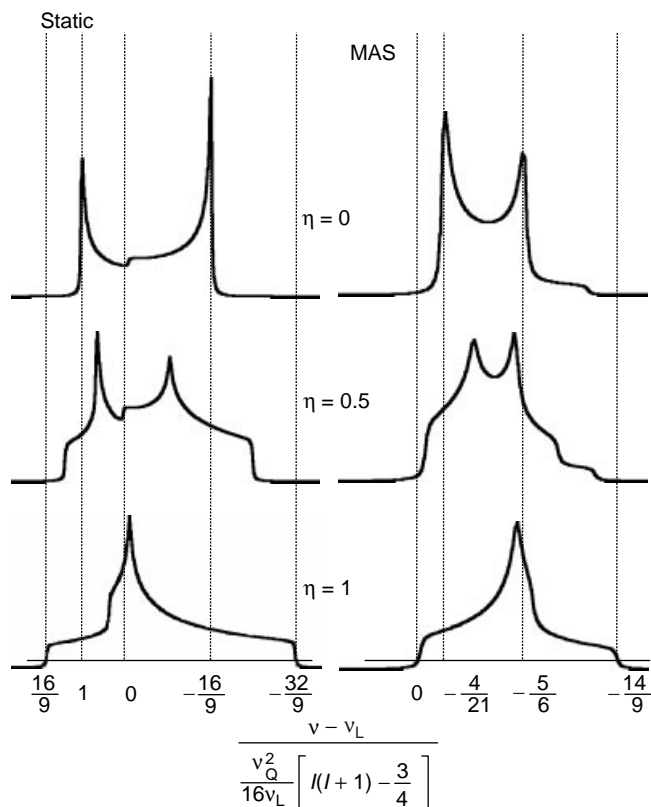
$$\nu_{iso Q} = -\frac{\nu_Q^2}{30\nu_L} \left[I(I+1) - \frac{3}{4} \right] \left(1 + \frac{\eta^2}{3} \right) \quad (44)$$

An important parameter of the powder line shape $f(\nu)$ is the second moment defined by Equation (45):

$$M_2 = \int (\nu - \nu_{iso})^2 f(\nu) d\nu \quad (45)$$

with $\int f(\nu) d\nu = 1$. The dimension Hz^2 of M_2 changes to s^{-2} or T^2 if the line shape is given as $f(\omega)$ or $f(B)$, respectively. The square root of M_2 characterizes the second-order broadening of the signal. Equations (46–48) give the second moments as a function of ν_{iso} for the static and for the MAS spectrum and in addition the narrowing factor, which can be achieved by the application of MAS to the second-order quadrupolar broadening of the central transition:

$$M_2^{\text{static}} = \nu_{iso}^2 \frac{23}{7} \quad (46)$$

**Figure 3** Examples of the line shapes, without and with MAS, of second-order quadrupolar broadened powder spectra of the central transition. The theoretical line shapes are slightly Gaussian broadened.

$$M_2^{\text{MAS}} = \nu_{iso}^2 \frac{1}{4} \quad (47)$$

$$\sqrt{\frac{M_2^{\text{static}}}{M_2^{\text{MAS}}}} = \sqrt{\frac{92}{7}} \approx 3.6 \quad (48)$$

Equations (46–48) in combination with Equation (44) allow the determination of $\nu_Q \sqrt{1 + \eta^2/3}$ from the second moment of the line shape, if the latter is exclusively broadened by second-order quadrupolar interaction. However, other contributions to the second moment of the static line shape should also be considered. The

anisotropy of the chemical shift gives Equation (49):

$$M_2^{\text{csa}} = \frac{4}{9} \frac{(\Delta\sigma v_L)^2}{5} \left(1 + \frac{\eta^2}{3}\right) \quad (49)$$

where $\Delta\sigma = \sigma_{ZZ} - (\sigma_{XX} - \sigma_{YY})/2$ denotes the total anisotropy and η is the asymmetry parameter (cf. Equations 20 and 21) and v_{iso} in Equation (45) must be taken as the isotropic value of the chemical shift.

If the dipolar interaction is small compared with the quadrupolar interaction, the spin flipping between different transitions is prohibited, and the second moment due to the dipolar interaction is modified.^(9,19) We will give here only the equations for dominating dipolar interaction. The dipolar second moment of a spin system consisting of N resonant spins of type I (homonuclear interaction) and M nonresonant spins of type S (heteronuclear interaction) can be determined by the dimensionless Equation (50):

$$\frac{M_2/\text{Hz}^2}{(\gamma_I/2\pi)^2} = \frac{M_2/\text{s}^{-2}}{\gamma_I^2} = M_2/T^2 = \frac{C_I}{r_I^6/\text{m}^6} + \frac{C_S}{r_S^6/\text{m}^6} \quad (50)$$

with (Equations 51–54)

$$C_I = \frac{3}{5} I(I+1) \left(\frac{\mu_0}{4\pi}\right)^2 \gamma_I^2 \hbar^2 \quad (51)$$

$$C_S = \frac{4}{15} S(S+1) \left(\frac{\mu_0}{4\pi}\right)^2 \gamma_S^2 \hbar^2 \quad (52)$$

$$\frac{1}{r_I^6} = \frac{1}{N} \sum_{i=1}^N \sum_{k \neq i}^N \frac{1}{r_{ik}^6} \quad (53)$$

$$\frac{1}{r_S^6} = \frac{1}{N} \sum_{i=1}^N \sum_{k=1}^M \frac{1}{r_{ik}^6} \quad (54)$$

The value C_S of a nonresonant nucleus can be easily calculated from the value of the same resonant nucleus C_I by $C_S = C_I \times 4/9$. If in Equation (50) the unit of the magnetic flux density T is substituted by 10^{-4} T (this corresponds to the old cgs unit gauss) and the unit m is substituted by the old unit Å, then the values C_I can be taken from Table 4.

Another dimensionless equation is very helpful in order to correlate the second moment of a line, which is broadened by any interaction, to the line width, which is commonly described by the full width at half-maximum ($\text{fwhm} \equiv \delta v_{1/2}$). Under the assumption of a gaussian line shape we obtain, for $M_2/\text{s}^{-2} = \gamma_I^2 M_2/T^2 = (\gamma_I/2\pi)^2 M_2/\text{Hz}^2$, cf. Equation (50), with T_2 as the transversal relaxation time and the line width δv given in hertz, Equation (55):

$$M_2/\text{s}^{-2} = \frac{2}{(T_2/\text{s})^2} = (\delta v_{1/2}/\text{Hz})^2 \frac{\pi^2}{\ln 4} \approx 7.12 (\delta v_{1/2}/\text{Hz})^2 \quad (55)$$

Table 4 Values of C_I in the equation

$$M_2/10^{-8}\text{T}^2 = \left(\frac{C_I}{r_I^6/\text{Å}^6} + \frac{C_S}{r_S^6/\text{Å}^6}\right)^a$$

¹ H	358.1	¹⁹ F	316.9	⁶³ Cu	125.8	¹²¹ Sb	239.2
² H	22.50	²³ Na	125.3	⁶⁵ Cu	144.3	¹²⁷ I	167.2
⁷ Li	270.4	²⁷ Al	283.6	⁷⁵ As	52.52	¹³³ Cs	129.4
⁹ Be	35.36	²⁹ Si	14.13	⁷⁷ Se	13.02	¹⁹⁵ Pt	16.55
¹⁰ B	66.16	³¹ P	58.68	⁷⁹ Br	112.4	¹⁹⁹ Hg	11.38
¹¹ B	184.3	³⁵ Cl	17.19	⁸¹ Br	130.6	²⁰¹ Hg	7.798
¹³ C	22.64	³⁷ Cl	11.91	⁸⁷ Rb	191.7	²⁰³ Tl	116.9
¹⁴ N	4.983	⁵¹ V	519.3	⁹³ Nb	706.0	²⁰⁵ Tl	119.2
¹⁵ N	3.677	⁵⁵ Mn	254.1	¹¹⁷ Sn	45.45	²⁰⁷ Pb	15.67
¹⁷ O	76.81	⁵⁹ Co	419.3	¹¹⁹ Sn	49.74	²⁰⁹ Bi	305.1

^a Values of C_S are given by $C_S = C_I \times 4/9$. The distances r_I and r_S denote in a simple model the internuclear distances of one resonant spin to another resonant spin and to a nonresonant spin, respectively. For the general case, see the definitions of r_I and r_S in Equations (53) and (54).

Now we go back to Equation (41) and consider the MAS spectra of the satellite transitions in addition to the central transition. Samoson⁽⁵¹⁾ has shown that the second-order quadrupolar shift of the $m \leftrightarrow m+1$ transition can be split into an isotropic part describing the center of gravity of the quadrupolar shift and an angular-dependent part (Equation 56):

$$v_{m,m+1} = -\frac{v_Q^2}{30v_L} [I(I+1) - 9m(m+1) - 3] \left[1 + \frac{\eta^2}{3}\right] - \left(\frac{v_Q^2}{30v_L} \left[I(I+1) - \frac{17}{3}m(m+1) - \frac{13}{6}\right]\right) \times ([A \cos^4 \beta + B \cos^2 \beta + C]) \quad (56)$$

with (Equations 57–59)

$$A = \frac{105}{16} - \frac{35}{8}\eta \cos 2\alpha + \frac{35}{48}\eta^2 \cos^2 2\alpha \quad (57)$$

$$B = -\frac{45}{8} + \frac{5}{12}\eta^2 + 5\eta \cos 2\alpha - \frac{35}{24}\eta^2 \cos^2 2\alpha \quad (58)$$

$$C = +\frac{9}{16} + \frac{1}{3}\eta^2 - \frac{5}{8}\eta \cos 2\alpha + \frac{35}{48}\eta^2 \cos^2 2\alpha \quad (59)$$

For the central transition, $m = -\frac{1}{2}$, Equation (56) corresponds to Equation (43) and the isotropic, upper part in Equation (56) corresponds to Equation (44). The true value of the isotropic chemical shift can be determined from the experimentally obtained isotropic shift (center of gravity of the signal), if the isotropic quadrupolar shift can be determined as shown below.^(10,51,52) For nonselective excitation, or at least partially selective excitation, MAS sidebands can be observed which are just outside of the spectral range of the static spectrum of the central transition. Their main intensity results from the $\pm\frac{1}{2} \leftrightarrow \pm\frac{3}{2}$ transitions, whereas the center band

results mainly from the $+\frac{1}{2} \leftrightarrow -\frac{1}{2}$ transition. The average resonance position of two equal-order sidebands can be obtained experimentally as the center of gravity of the corresponding sidebands. Thus, the difference $\Delta = \nu_{\text{iso } Q_{\pm 1/2, \pm 3/2}} - \nu_{\text{iso } Q_{-1/2, +1/2}}$ of the average resonance position of two first satellite sidebands to the center of gravity of the center band (central transition) can be measured and compared with the corresponding difference derived from Equation (56) (Equation 60):

$$\Delta = -\frac{\nu_Q^2}{30\nu_L} 9 \left(1 + \frac{\eta^2}{3} \right) \quad (60)$$

Finally, the combination of Equations (56) and (60) gives the isotropic quadrupolar shift of the center band, which for $I = \frac{5}{2}$ is equal to $\nu_{\text{iso } Q_{-1/2, +1/2}} = \Delta 8/9$.

This procedure for the determination of the quadrupolar shift or other quadrupolar parameters was introduced by Samoson.⁽⁵¹⁾ It is convenient for $I = \frac{5}{2}$ nuclei, because the linewidth of their $\pm\frac{1}{2} \leftrightarrow \pm\frac{3}{2}$ satellites is decreased by a factor of 0.3 with respect to the central line. Jäger used this sideband analysis for the study of various inorganic compounds⁽¹⁰⁾ and denoted it SATRAS (satellite-transition spectroscopy).

Now we go back to Equation (42) and use the representation of Amoureux⁽⁴⁸⁾ for the shift of a symmetric transition in the case of very fast sample rotation around the magic angle $\theta = \arccos 3^{-1/2} \approx 54.74^\circ$. Then, the contributions from the rank 2 components disappear and we obtain⁽⁵³⁾ Equation (61):

$$\begin{aligned} \nu_{p/2, -p/2} &= \nu_{\text{iso } Q(p)} + \nu_{\text{aniso } Q(p)} \\ &= \frac{p\nu_Q^2(3 + \eta^2)}{90\nu_L} \left\{ I(I+1) - \frac{3}{4}p^2 \right\} \\ &\quad - \left\{ \frac{p\nu_Q^2}{12960\nu_L} \right\} \left\{ (18 + \eta^2)d_{0,0}^{(4)} \right. \\ &\quad \left. + \sqrt{360}\eta d_{2,0}^{(4)} \cos 2\alpha + \sqrt{70}\eta^2 d_{4,0}^{(4)} \cos 4\alpha \right\} \\ &\quad \times \left\{ 36I(I+1) - 17p^2 - 10 \right\} \left\{ \left(-\frac{9}{28} \right) \right. \\ &\quad \left. \times (35 \cos^4 \theta - 30 \cos^2 \theta + 3) \right\} \quad (61) \end{aligned}$$

where p denotes the quantum level pQ and symmetric coherences with the notation $p/2 \leftrightarrow -p/2$ instead of $m \leftrightarrow -m$ are considered. The Euler angles (α, β) describe the spinner axis with respect to the PAS. The elements d of the reduced Wigner matrices are related to β by Equations (62–64):

$$d_{0,0}^{(4)} = \frac{1}{8}(35 \cos^4 \beta - 30 \cos^2 \beta + 3) \quad (62)$$

$$d_{2,0}^{(4)} = \frac{\sqrt{10}}{8}(7 \cos^2 \beta - 1) \sin^2 \beta \quad (63)$$

$$d_{4,0}^{(4)} = \frac{\sqrt{70}}{16} \sin^4 \beta \quad (64)$$

Equation (61) still contains a function of the rotor angle θ in the last brackets, in order to give one basic equation for MQMAS and DOR as well: if we insert the magic angle $\theta = \arccos \sqrt{1/3} \approx 54.74^\circ$, then the value of the last brackets is equal to one and Equation (61) can be used as the basic equation for MQMAS NMR (cf. section 6). If we consider a DOR and the second rotor angle is fixed to $\arccos \sqrt{(6 \pm \sqrt{96/5})/14} \approx 30.56^\circ$ or 70.12° , then the value of the last brackets in Equation (61) is equal to zero and the total anisotropic part of Equation (61) disappears. For the central transition, $p = -1$, only the isotropic quadrupolar shift remains, which can be directly observed by DOR NMR. The isotropic contribution in Equation (61) is identical with Equation (44) and with the isotropic part of Equation (56), if the central transition is considered ($p = -1$ and $m = -\frac{1}{2}$).

5 DOUBLE-ROTATION AND DYNAMIC-ANGLE SPINNING

Samoson et al.⁽⁵⁴⁾ succeeded in 1988 in building a double-rotor probe. The outer rotor, inclined by $\beta_2 = 54.74^\circ$ with respect to the external field, rotated at about 400 Hz, and had a diameter of 20 mm. The sample in the inner rotor, 5 mm diameter, rotated at about 2 kHz, and the angle between both axes of rotation was $\beta_1 = 30.56^\circ$.⁽⁵⁴⁾

A torque-free rotation can be achieved only for a certain ratio of $k = w_1/w_2$. The two contributions to the inner-rotor angular velocity are w_1 and the angular velocity w_2 imposed by the outer rotor. The latter can be decomposed into one component $w_2 \cos \beta_1$ along the z -axis of the inner rotor and another component $w_2 \sin \beta_1$ perpendicular to this axis in y -direction, so that y -direction, axis z of the inner rotor, and axis Z of the outer rotor are in one plane. Thus, $w_x = 0$, $w_y = w_2 \sin \beta_1$, $w_z = w_1 + w_2 \cos \beta_1$, and the resulting angular momentum \mathbf{L} must be in the Z -direction in order to be torque-free⁽⁵⁵⁾ (cf. Figure 4) (Equation 65):

$$\tan \beta_1 = \frac{J_y w_2 \sin \beta_1}{J_z (w_1 + w_2 \cos \beta_1)} \quad (65)$$

For $\beta_1 = \arccos \sqrt{(6 + \sqrt{96/5})/14} \approx 30.56^\circ$, we obtain Equation (66):

$$\begin{aligned} \frac{w_1}{w_2} \equiv \frac{\nu_{\text{inner}}}{\nu_{\text{outer}}} = k &= \sqrt{\frac{6 + \sqrt{96/5}}{14}} \left(\frac{J_y}{J_z} - 1 \right) \\ &\approx 0.86 \left(\frac{J_y}{J_z} - 1 \right) \quad (66) \end{aligned}$$

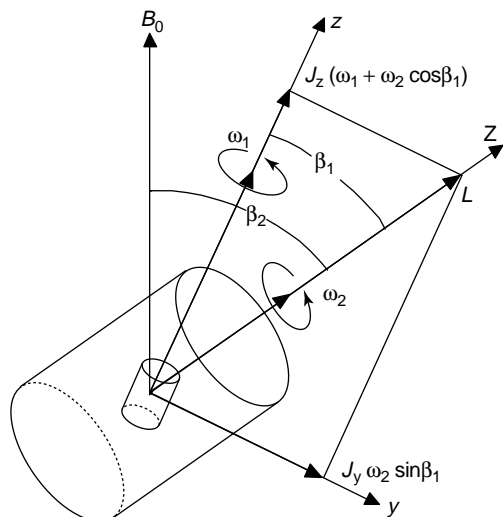


Figure 4 Moments of inertia for DOR after Wu et al.⁽⁵⁵⁾ By adjusting the ratio of moments, J_y/J_z , the addition of the two vector components of the angular momentum along the inner-rotor axis z and the y -axis can be made to point along the outer-rotor axis Z , so that spinning the outer rotor will not affect the orientation of the total angular momentum of the inner rotor.

and the usual design of the inner rotor gives values of J_y/J_z so that $5 < k < 6$. Wu et al.⁽⁵⁵⁾ explained that the spinning system is in a stable state when the torque-free condition, which is given by Equation (66), is slightly violated and the frequencies obey Equation (67):

$$\nu_{\text{inner}} = k\nu_{\text{outer}} + \Delta\nu_{\text{inner}} \quad (67)$$

where the excess of the inner frequency $\Delta\nu_{\text{inner}}$ is about 1 kHz.

The application of rotation-synchronized pulses has been shown to be effective in eliminating half of the DOR sidebands.⁽⁵⁶⁾ The total suppression of sidebands can be achieved by the application of additional pulses⁽⁵⁷⁾ and by application of the magic-angle turning technique.⁽⁵⁸⁾ A theoretical consideration of the DOR sidebands can be found in the literature.^(59–61)

DOR NMR gives accurate values of the isotropic shift, δ_{iso} , of the NMR of a quadrupolar nucleus. Two shift effects are superimposed: the isotropic quadrupolar shift, which is described in Equation (44), and the isotropic value of the chemical shift, which was introduced in Equation (16). We substitute σ_{iso} , the isotropic part of the shielding tensor, by the value of the chemical shift $\delta_{\text{CS iso}} = \sigma_{\text{ref}} - \sigma_{\text{iso}}$ (with respect to a given isotropic chemical shift of a reference compound). Then we substitute the second-order quadrupolar shift $\nu_{\text{iso Q}}$ in Equation (44) by the dimensionless value $\delta_{\text{Q iso}} = (\nu_{\text{iso Q}})/\nu_L$. In this notation we obtain for the observed isotropic shift in the DOR

experiment Equation (68):

$$\begin{aligned} \delta_{\text{DOR}} &= \delta_{\text{CS iso}} + \delta_{\text{Q iso}} \\ &= \delta_{\text{CS iso}} - \frac{\nu_{\text{Q}}^2}{30\nu_L^2} \left[I(I+1) - \frac{3}{4} \right] \left(1 + \frac{\eta^2}{3} \right) \quad (68) \end{aligned}$$

For common use the shifts can be expressed in parts per million (ppm) by multiplying the right-hand side of Equation (68) by 10^6 . Equation (68) reflects the fact that the value of the isotropic chemical shift cannot be obtained from *one* DOR experiment if the quadrupolar shift is unknown. However, two DOR experiments at different external field strengths, which means at different Larmor frequencies, give the value of the chemical shift $\delta_{\text{CS iso}}$ and also the quadrupolar parameter $\nu_{\text{Q}}\sqrt{1 + \eta^2/3}$.

The DOR technique has been applied, first, to the ^{23}Na resonance in sodium oxalate^(54,56,62) and later to NaNO_2 ^(56,63) to the ^{17}O resonance in diopside⁽⁶⁴⁾ and silicates⁽⁶⁵⁾ and to the ^{27}Al resonance of YAG.⁽⁶³⁾ The majority of the DOR NMR studies was devoted to zeolites of faujasite type^(66–75) and to zeolite-like materials such as aluminophosphates,^(47,66,76–86) zincosilicates⁽⁸⁷⁾ or sodalite.^(88,89) Other materials studied included aluminas⁽⁹⁰⁾ and aluminum borate⁽⁹¹⁾ (^{27}Al), gallium phosphate⁽⁹²⁾ (^{71}Ga) and boron nitride⁽⁹³⁾ (^{11}B). CP effects have been studied.^(47,79) Amoureux⁽⁹⁴⁾ proposed a combination of DOR and variable-angle spinning (VAS) in which the quadrupolar shift of DOR NMR can be deduced with a simulation of the second-dimension spectra obtained with stepped values of the angle of the outer rotor with respect to the external magnetic field.

The rotation frequencies of the inner and outer rotor at present do not exceed $\nu_{\text{inner}} = 12$ kHz and $\nu_{\text{outer}} = 2$ kHz, respectively. A pneumatic unit, which is controlled by a computer, simplifies the experimental set-up and makes it safer. However, compared with the MAS technique, a more complicated set-up and stronger wear of the rotors must still be accepted for DOR experiments.

A DAS experiment was first performed independently by Chmelka et al.⁽⁶⁴⁾ and Llor and Virlet.⁽⁹⁵⁾ The DAS technique uses a time-dependent angle of the rotor axis, which toggles in the simple experiment between 37.38° and 79.19° for two equal periods of time. During the hopping time, necessary for switching the angle (>30 ms), the evolution of the magnetization can be reduced by means of a selective $\pi/2$ pulse pair applied at a time t_1 after the preparation pulse. The signal consists of a second-order quadrupolar echo with a maximum at the time t_1 after the last pulse. The data acquisition of the FID starting at the echo maximum gives the data in the t_2 domain. The two-dimensional (2-D) spectrum is obtained after a 2-D Fourier transformation with respect to t_1 and t_2 . An advanced concept introduces a fourth $\pi/2$ pulse in order to retain two pathways from the t_1 evolution yielding a

pure absorption-phase spectrum and introduces a third angle of rotation of 54.74° , in order to correlate in two dimensions the DAS spectra with MAS spectra.^(96,97) A sideband pattern emerges if the evolution period of the 2-D DAS experiment is divided into unequal parts by RF pulses or spinner reorientation, as shown by Grandinetti et al.⁽⁹⁸⁾ Fyfe et al.⁽⁹⁹⁾ found that the switch to the magic angle after the CP step is useful for obtaining high-resolution spectra of slowly relaxing spin species. A 2-D heteronuclear correlation DAS NMR experiment with CP from ^{23}Na to ^{31}P was applied by Jarvie et al.⁽¹⁰⁰⁾ in order to find connectivities between the nuclei. Wenslow and Mueller⁽¹⁰¹⁾ demonstrated the increased information of this so-called DAS/CP/MAS NMR experiment for the study of cation sites in glasses. Medek et al.⁽¹⁰²⁾ introduced the three-dimensional dynamic-angle correlation spectroscopy (DACSY), which is based on the acquisition of DAS NMR signals as a function of different initial and final spinning axes.

Two drastic limitations for the application of the DAS technique compared with the DOR technique should be noted. First, the spin-lattice relaxation time T_1 , which is often short for quadrupolar nuclei, has to be larger than the time period necessary for flipping the rotor axis. Second, the spin exchange due to dipolar interactions, which cannot be eliminated during the relatively long flipping time of the rotor axis, has to be sufficiently small.

6 MULTIPLE-QUANTUM MAGIC-ANGLE SPINNING TECHNIQUE

In 1995, Frydman and Harwood⁽²⁵⁾ proved the feasibility of a 2-D NMR experiment that makes use of invisible multiple-quantum transitions combined with MAS to remove the anisotropy of the quadrupolar interaction. Symmetric $p/2 \leftrightarrow -p/2$ coherences with the quantum level pQ were selected, since the corresponding powder resonances are devoid of first-order quadrupolar effects.

The phase development $\varphi(t)$ of the single or multiple-quantum coherence can be written as Equation (69):

$$\begin{aligned} \frac{\varphi(t)}{2\pi t} &= \Delta\nu p + \nu_{p/2, -p/2} \\ &= \Delta\nu p + \frac{pv_Q^2(3 + \eta^2)[4I(I+1) - 3p^2]}{360\nu_L} \\ &\quad - \frac{pv_Q^2\{36I(I+1) - 17p^2 - 10\}}{12960\nu_L} \{(18 + \eta^2)d_{0,0}^{(4)} \\ &\quad + \sqrt{360}\eta d_{2,0}^{(4)} \cos 2\alpha + \sqrt{70}\eta^2 d_{4,0}^{(4)} \cos 4\alpha\} \quad (69) \end{aligned}$$

with $\nu_{p/2, -p/2}$ from Equation (61), which is reduced under MAS conditions. The contributions from the chemical

shift and from the resonance offset are included in $\Delta\nu = \sigma_{\text{iso}}\nu_L - \nu_{\text{offset}}$. Equation (69) shows that by going from the multiple-quantum level pQ to the $-1Q$ level of observation, the sign of the phase development can be inverted. Thus, the influence of the anisotropy of the second-order quadrupolar interaction is averaged out, if the times t_1 and t_2 spent on the quantum levels pQ and $-1Q$, respectively, fulfill the condition in Equation (70):

$$t_2 = p \frac{36I(I+1) - 17p^2 - 10}{36I(I+1) - 27} t_1 = R(I, p)t_1 \quad (70)$$

This relation describes the appearance of the isotropic echo, and thus gives the slope $R(I, p)$ of the anisotropic axis in the 2-D spectrum, which is obtained after the 2-D Fourier transformation with respect to t_2 and t_1 .

Several pulse sequences were used in order to excite a multiple-quantum coherence and convert it to the observable single-quantum coherence after the evolution time. The pulse sequence, which is shown in Figure 5, is mostly applied now. The highest possible RF power should be used for the first and second pulse, which excites the triple- (or quintuple-) quantum coherence and converts it back to zero-quantum coherence, respectively. The third pulse (z -filter) should be much weaker, in order to excite the central transition only. It converts nonobservable zero-quantum coherence and populations ($p = 0$) into observable single-quantum coherences ($p = -1$).

The symmetric 3Q coherence pathway in Figure 5 is $(0 \rightarrow \pm 3 \rightarrow 0 \rightarrow -1)$. The symmetric quintuple-quantum

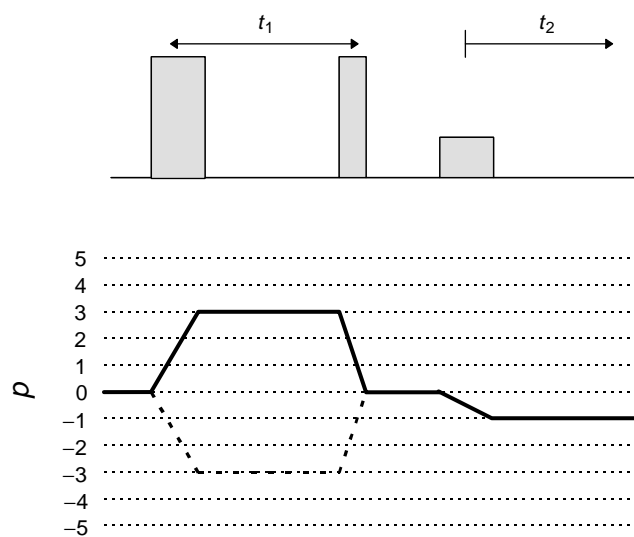


Figure 5 Pulse sequence and coherence transfer pathway for the echo (upper way) and antiecho (lower way) consisting of two strong pulses and a weak z -filter pulse. The triple-quantum MAS pathway is shown on the lines for the nuclear spin $I = \frac{5}{2}$.

(5Q) pathway is $(0 \rightarrow \pm 5 \rightarrow 0 \rightarrow -1)$. Two-pulse sequences (without z -filter) can be described by the notation $(0 \rightarrow \pm p \rightarrow -1)$. Although only one sign of p (cf. Equation 70) yields an echo which can be observed, it is needed to acquire both $\pm p$ coherence transfer pathways when trying to produce 2-D MQMAS spectra that are free from dispersive distortions.⁽¹⁰³⁾ Equally strong signals from both pathways must be collected, in order to obtain pure adsorptive spectra. This is more difficult if a two-pulse sequence is used, which includes the different transitions $+p \rightarrow -1$ and $-p \rightarrow -1$ for the last step in the echo and antiecho coherence transfer pathway, respectively. However, both pathways are completely symmetrical when considering the coherence jumps in the z -filter pulse sequence.^(104,105)

The flip angles of the first and second pulses should be optimized with respect to the best signal amplitude. In principle, this can be done by numerical calculations,⁽¹⁰⁶⁾ e.g. by the program PULSAR.⁽¹⁰⁷⁾ The result depends on the nuclear spin I and its Larmor frequency ν_L , the chosen coherence pQ and the ratio between the nutation frequency $\nu_{\text{rf}} = \gamma B_{\text{rf}}/2\pi$ and the quadrupolar frequency ν_Q . One conclusion is that the MQMAS NMR spectra, which are obtained by strong pulses, do not present quantitative results with respect to the concentration of species, since the multiple-quantum transition efficiency is different for nuclei with different quadrupolar frequency ν_Q .

The calculations need a full set of NMR parameters including the quadrupolar parameters and do not take into consideration second-order and spinning effects. Therefore, the optimization of the pulse duration should be performed at the beginning of the NMR experiment by variation of the pulse duration; and only the initial flip angles for this procedure should be taken from the numerical calculations. Nonselective flip angles of about 180° and 50° for the first and second pulse, respectively, can be used for any I and pQ , if the Larmor frequency is about 100 MHz and the ratio between the quadrupolar frequency ν_Q and the nonselective nutation frequency is $\nu_Q/\nu_{\text{rf}} \approx 10$. More precise flip angles are given in the literature^(106,108) as a function of I and pQ . (Note that definition of the quadrupolar frequency in the literature^(25,106,108) is different to the definition of Abragam;⁽¹⁹⁾ cf. Equation (25), which is used here: $\nu_Q^{\text{Frydman}} = \nu_Q^{\text{Abragam}}/6$.)

An alternative approach to the generation of multiple-quantum transitions by strong pulses is to use the adiabatic transfer by the interchange between the eigenstates 3Q and 1Q undergoing MAS.⁽⁴²⁾ Wu et al.⁽¹⁰⁹⁾ introduced a triple-quantum magic-angle spinning (3QMAS) experiment by rotation-induced adiabatic coherence transfer (RIACT) for $I = \frac{3}{2}$ nuclei and applied it to the study of sodium sites in inorganic salts. They claimed that

this method gives quantitative MQMAS NMR spectra, since the adiabatic coherence transfer is independent of the strength of the quadrupolar interaction. However, theoretical calculations⁽¹⁰⁸⁾ showed that, compared with the nonadiabatic excitation, the disturbing off-resonance effects are more extensive for RIACT. Lim and Grey⁽¹¹⁰⁾ performed numerical simulations of the RIACT experiment as a function of asymmetry parameter and pulse spacings and discussed the effect of very fast sample spinning. Mildner et al.⁽¹¹¹⁾ demonstrated by means of ^{17}O studies of silicates that RIACT can be applied to $I = \frac{5}{2}$ spins at the moderate RF field strength of $\nu_{\text{rf}} \approx 30$ kHz.

Ding and McDowell^(112,113) claimed that a shaped first excitation pulse would also achieve quantitative results in nonadiabatic 3QMAS NMR experiments and that properly shaped pulses can also reduce the requirements on the RF power and sample spinning speeds. The superior excitation of triple-quantum coherences by composite pulse schemes was also shown by Marinelli et al.⁽¹¹⁴⁾

Kentgens and Verhagen⁽³²⁾ showed that DFSs are very efficient for the conversion of triple- to single-quantum coherence in MQMAS spectroscopy. Goldbourn et al.⁽¹¹⁵⁾ used instead fast radiofrequency amplitude modulation (FAM) in the version FAM and FAM1 for $I = \frac{3}{2}$ and $I = \frac{5}{2}$ nuclei, respectively, and obtained a substantial intensity and resolution enhancement of the signal over the commonly used MQMAS pulse schemes. A very strong RF field, no resonance offset and a high spinning rate, if possible 30 kHz as shown by Rocha,⁽¹¹⁶⁾ are still the requirements for most MQMAS experiments.

For both the nonadiabatic and adiabatic MQMAS experiments described above, the selection of desired multiple-quantum coherences is done by phase cycling.^(111,117) Methods of hypercomplex or time-proportional phase increment (TPPI) 2-D Fourier transformation [cf. Ernst et al.⁽¹¹⁸⁾] are used for the acquisition of real and imaginary part with respect to the t_1/ν_1 dimension. Fyfe et al.⁽¹¹⁹⁾ used pulsed field gradients instead of phase cycling. The advantage is the simplification of the MQMAS pulse program, which allows the implementation of correlation experiments. However, the insertion of the field gradient coil reduces the maximum achievable RF power.

A shearing transform of the experimentally obtained 2-D spectrum, which aligns anisotropic ridges parallel to the ν_2 axis in such a way that the isotropic dimension can be displayed along the ν_1 axis, is described below. Brown et al.^(104,120,121) introduced an experiment with an additional pulse called split- t_1 MQMAS that is pure adsorptive and includes the shearing ratio into the pulse program so that anisotropic ridges

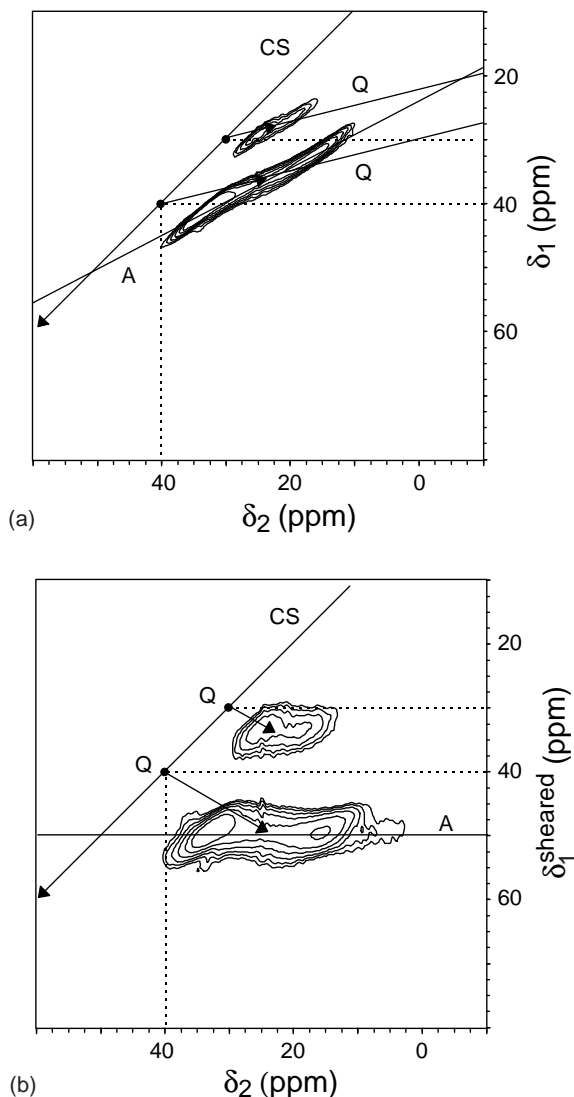


Figure 6 2-D ^{17}O 3QMAS NMR spectra of the zeolite Na-ZSM-5 (a) after the 2-D Fourier transformation and (b) after the following shearing transformation. The two signals were assigned to SiOSi and SiOAl fragments with concentrations of 80 and 20%, $\delta = 40$ and 30 ppm, $C_{\text{qcc}} = 5.3$ and 3.5 MHz, $\eta = 0.12$ and 0.29, respectively.⁽⁵³⁾ (The figure was provided by Ulf Pingel.)

are parallel to the ν_2 axis after the 2-D Fourier transformation.

Figure 6(a) and (b) shows the 2-D ^{17}O 3QMAS NMR spectra of the zeolite Na-ZSM-5 before and after the shearing procedure. The two signals in the spectra are due to Si–O–Si and Si–O–Al bonds.⁽⁵³⁾ The spectra demonstrate how the projection on the ν_1 axis is changed by the shearing. The analytical treatment starts from the isotropic part of Equation (69). Without resonance offset, the total shift is a superposition of the isotropic part of the chemical shift, $\sigma_{\text{iso}}\nu_L$, and the isotropic part of the

quadrupolar shift, $\nu_{\text{iso Q}}$ (Equation 71):

$$\begin{aligned} \nu_{\text{iso}} &= \sigma_{\text{iso}}\nu_L p + \nu_{\text{iso Q}} \\ &= \sigma_{\text{iso}}\nu_L p + \frac{p\nu_Q^2(3 + \eta^2)[4I(I + 1) - 3p^2]}{360\nu_L} \end{aligned} \quad (71)$$

Equation (71) can be transformed into relative units (ppm) by multiplication by $10^6/(-p\nu_L)$. The value $-p\nu_L$ describes the apparent Larmor frequency and includes the real Larmor frequency for $p = -1$. For the ν_1 axis (before shearing) and for the ν_2 axis, we have Equations (72) and (73), respectively:

$$\begin{aligned} \delta_1 &= \delta_{\text{CS iso}} + \delta_{\text{Q iso}} \\ &= \delta_{\text{CS iso}} - \frac{\nu_Q^2(3 + \eta^2)[4I(I + 1) - 3p^2]}{360\nu_L^2} \end{aligned} \quad (72)$$

$$\begin{aligned} \delta_2 &= \delta_{\text{CS iso}} + \delta_{\text{Q iso}} \\ &= \delta_{\text{CS iso}} - \frac{\nu_Q^2(3 + \eta^2)[4I(I + 1) - 3]}{360\nu_L^2} \end{aligned} \quad (73)$$

Equation (73) describes the shift δ_2 of the center of gravity of the anisotropic ridge, which is not influenced by the shearing transformation. The coordinate $\delta_1^{\text{shearing}}$ after the transformation is given by⁽¹⁰⁸⁾ Equation (74):

$$\begin{aligned} \delta_1^{\text{shearing}} &= \delta_{\text{CS iso}} + \delta_{\text{Q iso}}^{\text{shearing}} \\ &= \delta_{\text{CS iso}} + \frac{\nu_Q^2(3 + \eta^2)[4I(I + 1) - 3]}{612\nu_L^2} \end{aligned} \quad (74)$$

It can be seen that after shearing the quadrupolar shift becomes always positive and independent of p . Comparison of Equation (74) with Equation (73) gives the slope of two special lines in the sheared 2-D spectrum. One line with slope 1, which is denoted CS in Figure 6, describes the variable isotropic chemical shift in the case of zero quadrupolar shift. Only one line CS exists and crosses the coordinates (0, 0). Lines Q with slope $-10/17$ describe variable quadrupolar shifts at one value $\delta_{\text{CS iso}}$, which is given by the crossing of line Q with line CS. The shift difference between this crossing point and the center of gravity of a signal gives the corresponding quadrupolar shift $\delta_{\text{Q iso}}^{\text{shearing}}$. One-dimensional anisotropic slices A are obtained from the 2-D spectrum. These slices can be fit by a line-shape simulation, which gives values for ν_Q and η , whereas $\delta_{\text{Q iso}}$ is a measure of $\nu_Q\sqrt{1 + \eta/3}$. The quadrupolar parameter obtained from the 2-D spectrum can then be used for a simulation of the single-quantum MAS NMR spectrum. This procedure yields correct information about the relative concentration of the various species giving rise to the corresponding signals. The program REGULAR, which was developed by Delevoye,⁽¹²²⁾ takes full advantage of the information included in the 2-D MQMAS NMR spectrum and thereby

quantifies the distribution of nucleus surroundings also in badly crystallized and amorphous materials. A 2-D result is obtained which represents quadrupolar constants versus isotropic chemical shifts with correct relative intensities. Scaling and labeling of the isotropic axis (v_1 axis after shearing) was considered in detail by Man.⁽¹²³⁾

The residual line width of the MQMAS NMR spectra is a matter of current research. Wu and Wasylshen⁽¹²⁴⁾ showed that the heteronuclear dipolar interaction between two nuclei does not cause residual dipolar couplings in MQMAS NMR experiments.

The spinning sidebands in the multiple-quantum dimension are a common feature of dipolar-coupled spin $I = \frac{1}{2}$ and half-integer quadrupolar systems. Both cases were considered by Friedrich et al.⁽¹²⁵⁾ The case of half-integer spins is the subject of various studies.^(126–129) Spinning sidebands arise even in the absence of explicit time modulations of any spin interactions, due to orientation and time dependence characterizing the multiple- to single-quantum conversion process, as shown by Marinelli and Frydman.⁽¹²⁶⁾ The sidebands cause signal loss and misinterpretation of spectra. Rotor synchronization, which means setting the evolution dwell time equal to the rotation period, is useful for suppressing these spinning sidebands.⁽¹³⁰⁾ However, it limits the spectral width of the multiple-quantum dimension to the rotation frequency. This drawback increases on going from triple- to quintuple-quantum transitions.

Several combinations of MQMAS with other NMR techniques have been successfully applied. Vosegaard et al.⁽¹³¹⁾ added the Carr–Purcell–Meiboom–Gill (CPMG) pulse sequence to the MQMAS pulse program, in order to improve the sensitivity by splitting the line shape in the v_2 dimension into manifolds of spin-echo sidebands. High-power ^1H decoupling improves the resolution in both dimensions.^(132,133) Lacassagne et al.⁽¹³⁴⁾ demonstrated improved resolution for strong heteronuclear coupling by applying composite decoupling schemes during the evolution and acquisition time. Wang et al.⁽¹³⁵⁾ provided chemical shift anisotropy data by multiple-quantum variable-angle spinning (MQVAS). CP provides information about connectivities.^(136–139) REDOR^(139–141) and heteronuclear chemical shift correlation (HETCOR)^(138,142) were also applied in addition to MQMAS. The most difficult combination, DOR in addition to MQMAS, was presented by Samoson et al.^(143,144) The advantage of multiple-quantum double-rotation (MQDOR) compared with MQMAS is that the need for simulations is avoided.⁽¹⁴³⁾ However, although in principle most informative, experimental difficulties and low multi-quantum conversion efficiency make the applicability of the MQDOR technique currently relatively limited.⁽¹⁴⁴⁾

MQMAS NMR studies have been carried out on all half-integer quadrupolar spins from $I = \frac{3}{2}$ to $I = \frac{9}{2}$ [^{93}Nb ⁽¹⁰⁶⁾]. The nucleus ^{59}Co ($I = \frac{7}{2}$) in nitrogen compounds was studied to show the interplay between the chemical shift anisotropy and the quadrupolar interaction. However, the majority of the studies were focused on the two nuclei ^{27}Al ($I = \frac{5}{2}$) and ^{23}Na ($I = \frac{3}{2}$). Two examples are the study of the aluminum coordination in $\text{SrAl}_{12}\text{O}_{19}$ by Jansen et al.⁽¹⁴⁵⁾ and the study of sodium cations in dehydrated zeolites by Hunger et al.⁽¹⁴⁶⁾ Zeolites, zeolite-like materials and glasses^(147,148) have been investigated in many studies.

7 NUTATION TECHNIQUE

Nutation NMR spectroscopy represents a 2-D experiment: a strong RF field is irradiated during the evolution period t_1 , and the FID is observed during the detection period t_2 . In the rotating frame, the spins *nutate* (precess) around the strong RF field with specific nutation frequencies w_1 ; here the subscript 1 denotes the frequency axis w_1 in the 2-D spectrum corresponding to the Fourier transform with respect to t_1 and should not be confused with $w_{\text{rf}} = \gamma B_{\text{rf}}$ which is a constant for the 2-D experiment. The original one-dimensional nutation experiment of Torrey⁽¹⁴⁹⁾ uses only one point of the FID.

Samoson and Lippmaa^(150,151) introduced 2-D nutation NMR studies of half-integer quadrupolar nuclei. A corresponding one-dimensional experiment was performed by Fenzke et al.⁽¹⁵²⁾ For quadrupolar nuclei, the effective nutation frequencies w_1 depend on the strength of the quadrupolar interaction, as has been shown in section 3. If $w_Q \ll w_{\text{rf}}$, then the transverse magnetization responds to the RF pulse like spin- $\frac{1}{2}$ nuclei, thus $w_1 = w_{\text{rf}}$. If $w_Q \gg 10w_{\text{rf}}$, the central transition can be treated as a two-level system and an effective nutation frequency is expected, that is, increased by a factor $I + \frac{1}{2}$, i.e. $w_1 = (I + \frac{1}{2})w_{\text{rf}}$ (cf. Equation 39). For the intermediate case, $0.1 < w_Q/w_{\text{rf}} < 100$, the nutation spectra are complicated because of the influence of the partly excited outer satellite transitions.

Nutation spectra can be calculated using numerical procedures or by means of an analytical description which is the more complicated the larger the spin quantum number. The powder average, which produces complicated nutation spectra, is necessary, in order to deduce quadrupolar parameters from the spectra and to compare the experimental spectrum with a set of calculated spectra. An analytical approach was found for $I = \frac{3}{2}$,^(153–156) for $I = \frac{5}{2}$,^(157,158) and for $I = \frac{7}{2}$ ^(159,160) yielding $(I + \frac{1}{2})^2$ different nutation frequencies of the central transition. Each frequency gives rise to a powder

pattern, and $2I$ of the $(I + \frac{1}{2})^2$ frequencies are dominant. Calculated line shapes of nutation spectra can be found in papers by Kentgens et al.^(161,162) and in a review by Freude and Haase.⁽⁹⁾ The latter reviews the quadrupolar nutation literature from 1983 to 1992 (about 40 papers), including experimental aspects such as inhomogeneity of the RF field, resonance offset, influence of MAS, spin–lattice relaxation, spin–spin relaxation in the rotating frame and some advanced concepts in nutation spectroscopy. Since 1993, another 15 papers were published, among them recent work about nutation MAS NMR by Ding and McDowell.^(46,163)

The most advanced concept, the off-resonance nutation NMR of half-integer nuclei, was introduced by Kentgens.⁽¹⁶⁴⁾ The large resonance offset, $\nu_{\text{offset}} \gg \nu_{\text{rf}}$, during the irradiation causes an evolution of the spin system in the effective field, $\mathbf{B}_{\text{eff}} = \mathbf{B}_{\text{offset}} + \mathbf{B}_{\text{rf}}$, whereas the signal is as usually observed in resonance. The off-resonance technique extends the range of applicability at given \mathbf{B}_0 and \mathbf{B}_{rf} to larger values of C_{qcc} . The acquisition of several spectra with different ν_{offset} improves the reliability of the fitting process, which is essential for obtaining information from nutation spectra. A loss of signal intensity due to the uninformative zero-frequency peak, which is typical for off-resonance irradiation, can be avoided by a soft selective pulse or by using an FSAHP (cf. section 3), for the preparation of the central transition magnetization only. A recent review including the perspectives of the nutation NMR of half-integer quadrupolar nuclei was given by Kentgens.⁽¹⁶²⁾ He proposed a combination of MQMAS, off-resonance nutation and echo techniques for sites with very large C_{qcc} .

8 ECHO TECHNIQUES

Echo techniques provide two data sets in the NMR time domain. First, the echo decay dependence on the time t_2 starting from zero at the maximum of the echo gives similar information to the initial FID after the preparation pulse, but the loss of signal during the ring down of the probe and the recovery of the receiver immediately after the pulse is overcome in the echo technique. Second, by varying the pulse distance t_1 between the preparation pulse and the refocusing second pulse, the resulting envelope of the echo decay gives additional information about the spin system. The refocusing effect of a second pulse after a preceding $\pi/2$ pulse for an interaction that is proportional to I_z is called the Hahn echo. The original experiment by Hahn⁽¹⁶⁵⁾ was performed with identical phase incoherent pulses in an inhomogeneous external magnetic field. The term Hahn echo is now in use for the spin-echo (after $\pi/2-t_1-\pi-t_1$) of spin- $\frac{1}{2}$ nuclei or of

quadrupolar nuclei with half-integer spins, if the central transition is selectively excited.

However, the quadrupolar interaction strongly influences the formation of an echo: homonuclear dipolar interactions which mainly cause the decay of the spin-echo amplitude become less effective since spin-flipping between different transitions is forbidden. Owing to the nature of the quadrupolar coupling, which is to first order proportional to I_z^2 , refocusing is not complete. Also, the limited range of excitation for very broad lines of powder samples causes complicated spin-echo behavior.

Echo studies on quadrupolar nuclei with half-integer spin (for integer spin, see section 9) were reviewed by Freude and Haase,⁽⁹⁾ beginning with the pioneering work of Das and Saha⁽⁶⁾ in 1955 up to the publications in 1993, e.g. Haase and Oldfield.⁽¹⁶⁶⁾ Several cases, which can be mainly divided into nonselective and selective excitation, were considered, as follows.⁽⁹⁾

Nonselective and hard pulses without dipole interaction cause several echoes at times $k \times t_1$ with $k = \frac{1}{2}, 1, \frac{3}{2}$ and $k = \frac{1}{2}, 1, \frac{3}{2}, 2, 3$ for $I = \frac{3}{2}$ and $I = \frac{5}{2}$, respectively. Some of these are forbidden echoes: $k = \frac{1}{2}, \frac{3}{2}$ and $k = \frac{3}{2}, 3$ for $I = \frac{3}{2}$ and $I = \frac{5}{2}$, respectively. On going from hard to soft pulses (cf. section 3), the influence of the quadrupolar interaction during the pulse has to be considered and the selection rule is changed. Then also the forbidden echoes can be observed. The consideration of dipole interaction for first-order quadrupolar echoes can be divided into two parts. First, the heteronuclear dipole interaction, which is proportional to $I_z S_z$, can generally be removed by the application of a second π -pulse. However, strong coupling among the S spins, and also a short spin–lattice relaxation time of the S spins, can destroy the formation of the I spin echo. Second, if the homonuclear dipolar interaction is large compared with the quadrupolar interaction, $\|\mathcal{H}_{\text{D}}\| \gg \|\mathcal{H}_{\text{Q}}\|$, its influence is essentially the same as for spin- $\frac{1}{2}$ nuclei. If the quadrupolar interaction is large compared with the dipolar interaction, $\|\mathcal{H}_{\text{Q}}\| \gg \|\mathcal{H}_{\text{D}}\|$, spin exchange due to homonuclear dipole interaction between adjacent levels can be considered as being suppressed completely and the echo decay can be investigated by selective excitation of each transition, separately.

$\|\mathcal{H}_{\text{Q}}\| \gg \|\mathcal{H}_{\text{rf}}\| \gg \|\mathcal{H}_{\text{D}}\|$ and $\|\mathcal{H}_{\text{Q}}\| \gg \|\mathcal{H}_{\text{rf}}\| \approx \|\mathcal{H}_{\text{D}}\|$ denote the cases of selective excitation of a single transition without and with dipole interaction, respectively. For powder we can mainly excite the central transition, and for single crystals we can tune to any transition and describe it by the reduced spin- $\frac{1}{2}$ formalism.⁽¹⁹⁾ Without the dipole interaction an echo is observed at the time t_1 after the π pulse in full analogy with spin- $\frac{1}{2}$ nuclei subjected to an inhomogeneous interaction. Since the calculation of the spin-echo amplitude in the presence of dipolar interactions can be complicated,

the spin-echo decay has been discussed by Haase and Oldfield⁽¹⁶⁶⁾ in terms of the second moment spin-echo decay (cf. section 5.2.5 in Freude and Haase⁽⁹⁾).

Echo techniques in combination with coherence selection (multiple-quantum filter) reduce the overlap of signals of quadrupolar nuclei in anisotropic soft matter, as demonstrated by Furo and Halle.^(167,168) Recent progress in this field was presented by Eliav et al.^(169–172) The use of echoes for the editing of ²⁷Al MAS NMR spectra of zeolite catalysts was shown by Schmitt et al.⁽¹⁷³⁾ The connection between all NMR interactions (except the homonuclear dipole interaction) and the optimum experimental conditions for the avoidance of spectral distortions was described by Dumazy et al.⁽¹⁷⁴⁾

The leading authority in the field of quadrupolar echoes is Pascal Man, who has published more than 10 papers on this topic during the last decade. Most of them are discussed in recent publications.^(175–177)

The CPMG^(178,179) pulse sequence $\pi/2_x, (t_1, \pi_y, t_1)_n$ can be considered as an advanced concept of the Hahn echo. Larsen et al. reconsidered the quadrupolar version of CPMG (QCPMG) without MAS⁽¹⁸⁰⁾ and with MAS.⁽¹⁸¹⁾ For MQMAS NMR and ²H NMR, see sections 6 and 9, respectively. More than one order of magnitude can be gained in sensitivity by the application of this QCPMG technique.

9 ²H NUCLEAR MAGNETIC RESONANCE SPECTROSCOPY

²H is the most important NMR isotope with an integer nuclear spin $I = 1$, rather seldom ⁶Li and ¹⁴N NMR studies can be found in the literature. About 10% of the solid-state NMR studies of quadrupolar nuclei concern deuterium magnetic resonance spectroscopy, which is a powerful technique for investigating molecular structure and dynamics. This small section does not correspond to the importance of the deuterium NMR, especially for the study of dynamics. The textbook by Schmidt-Rohr and Spiess, *Multidimensional Solid-state NMR and Polymers*⁽¹⁸⁾ and the reviews by Hoatson and Vold, *²H-NMR Spectroscopy of Solids and Liquid Crystals*,⁽¹¹⁾ and Ulrich and Grage, *²H NMR (Solid-state NMR of Polymers)*,⁽¹⁴⁾ demonstrate the wealth of modern applications of solid-state ²H NMR.

The experimental techniques for nuclei with the spin $I = 1$ are different to the techniques for nuclei having half-integer spins mainly for one reason, that no central transition exists. There are only two transitions for the magnetic quantum number m : $-1 \leftrightarrow 0$ and $0 \leftrightarrow 1$. They cause a line splitting that is symmetric with respect to the Larmor frequency if the quadrupolar interaction

is considered in first-order perturbation theory with respect to the Zeeman interaction (cf. Equation 40). From Equation (41) it follows that the second-order shifts for both transitions are identical. Thus, the splitting between the two lines (difference frequency), which is the experimentally observed parameter in studies of single crystals, is not influenced by the second-order quadrupolar interaction.

Equations (40) and (41) can be used for nuclei with the spin $I = 1$, but the quadrupolar frequency should be substituted by the quadrupolar coupling constant using $\nu_Q = 3C_{qcc}/2$. The definition of the quadrupolar frequency for half-integer spins in Equations (25) and (26) is rather unusual for integer spins. The use of the quadrupolar coupling constant C_{qcc} after Equation (24) is commonly accepted, but for integer spins no notational consistency exists with respect to the quadrupolar frequency ν_Q .

The asymmetry parameter η (cf. Equations 19 and 20), is relatively small for the majority of the ²H NMR studies due to a rotation symmetry of the hydrogen bonding. The theoretical powder line shape of nuclei with $I = 1$ and $\eta = 0$ is equal to the line shape of isolated pairs of nuclei with the spin $I = \frac{1}{2}$. Therefore, the typical ²H NMR pattern of the so-called static powder (no sample rotation and no internal rotation) is often referred to as the Pake powder pattern. Pake in 1948 studied the ¹H NMR spectra of gypsum and discussed the angular dependence of the doublets in the spectra of a single crystal and the powder pattern in the spectrum of a powder sample as well.⁽¹⁸²⁾

The splitting of lines of single crystals or the full width of powder patterns reach values up to 300 kHz. From $\delta\nu_{1/2} \approx 0.886/\tau$ (cf. Equations 32–34), it follows that a duration $\tau \leq 2 \mu\text{s}$ for the $\pi/2$ pulse is necessary, in order to obtain a quite uniform excitation of the whole spectrum. In addition to the need for high RF power, an echo pulse sequence must be applied in order to overcome the dead time problem of the receiver. A simple pulse sequence consisting of two $\pi/2$ pulses with a pulse duration of $2 \mu\text{s}$ and a pulse separation of $20 \mu\text{s}$ with phase cycling (the phase of the first pulse is cycled with respect to the synthesizer, and in addition the phase of the second pulse is cycled with respect to the first pulse) is the standard for solid-state ²H NMR experiments. The pulse separation must be adjusted to one rotation period if MAS is applied. Hoatson discussed the broadband composite excitation sequences⁽¹⁸³⁾ and the Hadamard pulse excitation^(184,185) for detecting quadrupolar order in ²H NMR. Noise spectroscopy provides broad-bandwidth excitation with minimal applied RF field strengths. The state-of-the-art for applications to the ²H solid-state NMR was described by Yang et al.^(186,187) More detailed consideration of the quadrupolar echo in ²H NMR can be found in the review by Hoatson and Vold,⁽¹¹⁾ Chapter 2.2, and the references

therein. (The NMR echo for nuclei with half-integer spin is discussed in section 8 of this article.) The excitation with symmetric quadrupolar-shaped (SQUASH)⁽¹⁸⁸⁾ and time-asymmetric-shaped (QUASH) pulses⁽¹⁸⁹⁾ improves the excitation bandwidth.

Deuterium labels are introduced synthetically or by a postsynthesis treatment of the material. The labeled hydrogen segment can be investigated in terms of its specific structural and dynamic properties. The natural abundance of ^2H is only 150 ppm. The relative sensitivity of naturally abundant ^2H with respect to the ^1H NMR sensitivity at constant external field is only 1.5 ppm. Nevertheless, natural abundance high-resolution solid-state ^2H NMR investigations can be performed if MAS, high-power ^1H decoupling and ^1H - ^2H CP are used.^(190,191)

^1H - ^2H CP effects in single- and double-quantum (DQ) transitions of the ^2H NMR were theoretically and experimentally investigated by Vega et al.⁽¹⁹²⁾ in 1980. There are two reasons why CP is rarely used in the solid-state ^2H NMR: the maximum increase in the ^2H NMR intensity due to the CP from ^1H spins is given by the gyromagnetic ratio $\gamma_{\text{H}}/\gamma_{\text{D}} \approx 6.5$ for infinitely diluted ^2H nuclei. This value decreases if the concentration of ^2H nuclei increases with the deuterium enrichment. However, the increasing level of deuteration increases the ^2H NMR intensity more effectively. The second point is that the high-power decoupling of the protons close to the deuterons causes some problems. However, ^1H - ^2H CP is invaluable for the investigation of the interfaces of the deuterated segments, e.g. in polymer blends. Ba et al.⁽¹⁹³⁾ proposed a quadrupolar echo double resonance (QEDOR) and a solid echo double resonance (SOLEDOR) NMR experiment in order to provide information about deuteron-proton distances. A new theoretical model that describes CPMAS experiments for abundant $I = \frac{1}{2}$ spins coupled to a single spin $S = 1$ was presented by Marks et al.⁽¹⁹⁴⁾ Gan and Robyr⁽¹⁹⁵⁾ described a new 2-D CPMAS experiment with a three-pulse sequence for the determination of the relative orientation between ^2H quadrupolar coupling tensors.

The MAS technique for powder materials offers a more sensitive technique (compared with the quadrupolar echo technique) and the opportunity for an accurate measurement of the chemical shift.⁽¹⁹⁶⁾ A simple variation of the processing procedure of the FID, which is obtained in a one-pulse experiment, gives a 2-D spectrum with quadrupolar pattern in one dimension and the isotropic chemical shift in the other dimension.^(197,198) The 2-D data set in the time domain can be constructed from the one-dimensional set, which should be acquired with a dwell time τ_{dwell} and a rotation frequency ν_{rot} in the order of magnitude of 1 μs and 5 kHz, respectively. $N = (2\nu_{\text{rot}}\tau_{\text{dwell}})^{-1}$ points with the time distance of $2\tau_{\text{dwell}}$

starting at the top of each rotational echo define the t_2 domain, and the increments of t_1 as the rotation period $1/\nu_{\text{rot}}$ give the t_1 domain. Spaniol et al.⁽¹⁹⁹⁾ recently used a 2-D ^2H MAS NMR experiment for the separation of paramagnetic and quadrupolar interactions.

Quadrupolar effects do not shift (or broaden in the case of powder) the signals arising from DQ transitions. Therefore, 2-D ^2H DQ NMR spectra provide information about the chemical shift of the deuterons.⁽²⁰⁰⁾ Advantages of the MAS NMR technique compared with the DQ NMR technique are the higher sensitivity of the single-quantum compared with the DQ transition and the higher sensitivity of the MAS technique compared with the static echo technique. Multiple-quantum effects in combination with MAS are less often used for ^2H nuclei⁽²⁰¹⁻²⁰³⁾ compared with nuclei with half-integer spin (cf. section 6). Chandrakumar et al.⁽²⁰³⁾ use a four-pulse experiment (QUADSHIFT) with a t_1 interval in the middle (which is incremented by the rotation period) in order to obtain chemical shift values and quadrupolar parameters from DQ coherences under MAS conditions [see also Chandrakumar⁽¹³⁾]. ^2H MAS NMR imaging experiments were described by Blümich.⁽¹⁸⁵⁾

Deuterium NMR spectroscopy of single-crystal systems is an active field of research. The original approach of Volkoff et al.^(4,5) is still in use, in order to obtain the quadrupolar parameters from the angular dependence of the line splitting, and new aspects were found and applied by Haebleren et al.^(204,205) The work up until 1994 is reviewed by Chandrakumar⁽¹³⁾ and recent results are also available^(204,205) The ordering behavior at the phase transition in single crystals of betaine phosphate and betaine phosphite has also been studied by one-dimensional and 2-D ^2H NMR.⁽²⁰⁶⁾

The majority of ^2H NMR studies concern molecular dynamics. Many polymer systems are studied, because ^2H NMR is ideally suited to explore molecular motions in polymers.⁽¹⁴⁾ There is a wide range of timescales for the correlation times that are accessible by various methods: 10^2 - 10^{-4} s (2-D exchange spectroscopy), 10^2 - 10^{-5} s (selective inversion), 10^{-4} - 10^{-8} s (line-shape analysis), 10^2 - 10^{-4} s (T_2 anisotropy), 10^{-8} - 10^{-12} s (T_{1Z} anisotropy) and 10 - 10^{-12} s (T_{1Q} anisotropy).⁽¹¹⁾ For exchange spectroscopy we refer to the textbook by Schmidt-Rohr and Spiess.⁽¹⁸⁾ The introduction of multi-dimensional exchange experiments by Spiess et al. gave rise to strong developments in this field. Kubo et al.⁽²⁰⁷⁾ recently combined deuterium selective-excitation exchange spectroscopy with the Hadamard method for the measurement of reorientation rates. The technique of selective inversion is based on the selective excitation or the so-called hole burning that has been well known in NMR from the very beginning.⁽²⁰⁸⁾ Recent applications to ^2H NMR have been reviewed by Hoatson and Vold.⁽¹¹⁾

Table 5 Quadrupolar coupling constant $C_{\text{qcc}} = e^2qQ/h$, the asymmetry parameter η and the isotropic value of the chemical shift δ (referred to 1.0 M $\text{AlCl}_3 \cdot 6\text{H}_2\text{O}$) for the ^{27}Al NMR of powder compounds at ambient temperature^a

Compound	Site	C_{qcc} (MHz)	η	δ (ppm)	Refs.
Aluminates					
$\text{CaO} \cdot 6\text{Al}_2\text{O}_3$	AlO_4	2.0	0 _{assumed}	65	261
	AlO_5	6.7	0 _{assumed}	27.5	262
	$\text{AlO}_6\text{-I}$	1.5	0 _{assumed}	9	261
	$\text{AlO}_6\text{-II}$	<1	0 _{assumed}	16	261
$\text{CaO} \cdot 2\text{Al}_2\text{O}_3$	$\text{AlO}_4\text{-I}$	6.7	0.8	78	261
	$\text{AlO}_4\text{-II}$	13	0.1	~60	261
$\text{CaO} \cdot \text{Al}_2\text{O}_3$	$\text{AlO}_4\text{-I}$	2.7	0.85	80	261
	$\text{AlO}_4\text{-II}$	2.7	0.85	83	261
$4\text{CaO} \cdot 3\text{Al}_2\text{O}_3$	AlO_4	2.4	0.95	80	261
$12\text{CaO} \cdot 7\text{Al}_2\text{O}_3$	$\text{AlO}_4\text{-I}$	3.7	0.9	79	261
	$\text{AlO}_4\text{-II}$	11	0.2	85	263
$3\text{CaO} \cdot \text{Al}_2\text{O}_3$	AlO_4	9.7	0.3	85	263
	$\text{AlO}_4\text{-I}$	8.69	0.32	79.5	264
	$\text{AlO}_4\text{-II}$	9.3	0.54	78.25	264
$4\text{CaO} \cdot 3\text{Al}_2\text{O}_3 \cdot 3\text{H}_2\text{O}$	$\text{AlO}_4\text{-I}$	1.8	0.5	78	261
	$\text{AlO}_4\text{-II}$	5.4	0.45	79	261
KAlO_2	AlO_4	1.1	0.7	76	263
$\text{KAlO}_2 \cdot 0.5\text{H}_2\text{O}$	AlO_4	5.6	0.0	77	263
$\text{KAlO}_2 \cdot \text{H}_2\text{O}$	AlO_4	6.5	0.6	83	263
$\text{KAlO}_2 \cdot 1.5\text{H}_2\text{O}$	AlO_4	5.0	0.25	81	263
$5\text{BaO} \cdot \text{Al}_2\text{O}_3$	AlO_4	2.3	0.8	80	263
$\text{BaO} \cdot \text{Al}_2\text{O}_3$	AlO_4	2.4	0.4	78	263
$\alpha\text{-BaO} \cdot \text{Al}_2\text{O}_3 \cdot 2\text{H}_2\text{O}$	$\text{AlO}_4\text{-I}$	3.4	0.5	81	263
	$\text{AlO}_4\text{-II}$	5.1	0.9	80	263
$\alpha\text{-LiAlO}_2$	AlO_6	2.8	0.05	16	265
$\beta\text{-LiAlO}_2$	AlO_4	1.8	0.55	82	265
	AlO_4	1.86	0.56	83.0	266
$\gamma\text{-LiAlO}_2$	AlO_4	3.2	0.7	81	265
$\beta\text{-NaAlO}_2$	AlO_4	1.4	0.5	80	263
$\alpha\text{-Al}_2\text{O}_3$	AlO_6	2.40	0.01	18.8	267
$\gamma\text{-Al}_2\text{O}_3$	AlO_4	>5.0	~0	>67	268, 269
	AlO_6	4.5	~0	>9	268, 269
	AlO_4	5.1	–	71.5	270
$\gamma\text{-Al}_2\text{O}_3$ (rehydrated)	AlO_5	5.1	–	44.0	270
	AlO_6	3.55	–	10.0	270
	AlO_4	7.6	0.3	81.5	271
$\kappa\text{-Al}_2\text{O}_3$	$\text{AlO}_6\text{-(1)}$	5.0	–	ca. 13	271
	$\text{AlO}_6\text{-(4)}$	8.5	–	18	271
	AlO_4	5.0	0.3	71.5	272
$\chi\text{-Al}_2\text{O}_3$	AlO_5	2.7	0.3	38.5	272
	AlO_6	4.5	0.3	11.5	272
	AlO_4	2.00	<0.1	80.4	273
$\text{Ca}_8(\text{AlO}_2)_{12} \text{S}_2$ (sodalite)	AlO_4	3.55	<0.1	79.1	273
$\text{Cd}_8(\text{AlO}_2)_{12} \text{Se}_2$ (sodalite)	AlO_4	3.95	<0.1	78.7	273
$\text{Cd}_8(\text{AlO}_2)_{12} (\text{SO}_4)_2$ (sodalite)	AlO_4	3.24	<0.1	79.1	273
$\text{Sr}_8(\text{AlO}_2)_{12} \text{S}_2$ (sodalite)	AlO_4	4.65	<0.1	76.9	273
$\text{Sr}_8(\text{AlO}_2)_{12} \text{Se}_2$ (sodalite)	AlO_4	5.10	<0.1	76.6	273
$\text{Sr}_8(\text{AlO}_2)_{12} (\text{CrO}_4)_2$ (sodalite)	AlO_4	6.75	<0.1	75.5	273
$\text{SrAl}_{12}\text{O}_{19}$	AlO_4	3.45	0.1	68.0	145
	AlO_5	2.1	0.7	18.0	145
	$\text{AlO}_6\text{-(1)}$	0.6	1	17.1	145
	$\text{AlO}_6\text{-(2)}$	1.3	1	9.6	145
	$\text{AlO}_6\text{-(3)}$	4.9	0.63	21.7	145
Alumoborates					
$2\text{SrO} \cdot \text{Al}_2\text{O}_3 \cdot \text{B}_2\text{O}_3$	AlO_4	4.3	0.65	83.5	91
$2\text{CaO} \cdot \text{Al}_2\text{O}_3 \cdot \text{B}_2\text{O}_3$	AlO_4	6.25	0.45	79.5	91

(continued overleaf)

Table 5 (continued)

Compound	Site	C_{qcc} (MHz)	η	δ (ppm)	Refs.
$2\text{Li}_2\text{O}\cdot\text{Al}_2\text{O}_3\cdot\text{B}_2\text{O}_3$	AlO_4	6.0	0.45	76	91
$3\text{Li}_2\text{O}\cdot\text{Al}_2\text{O}_3\cdot 2\text{B}_2\text{O}_3$	AlO_4	6.7	0.83	70	91
$9\text{Al}_2\text{O}_3\cdot 2\text{B}_2\text{O}_3$	AlO_4	6.8	0.1	53	91
	AlO_5	4.8	0.3	31	91
	AlO_6	6.2	0.4	10.5	91
Aluminum phosphates					
AlPO_4 (quartz)	AlO_4	4.2	0.35	44.8	274
AlPO_4 (tridimite)	AlO_4	0.75	0.95	39.8	274
AlPO_4 (cristobalite)	AlO_4	1.2	0.75	42.5	274
$\text{Al}_2\text{PO}_4(\text{OH})_3$ (augelite)	AlO_5	5.5	0.78	30	275
	AlO_6	4.7	0.2	-3	275
$\text{Al}_2\text{PO}_4(\text{OH})_3\cdot\text{H}_2\text{O}$ (senegalite)	AlO_5	2.87	0_{assumed}	30	275
	AlO_6	4.09	0_{assumed}	1.7	275
	AlO_6	1.2	0.25	-16	276
KAIP_2O_7	AlO_6	1.2	0.25	-16	276
AlPO_4 -5 (molecular sieve)	AlO_4	2.3	0.95	40.4	274
AlPO_4 -8 (dehydrated sieve)	AlO_4 -(1)	3.9	0.5_{assumed}	40.1	84
	AlO_4 -(2)	3.6	0.5_{assumed}	40.6	84
	AlO_4 -(3)	3.6	0.5_{assumed}	47.0	84
	AlO_4 -(4)	3.0	0.5_{assumed}	42.9	84
	AlO_4 -(5)	3.4	0.5_{assumed}	42.6	84
AlPO_4 -14 (molecular sieve)	AlO_4 -(3)	1.75/1.74	0.70/0.63	43.2/42.9	83/277
	AlO_4 -(2)	4.15/4.08	0.82/0.82	44.0/43.5	83/277
	AlO_5 -(1)	5.66/5.58	0.89/0.97	27.2/27.1	83/277
	AlO_6 -(4)	2.60/2.57	0.68/0.70	-0.9/-1.3	83/277
AlPO_4 -21 (molecular sieve)	AlO_4	3.7	0.15	47.3	78
	AlO_5 -I	5.9	0.68	14.6	78
	AlO_5 -II	7.4	0.52	15.7	78
AlPO_4 -25 (molecular sieve)	AlO_4 -I	1.9	0.67_{assumed}	40.8	78
	AlO_4 -II	0.8	0.67_{assumed}	39.5	78
AlPO_4 -25 (dehydrated molecular sieve)	AlO_4 -I	2.3	0.67_{assumed}	39.2	78
	AlO_4 -II	1.1	0.67_{assumed}	37.5	78
Alumosilicates					
Al_2SiO_5 (sillimanite)	AlO_4	6.77	0.53	64.5	278
	AlO_6	8.93	0.46	4.0	278
Al_2SiO_5 (andalusite)	AlO_5	5.73	0.7	35	279
	AlO_6	15.5	0.0	10	279
Al_2SiO_5 (kyanite)	AlO_6 -(1)	10.1	0.27	13.0	280
	AlO_6 -(2)	3.8	0.85	4.0	280
	AlO_6 -(3)	6.4	0.70	5.7	280
	AlO_6 -(4)	9.2	0.38	5.9	280
Mullite ($\sim 3\text{Al}_2\text{O}_3\cdot 1\text{SiO}_2$)	AlO_6	7.3	0	6.3	281
	AlO_4 (T)	7.3	0	68	281
	AlO_4 (T')	6	0.5	53	281
	AlO_4 (T*)	4	0.5	45	281
	AlO_4	2.8	-	72	278
Pennine	AlO_6	1.4	-	10	278
KAlSi_2O_6 (leucite)	T1-T3	2.1-2.3	0_{assumed}	61-69	282
$\text{CaAl}_2\text{Si}_2\text{O}_8$ (anorthite)	T1-T6	2.7-8.2	0.45-0.70	61-66	282
$\text{KAl}_2\{(\text{OH},\text{F})_2/\text{AlSi}_3\text{O}_{10}\}$ (muscovite)	AlO_4	2.1	-	72	278
	AlO_6	2.2	-	5	278
$\text{CaAl}_2\{(\text{OH})_2/\text{Al}_2\text{Si}_2\text{O}_{10}\}$ (margarite)	AlO_4	4.2	-	76	278
	AlO_6	6.3	-	11	278
Xantophyllite	AlO_4	2.8	-	76	278
	AlO_6	2.0	-	11	278
$\text{Na}_8\text{Al}_2\text{Be}_2\text{Si}_8\text{O}_{24}\text{Cl}_2$ (tugtupide)	AlO_4	1.36	0.08	63.4	218

Table 5 (continued)

Compound	Site	C_{qcc} (MHz)	η	δ (ppm)	Refs.
NaAlSi ₃ O ₈ (low albite)	AlO ₄	3.29	0.62	62.7	283
KAlSi ₃ O ₈ (microcline)	AlO ₄	3.22	0.21	58.5	283
(Mg, Fe)Al ₃ SiBO ₉ (grandidierite)	AlO ₅	8.7	0.95	41.0	284
	AlO ₆ -(1)	3.5	0.5	9.0	284
	AlO ₆ -(2)	8.6	0.95	11.0	284
Natrolite	AlO ₄	1.67	0.50	64	278
LiCl-sodalite	AlO ₄	0.98	0.59	71.9	217
LiBr-sodalite	AlO ₄	0.71	0.61	70.9	217
NaCl-sodalite	AlO ₄	0.94	0.32	62.9	217
NaBr-sodalite	AlO ₄	0.81	0.29	61.8	217
NaI-sodalite	AlO ₄	0.57	0.34	60.4	217
Na-A, hydrated zeolite	AlO ₄	1.1	0.75	59.2	278
Na-Y, hydrated zeolite	AlO ₄	2.0	0.5	62.8	278
Na-Y, dehydrated zeolite	AlO ₄	5.5	0.3	ca. 60	285
H-Y, dehydrated zeolite	AlO ₃	13.1	0.75	105 ± 20	285
	AlO ₃	13.5	0.4	–	286
	AlO ₃	15.3	0.4	60	287
	AlO ₄	6.0	0.7	–	286
H-Y, dealuminated, dehydr.	AlO ₃	13.7	0.5	–	286
	AlO ₄	7.0	0.7	–	286
USY	AlO ₄	2.8	–	60.0	270
	AlO ₅	4.1	–	34.5	270
	AlO ₆	2.9	–	4.0	270
HMOR, dehydrated zeolite	AlO ₃	15.0	0.35	–	286
	AlO ₄	6.8	0.7	–	286
Na-ZSM-5, dehydrated zeolite	AlO ₄	4.7	0.5	ca. 60	285
H-ZSM-5, dehydrated zeolite	AlO ₃	16.0/15.5	0.1/0.5	82 ± 20/–	285/286
	AlO ₄	7.3	0.7	–	286
H, Al-MCM-41 (as synthesized)	AlO ₄	2.3	0 _{assumed}	52.6	288
Fluoroaluminates					
H ₃ AlF ₆ ·6H ₂ O	AlF ₆	0.3	0.0	–2.8	289
K ₂ AlF ₅ ·H ₂ O	AlF ₆	12	0.0	0	289
Rb ₂ AlF ₅ ·H ₂ O	AlF ₆	13	0.0	0	289
CsAlF ₅ ·H ₂ O	AlF ₆	7.5	0.15	–10	289
NH ₄ AlF ₄	AlF ₆	10	0.1	–6	289
KAlF ₄	AlF ₆	12	0.0	–5	289
RbAlF ₄	AlF ₆	13	0.1	–4	289
Al ₂ SiO ₄ F ₂ (topas)	AlF ₆	1.7	0.4	0.3	289
Others					
Al(acac) ₃	AlO ₆	3.03	0.15	0.0	290
Al(trop) ₃		4.43	0.08	36.6	290
Al(TMHD) ₃	AlO ₆	3.23	0.10	1.5	290
AlCl ₃ ·3Al(OH) ₃ ·6H ₂ O	AlO ₆	6.9	0.4	7	291
AlCl ₃ ·4Al(OH) ₃ ·7H ₂ O	AlO ₆	5.7	0.7	3	291
AlCl ₃ ·OPCl ₃	AlCl ₃ O	6.0	0.15	88	292
Al ₂ Ge ₂ O ₇	AlO ₅	8.8	0.4	36	293
AlLaGe ₂ O ₇	AlO ₅	7.2	0.37	36	293
Al ₂ (MoO ₄) ₃	AlO ₆ -(1)	1.12	0.65	–12.4	272
	AlO ₆ -(2)	0.88	0.95	–13.4	272
	AlO ₆ -(3)	1.21	1.0	–10.3	272
	AlO ₆ -(1)	0.78	0.8	–11.1	272
Al ₂ (OH) ₂ (H ₂ O) ₈ (SO ₄) ₂ ·2H ₂ O	AlO ₆	4.6	0.4	3	291
Al ₂ (OH) ₄ SO ₄ ·7H ₂ O (aluminite)	AlO ₆ -I	10.1	0.1	6.9	291
	AlO ₆ -II	11.6	0.15	6.4	291
KAl(SO ₄) ₂ ·12H ₂ O	AlO ₆	0.400	0.00	–4.1	266
NH ₄ Al(SO ₄) ₂ ·12H ₂ O	AlO ₆	0.456	0.00	–0.4	266

^a The data published in 1983–92 were compiled by Dirk Müller.

Table 6 Quadrupolar coupling constant $C_{\text{qcc}} = e^2qQ/h$, the asymmetry parameter η and the isotropic value of the chemical shift δ (referred to 1.0 M NaCl) for the ^{23}Na NMR of powdered substances at ambient temperature^a

Compound	Site	C_{qcc} (MHz)	η	δ (ppm)	Ref.
Sodium–nitrogen compounds					
NaNO_3		0.337	0.00	−8.0	266
NaNO_2		1.09	0.11	−0.1	266
NaN_3		0.297	0.12	−3.8	266
Aluminosilicates					
NaX (Si/Al = 1.0)	I	1.1	0.5	5.2*	294
	I'	5.8	0.0	−12.8*	294
	II	5.0	0.0	−8.8*	294
	III'(1,2)	2.2	0.7	−10.8*	294
	III'(3)	1.2	0.9	−22.8*	294
NaX (Si/Al = 1.23)	I	0.0	0.0	1.2*	74
	I'	5.2	0.0	−11.8*	74
	II	4.6	0.0	−7.8*	74
	III'(1,2)	2.6	0.7	−5.8*	74
	III'(3)	1.6	0.9	−21.8*	74
NaY (Si/Al = 2.5)	I	1.2	0 _{assumed}	2.2*	146
	I'	4.8	0.0	3.2*	74
	II	3.9	0.0	−4.8*	74
EMT (Si/Al = 3.7)	I	1.0	0 _{assumed}	0.7*	146
	I' + II	4.1	0.3	0.2*	146
NaMOR (Si/Al = 7.1)	12-ring	2.0	0 _{assumed}	−6.8*	146
	Sidepockets	3.1	0 _{assumed}	−16.8*	146
NaZSM-5 (Si/Al = 18)		2.0	0 _{assumed}	−10.8*	146
$\text{NaAlSi}_3\text{O}_8$ (albite)		2.69	0.25	−7.1	295
$\text{Na}_8\text{Al}_2\text{Be}_2\text{Si}_8\text{O}_{24}\text{Cl}_2$ (tugtupide)		1.41	0.44	7.7	218
Amphibole HSMC	M(4)	3.9	0.49	9.3	296
	A	2.9	0.26	5.5	296
NaCl -sodalite, dehydrated		0–0.5	–	−8.8	217
		~0	0.67 _{assumed}	6.3	71
NaCl -sodalite, hydrated		≤0.1	–	–	297
NaBr -sodalite, dehydrated		0.72	0.12	−9.9	217
		1	0.67 _{assumed}	8.5	71
NaBr -sodalite, hydrated		0.6–0.8	–	–	297
NaI -sodalite, dehydrated		1.73	0.06	−20.6	217
		1.9	0.67 _{assumed}	9.3	71
NaI -sodalite, hydrated		1.5–1.8	0	–	297
Na -hydroxosodalite		2.00	0.10	3.2*	298
Na -nitride sodalite		1.00	0.18	0.4*	298
Silicates					
$\text{Na}_2\text{H}_2\text{SiO}_4 \cdot 8\text{H}_2\text{O}$		1.11	0.72	3.8*	298
$\text{Na}_2\text{H}_2\text{SiO}_4 \cdot 5\text{H}_2\text{O}$	I	1.35	0.45	5.7*	298
	II	2.01	0.70	0.0*	298
$\text{Na}_2\text{H}_2\text{SiO}_4 \cdot 4\text{H}_2\text{O}$	I	1.80	0.75	9.0*	298
	II	2.83	0.17	9.5*	298
Others					
NaOH		3.5	0.00	19.4*	298
$\text{Na}_3\text{P}_3\text{O}_9$	I	1.57	0.55	1.6*	298
	II	2.20	0.70	−7.6*	298
$\text{Na}_2(\text{OOCCH})_2 \cdot \text{H}_2\text{O}$	I	1.34	0.80	−2.2*	298
	II	0.80	0.75	0.9*	298
$\text{Na}_2\text{C}_2\text{O}_4$		2.50	0.74	17.9	266
$\text{CH}_3\text{COONa} \cdot 3\text{H}_2\text{O}$		0.779	0.38	2.1	266
Na_2SO_4		2.60	0.58	−1.3*	298

^a An asterisk denotes values of the chemical shift which were originally referred to solid NaCl and transformed by $\delta(1\text{ M NaCl}) = \delta(\text{solid NaCl}) + 7.2\text{ ppm}$. Zeolite samples listed in this table were dehydrated.

Table 7 Quadrupolar coupling constant $C_{\text{qcc}} = e^2qQ/h$, the asymmetry parameter η and the isotropic value of the chemical shift δ (referred to H_2O) for the ^{17}O NMR of powder compounds at ambient temperature^a

Compound	Site	C_{qcc} (MHz)	η	δ (ppm)	Ref.
Aluminum oxides and hydroxides					
α - Al_2O_3 (corundum)	OAl ₄	2.17	0.55	75	299
AlO(OH) (boehmite)	OAl ₄	1.20	0.1	70	299
	OAl ₄	1.15	0.13	70.0	266
	Al ₂ OH	5.0	0.5	40	299
Al(OH) ₃ (bayerite)	Al ₂ OH	6.0	0.3	40	299
γ - Al_2O_3	OAl ₄	1.8	0 _{assumed}	73	299
η - Al_2O_3	OAl ₄	1.6	0 _{assumed}	73	299
δ - Al_2O_3	OAl ₄	1.6	0 _{assumed}	72	299
θ - Al_2O_3	OAl ₄	1.2	0 _{assumed}	72	299
	OAl ₃	4.0	0.6	79	299
Al ₁₃ O ₄₀ cluster	AlOAl	1.2	0	50	300
Microporous materials					
AlPO ₄ -5	AlOP	5.7	0.0	63	301
AlPO ₄ -11	AlOP	5.7	0.0	64	301
AlPO ₄ -17	AlOP	5.6	0.1	67	301
Ga-sodalite	SiOGa	4.0	0.3	29	301
	SiOSi	5.1	0.0	52	301
NaBa-Ga-sodalite	SiOGa	4.0	0.3	29	301
	SiOSi	5.1	0.0	52	301
Ga-X	SiOGa	4.0	0.3	28	301
	SiOSi	5.0	0.0	50	301
Na-Y	SiOAl	3.1	0.2	31	302
	SiOSi	4.6	0.2	46	302
Ba, Na-Y	SiOAl	3.4	0.2	45	302
	SiOSi	5.1	0.1	57	302
NH ₄ -Y	SiOAl	3.2	0.2	31	302
	SiOSi	5.0	0.1	47	302
Na-Y, dealuminated	SiOSi	5.2	0.1	47	302
Sil-Y, dehydrated	SiOSi O1	5.1	0.3	42.3	85
	SiOSi O4	5.28	0.2	34.8	85
	SiOSi O3	5.14	0.1	47.3	85
	SiOSi O2	5.39	0.2	37.2	85
Na-A, dehydrated	SiOAl	3.2	0.2	33	302
Na-A, hydrated	SiOAl O1	3.4	0	43.6	86
	SiOAl O3	3.4	0.25	40.5	86
	SiOAl O2	3.4	0	31.0	86
Na-LSX, hydrated	SiOAl O1	3.2	0.4	50.3	86
	SiOAl O3	3.4	0.3	45.0	86
	SiOAl O2	3.3	0.3	41.7	86
	SiOAl O4	3.6	0.15	36.9	86
Na-ZSM-5, hydrated	SiOSi	5.3	0.12	40.0	53
	SiOAl	3.5	0.29	30.0	53
Stilbite	SiOSi	5.1	0.18	43	303
	SiOAl	3.5	0.28	33	303
Silicates					
SiO ₂ (low cristobalite)	SiOSi	5.3	0.0	46	302
SiO ₂ (cristobalite)	SiOSi	5.3	0.125	40	304
SiO ₂ (amorphous)	SiOSi	5.8	0.0	50	305
	SiOH	4.0	0.3	20	305
SiO ₂ (stishovite)	SiOSi	6.5	0.125	109	306
SiO ₂ (coesite)	SiOSi O5	5.16	0.292	58	307
	SiOSi O2	5.43	0.166	41	307
	SiOSi O3	5.45	0.168	57	307
	SiOSi O4	5.52	0.169	53	307
	SiOSi O1	6.05	0.000	29	307

(continued overleaf)

Table 7 (continued)

Compound	Site	C_{qcc} (MHz)	η	δ (ppm)	Ref.
Mg_2SiO_4 (forsterite)	SiOMg-I	2.35	0.2	61	308
	SiOMg-II	2.35	1.0	62	308
	SiOMg-III	2.70	0.3	47	308
	SiOMg-I	2.8	0 _{assumed}	64	309
	SiOMg-II	3.3	0 _{assumed}	72	309
	SiOMg-III	3.0	0 _{assumed}	49	309
MgSiO_3 (clinoenstatite)	SiOMg-I	3.2	0.0	60	310
	SiOMg-II	3.2	0.0	42	310
	SiOSi	5.1	0.3	62	310
	SiO-?	2.9–5.2	0 _{assumed}	57–70	309
$\text{CaMgSi}_2\text{O}_6$ (diopside)	SiOCa	2.7	0.0	84	310
	SiOMg	2.7	0.1	63	310
	SiOSi	4.4	0.3	69	310
	SiOCa	2.8	0 _{assumed}	86	309
	SiOMg	2.7	0 _{assumed}	64	309
	SiOSi	4.5	0 _{assumed}	69	309
$\text{Mg}_3\text{Si}_4\text{O}_{10}(\text{OH})_2$ (talc)	SiOMg	3.2	0.0	40	305
	SiOSi	5.8	0.0	50	305
	MgOH	7.3	0.0	0	305
$\text{Li}_2\text{Si}_2\text{O}_5$	br O1	5.6	0.55	108	311
	br O2	4.05	0.05	35	311
	nb O3	2.45	0.1	38	311
$\alpha\text{-Na}_2\text{Si}_2\text{O}_5$	br O1	5.74	0.2	52	311
	br O2	4.67	0.3	74	311
	nb O3	2.4	0.2	36	311
$\text{K}_2\text{Si}_2\text{O}_5$	br O1	5.1	0.1	114	311
	br O2	4.7	0.2	69	311
	nb O3	2.1	0.5	72	311
$\text{Rb}_2\text{Si}_2\text{O}_5$	br O1	4.4	0.1	124	311
	br O2	4.7	0.5	59	311
	nb O3	1.9	0.5	93	311
$\text{K}_2\text{Si}_4\text{O}_9$ (wadeite)	br O1	4.45	0.35	62.5	306
	SiOSi O2	4.9	0.2	97	306
BaSiO_3	br O	3.7	0.4	87	310
$\alpha\text{-SrSiO}_3$	br O	4.1	0.4	80	310
$\alpha\text{-CaSiO}_3$	br O	3.8	0.2	75	310
CaSiO_3 (wollastonite)	SiO-?	2.3–4.7	0 _{assumed}	115–167	309
Ca_2SiO_4 (larnite)	SiO-?	2.5–2.8	0 _{assumed}	122–134	309
Na-ilerite (RUB-18)	SiOSi	5.1	0	42.6	312
	SiOH	3.1	0	61.2	312
Aluminosilicate glasses					
YAS	br O	3.1	–	54	313
	nb O			143	313
	nb O			210	313
LAS	br O	3.1	–	58	313
	nb O			178	313
$\text{NaAlSi}_3\text{O}_8$	SiOSi	5.1	0.15	49	314
	SiOAl	3.2	0.05	33	314
$\text{NaAlSi}_3\text{O}_8$	SiOSi	5.2	0.2	40	315
	SiOAl	3.8	0.2	25	315
Analcime	H_2O	7.6	0	18	316
Silicate glasses					
$\text{Na}_2\text{Si}_4\text{O}_9$	SiOSi	5.2	0.22	51	315
	nb O	2.7	0.25	40	315
	H_2O	6.0	0.7	20	315
$\text{Na}_2\text{Si}_2\text{O}_5$	br O	4.9	0.1	69	311
	nb O	2.35	0.2	37	311

Table 7 (continued)

Compound	Site	C_{qcc} (MHz)	η	δ (ppm)	Ref.
Na ₂ Si ₃ O ₇	br O	5.0	0	60	306
	nb O	2.3	0	39	306
Li ₂ Si ₂ O ₅	br O	5.0	0.15	68	311
	nb O	2.55	0.2	42	311
K ₂ Si ₂ O ₅	br O	4.7	0.25	60	311
	nb O	2.5	0.45	84	311
K ₂ Si ₄ O ₉	br O	4.9	0	52	306
	nb O	2.3	0	76	306
Cs ₂ Si ₂ O ₅	br O	4.55	0.3	68	311
	nb O	3.1	0.55	145	311
Ba Si glass	br O	4.0	0.3	78	317
Ba Ca Si glass	br O	4.1	0.3	68	317
Ca Si glass	br O	4.7	0.3	59	317
	br O	4.6	0.0	66	318
	nb O	2.1	0.2	110	318
Na₂O–GeO₂ crystals and glasses					
GeO ₂ (quartz)	GeO ₄	7.3	0.48	70	319
GeO ₂ (rutile)	GeO ₆	7.5	0.10	160	319
Na ₂ GeO ₃ (crystal)	GeO ₄	5.2	0.5	70	319
	NBO	2.5	0.5	47	
Na ₂ O·9GeO ₂	GeO ₄	7.0	0.5	165	319
	GeO ₆				
2 Na ₂ O·9GeO ₂	GeO ₄	6.0	0.5	80	319
Others					
TiO ₂ (rutile)	TiOTi	1.5	0.87	596.5	249
HfGeO ₄	HfOGe	5.2	0.65	185	320
Mg(OH) ₂ (brucite)	MgOH	6.8	0	20	321
Mg(OH) ₂ polycrystalline	MgOH	6.8	0.0	25	305
Mg(OH) _x (OCH ₃) _{2-x}	MgOH	7.25	0	-25	321
Hydroxyapatite Ca ₅ (P ¹⁷ O ₄) ₃ (OH)		4.0/4.1	0.0/0.1	108/115	322
CaHP ¹⁷ O ₄ ·2H ₂ O		4.2/4.3	0/0	98/96	322
KH ₂ PO ₄		5.2	0.55	92	322
NH ₄ H ₂ PO ₄		5.1	0.55	93	322
Ba(ClO ₃) ₂ ·H ₂ ¹⁷ O	H ₂ O	6.8	1.00	22	322
Ca(OH) ₂		6.5	0.00	62	322
CaCO ₃		6.97	1	204	323

^a The data published after 1989 were compiled by Ulf Pingel. A site nb O and br O denotes nonbridging and bridging oxygen, respectively.

If the quadrupolar echo decay ($\pi/2, t_1, \pi/2, t_1, t_2$) is monitored as a 2-D data set, the doubly Fourier transformed 2-D spectrum can be influenced by a slow motion. Schleicher et al.⁽²⁰⁹⁾ applied this technique for the observation of dynamics in alanine. Müller et al.⁽²¹⁰⁾ used a multiple-pulse quadrupolar echo sequence, in order to obtain information about the chemical exchange. For other examples, including the influence of dynamics on the longitudinal relaxation time in the Zeeman reservoir T_{1Z} or the relaxation time in the quadrupolar reservoir T_{1Q} , see Vold et al.^(11,211)

Larsen et al.⁽²¹²⁾ applied the CPMG experiment to deuterons (²H QCPMG) and thereby enhanced the sensitivity by about one order of magnitude and the dynamic range by two orders of magnitude.

Dynamic experiments were mainly performed with nonrotating samples. However, dynamic ²H MAS NMR is now in progress. Weintraub and Vega⁽²¹³⁾ studied dimethyl sulfone by MAS and off-MAS techniques. Kristensen et al. investigated multiaxial dynamics⁽²¹⁴⁾ and effects of restricted rotational diffusion.⁽²¹⁵⁾

10 SURVEY OF NUCLEAR MAGNETIC RESONANCE PARAMETERS FOR SELECTED COMPOUNDS

Collections of electric field gradient and chemical shift data for the most commonly studied quadrupolar nuclei with half-integer spins ²⁷Al, ²³Na and ¹⁷O are presented in Tables 5, 6 and 7, respectively. For

solid-state NMR studies of other quadrupolar nuclei we give only a few references to recent publications: lithium-6,⁽²¹⁶⁾ lithium-7,^(74,217) beryllium-9,⁽²¹⁸⁾ boron-11,^(219–221) nitrogen-14,⁽²²²⁾ magnesium-25,⁽²²³⁾ sulfur-33,^(224,225) chlorine-35/37,⁽²²⁶⁾ potassium-39,^(227,228) calcium-43,^(229–231) scandium-45,⁽²³²⁾ titanium-47/49,^(233,234) vanadium-51,^(235,236) chromium-53,⁽²³⁷⁾ cobalt-59,^(236,238,239) copper-65,⁽²⁴⁰⁾ zinc-67,^(241,242) gallium-69/71,^(243–245) bromine-81,⁽²⁴⁶⁾ rubidium-85/87,^(247,248) zirconium-91,⁽²⁴⁹⁾ niobium-93,^(33,249) molybdenum-95,⁽²⁵⁰⁾ indium-115,⁽²⁵¹⁾ antimony-121,⁽²⁵²⁾ iodine-127,^(253,254) cesium-133,^(255,256) barium-137,^(257,258) lanthanum-139^(73,259) and lutetium-175.⁽²⁶⁰⁾

ACKNOWLEDGMENTS

I am grateful to Jean-Paul Amoureux, Horst Ernst, Jürgen Haase, Michael Hunger, Christian Jäger, Dieter Michel, Toralf Mildner, Dirk Müller, Ulf Pingel, Dagmar Prager, Ago Samoson, Mark E. Smith, Daniel Prochnow, and Ingo Wolf for contributions and advice. This work was supported by the Deutsche Forschungsgemeinschaft, SFB 294, project Fr 902/9, and the Graduiertenkolleg Physikalische Chemie der Grenzflächen.

ABBREVIATIONS AND ACRONYMS

CP	Cross-polarization
CPMAS	Cross-polarization Magic-angle Spinning
CPMG	Carr–Purcell–Meiboom–Gill
DACS	Dynamic-angle Correlation Spectroscopy
DAS	Dynamic-angle Spinning
DFS	Double-frequency Sweeps
DOR	Double-rotation
DQ	Double-quantum
FAM	Fast Radiofrequency Amplitude Modulation
FID	Free Induction Decay
FSAHP	Frequency-stepped Adiabatic Half-passage
fwhm	Full Width at Half-maximum
HETCOR	Heteronuclear Chemical Shift Correlation
LAB	Laboratory Axis System
MAS	Magic-angle Spinning
MQDOR	Multiple-quantum Double-rotation
MQMAS	Multiple-quantum Magic-angle Spinning

MQVAS	Multiple-quantum Variable-angle Spinning
NMR	Nuclear Magnetic Resonance
NQR	Nuclear Quadrupolar Resonance
PAS	Principal Axis System
QEDOR	Quadrupolar Echo Double Resonance
REDOR	Rotational-echo Double Resonance
RF	Radiofrequency
RIACT	Rotation-induced Adiabatic Coherence Transfer
SATRAS	Satellite-transition Spectroscopy
SOLEDOR	Solid Echo Double Resonance
TPPI	Time-proportional Phase Increment
TRAPDOR	Transfer-of-populations Double-resonance
VAS	Variable-angle Spinning
2-D	Two-dimensional
3QMAS	Triple-quantum Magic-angle Spinning

RELATED ARTICLES

Nuclear Magnetic Resonance and Electron Spin Resonance Spectroscopy (Volume 13)

Nuclear Magnetic Resonance and Electron Spin Resonance Spectroscopy: Introduction • Chemical Shifts in Nuclear Magnetic Resonance

Nuclear Magnetic Resonance and Electron Spin Resonance Spectroscopy cont'd (Volume 14)

Nuclear Magnetic Resonance Instrumentation • Parameters, Calculation of Nuclear Magnetic Resonance • Quadrupole Couplings in Nuclear Magnetic Resonance, General

REFERENCES

1. T. Vosegaard, E. Hald, V. Langer, H. Skov, P. Daugaard, H. Bildsoe, H. Jakobsen, 'Improved Hardware and Software for Single-crystal NMR Spectroscopy', *J. Magn. Reson.*, **135**, 126–132 (1998).
2. T. Vosegaard, E. Hald, P. Daugaard, H.J. Jakobsen, 'A Two-axis Goniometer for Sensitivity Enhancement in Single-crystal NMR Spectroscopy', *Rev. Sci. Instrum.*, **70**, 1771–1779 (1999).
3. O. Kanert, M. Mehring, 'Static Quadrupole Effects in Disordered Cubic Solids', *NMR Basic Principles Prog.*, **3**, 1–81 (1971).

4. B.V.G. Volkoff, H.E. Petch, D.W.I. Smellie, 'Nuclear Electric Quadrupole Interaction in Single Crystals', *Can. J. Phys.*, **30**, 270–289 (1952).
5. B.G.M. Volkoff, 'Second Order Nuclear Quadrupole Effects in Single Crystals', *Can. J. Phys.*, **31**, 820–836 (1953).
6. T.P. Das, A.K. Saha, 'Electric Quadrupole Interaction and Spin Echoes in Crystals', *Phys. Rev.*, **98**, 516–524 (1955).
7. M.H. Cohen, F. Reif, 'Quadrupole Effects in Nuclear Magnetic Resonance Studies of Solids', *Solid State Phys.*, **5**, 321–438 (1957).
8. H.W. Spiess, 'Deuteron NMR – A New Tool for Studying Chain Mobility and Orientation in Polymers', *Adv. Polym. Sci.*, **66**, 23–58 (1985).
9. D. Freude, J. Haase, 'Quadrupole Effects in Solid-state NMR', *NMR Basic Principles Prog.*, **29**, 1–90 (1993).
10. C. Jäger, 'Satellite Transition Spectroscopy of Quadrupolar Nuclei', *NMR Basic Principles Prog.*, **31**, 133–170 (1994).
11. G.L. Hoatson, R.L. Vold, '²H-NMR Spectroscopy of Solids and Liquid Crystals', *NMR Basic Principles Prog.*, **32**, 1–67 (1994).
12. B.F. Chmelka, J.W. Zwanziger, 'Solid-state NMR Line Narrowing Methods for Quadrupole Nuclei – Double Rotation and Dynamic-angle Spinning', *NMR Basic Principles Prog.*, **33**, 79–124 (1994).
13. N. Chandrakumar, 'Spin-1 NMR', *NMR Basic Principles Prog.*, **34**, 1–117 (1996).
14. A.S. Ulrich, S.L. Grage, 'H-2 NMR (Solid-state NMR of Polymers)', *Stud. Phys. Theor. Chem.*, **84**, 190–211 (1998).
15. M.E. Smith, E.R.H. van Eck, 'Recent Advances in Experimental Solid State NMR Methodology for Half-integer Spin Quadrupole Nuclei [Review]', *Prog. Nucl. Magn. Reson. Spectrosc.*, **34**, 159–201 (1999).
16. H. Chihara, N. Nakamura, *Nuclear Quadrupole Resonance Spectroscopy Data, Landold-Börnstein, New Series, Group III*, Springer, Berlin, Vol. 20, 1988.
17. J. Mason, *Multinuclear NMR*, Plenum Press, New York, 1989.
18. K. Schmidt-Rohr, H.W. Spiess, *Multidimensional Solid-state NMR and Polymers*, Academic Press, London, 1994.
19. A. Abragam, *Principles of Nuclear Magnetism*, Oxford University Press, Oxford, 1961.
20. M. Weissbluth, *Atoms and Molecules*, Academic Press, New York, London, 1978.
21. Z.W. Zheng, Z.H. Gan, N.K. Sethi, D.W. Alderman, D.M. Grant, 'An Efficient Simulation of Variable-angle Spinning Lineshapes for the Quadrupole Nuclei with Half-integer Spin', *J. Magn. Reson.*, **95**, 509–522 (1991).
22. M.E. Rose, *Elementary Theory of Angular Momentum*, John Wiley, New York, 1967.
23. U. Haeberlen, *High Resolution NMR in Solids, Selective Averaging*, Academic Press, New York, 1976.
24. T.P. Das, E.L. Hahn, 'Nuclear Quadrupole Resonance Spectroscopy', *Solid State Phys., Suppl.*, **1**, 1–223 (1958).
25. L. Frydman, J.S. Harwood, 'Isotropic Spectra of Half-integer Quadrupole Spins from Bidimensional Magic-angle Spinning NMR', *J. Am. Chem. Soc.*, **117**, 5367–5368 (1995).
26. S. Wimperis, 'Broadband and Narrowband Composite Excitation Sequences', *J. Magn. Reson.*, **86**, 46–59 (1990).
27. A.P.M. Kentgens, 'Quantitative Excitation of Half-integer Quadrupole Nuclei by a Frequency-stepped Adiabatic Half-passage', *J. Magn. Reson.*, **95**, 619–625 (1991).
28. D.W. Sindorf, V.J. Bartuska, 'Wide-line NMR Spectroscopy in Solids Using Variable Frequency Pulses', *J. Magn. Reson.*, **85**, 581–585 (1989).
29. R.Q. Fu, V.L. Ermakov, G. Bodenhausen, 'Divergent Double Chirp Pulses for Refocusing Quadrupole Interactions', *Solid State NMR*, **7**, 1–10 (1996).
30. J. Haase, M.S. Conradi, 'Sensitivity Enhancement for NMR of the Central Transition of Quadrupole Nuclei', *Chem. Phys. Lett.*, **209**, 287–291 (1993).
31. J. Haase, E. Oldfield, 'Aluminum to Oxygen Cross-polarization in Alpha-Al₂O₃ (Corundum)', *Solid State NMR*, **3**, 171–175 (1994).
32. A.P.M. Kentgens, R. Verhagen, 'Advantages of Double Frequency Sweeps in Static, MAS and MQMAS NMR of Spin $I = \frac{3}{2}$ Nuclei', *Chem. Phys. Lett.*, **300**, 435–443 (1999).
33. A.F. McDowell, M.S. Conradi, J. Haase, 'First-satellite Spectroscopy, a New Method for Quadrupole Spins', *J. Magn. Reson. A*, **119**, 211–218 (1996).
34. J. Haase, N.J. Curro, R. Stern, C.P. Slichter, 'New Double Resonance Technique for Quadrupole Nuclei', *Mol. Phys.*, **95**, 891–896 (1998).
35. T. Gullion, 'Measurement of Dipolar Interactions Between Spin- $\frac{1}{2}$ and Quadrupole Nuclei by Rotational-echo, Adiabatic-passage, Double-resonance NMR', *Chem. Phys. Lett.*, **246**, 25–330 (1995).
36. T. Gullion, 'Introduction to Rotational-echo, Double Resonance NMR', *Concepts in Magn. Reson.*, **10**, 277–289 (1998).
37. C.P. Grey, W.S. Veeman, A.J. Vega, 'Referenz', *J. Chem. Phys.*, **98**, 7711 (1993).
38. S.R. Hartmann, E.L. Hahn, 'Nuclear Double Resonance in the Rotating Frame', *Phys. Rev.*, **128**, 2042–2053 (1962).
39. C.P. Slichter, *Principles of Magnetic Resonance*, Springer, Berlin, 1990.
40. S. Vega, 'Multiple-quantum Cross-polarization NMR on Spin Systems with $I = \frac{1}{2}$ and $S = \frac{3}{2}$ in Solids', *Phys. Rev. A*, **23**, 3152–3173 (1981).
41. A.J. Vega, 'CP/MAS of Quadrupole $S = \frac{3}{2}$ Nuclei', *Solid State NMR*, **1**, 17–32 (1992).
42. A.J. Vega, 'MAS NMR Spin Locking of Half-integer Quadrupole Nuclei', *J. Magn. Reson.*, **96**, 50–68 (1992).

43. S. Hayashi, K. Hayamizu, 'Line Shapes in CP/MAS NMR Spectra of Half-integer Quadrupole Nuclei', *Chem. Phys. Lett.*, **203**, 319–324 and **205**, 597 (1993).
44. S. Hayashi, 'MAS NMR of Half-integer Quadrupole Nuclei – Effect of Spin-locking Efficiency on Powder Lineshapes', *Solid State NMR*, **3**, 93–101 (1994).
45. S.W. Ding, C.A. McDowell, 'Theoretical Calculations of the CPMAS Spectral Lineshapes of Half-integer Quadrupole Systems', *J. Magn. Reson. A*, **114**, 80–87 (1995).
46. S.W. Ding, C.A. McDowell, 'Application of Floquet Theory to Quadrupole Nuclear Spin- $\frac{3}{2}$ Nuclei in Solids Undergoing Sample Rotation', *Mol. Phys.*, **95**, 841–848 (1998).
47. W. Sun, J.T. Stephen, L.D. Potter, Y. Wu, 'Rotation-induced Resonance and Second-order Quadrupole Effects on Spin Locking of Half-integer Quadrupole Nuclei', *J. Magn. Reson. A*, **116**, 181–188 (1995).
48. J.P. Amoureux, 'High-resolution Solid-state NMR for Spin $\frac{3}{2}$ and $\frac{9}{2}$: The Multi-quantum Transitions Method', *Solid State NMR*, **2**, 83–88 (1993).
49. K. Narita, J.J. Umeda, H. Kusumoto, 'NMR Powder Patterns of the Second-order Nuclear-Quadrupole Interaction on the Central Line in Solids with Asymmetric Field Gradient', *J. Chem. Phys.*, **44**, 2719–2723 (1966).
50. D. Müller, 'Zur Bestimmung Chemischer Verschiebungen der NMR-Frequenzen bei Quadrupolkernen aus den MAS NMR-Spektren', *Ann. Phys.*, **39**, 451–460 (1982).
51. A. Samoson, 'Satellite Transition High-resolution NMR of Quadrupole Nuclei in Powders', *Chem. Phys. Lett.*, **119**, 29–32 (1985).
52. H.J. Jakobsen, J. Skibsted, H. Bildsoe, N.C. Nielsen, 'Magic-angle Spinning NMR Spectra of Satellite Transitions for Quadrupole Nuclei in Solids', *J. Magn. Reson.*, **85**, 173–180 (1989).
53. J.-P. Amoureux, F. Bauer, H. Ernst, C. Fernandez, D. Freude, D. Michel, U.-T. Pingel, 'O-17 Multiple-quantum and ^1H MAS NMR Studies of Zeolite ZSM-5', *Chem. Phys. Lett.*, **285**, 10–14 (1998).
54. A. Samoson, E. Lippmaa, A. Pines, 'High Resolution Solid State NMR Averaging of Second-order Effects by Means of a Double-rotor', *Mol. Phys.*, **65**, 1013–1018 (1988).
55. Y. Wu, B.Q. Sun, A. Pines, A. Samoson, E. Lippmaa, 'NMR Experiments with a New Double Rotor', *J. Magn. Reson.*, **89**, 297–309 (1990).
56. A. Samoson, E. Lippmaa, 'Synchronized Double-rotation NMR Spectroscopy', *J. Magn. Reson.*, **84**, 410–416 (1989).
57. A. Samoson, J. Tegenfeldt, 'Suppression of DOR Sidebands', *J. Magn. Reson. A*, **110**, 238–244 (1994).
58. D. Kuwahara, T. Nakai, 'Spinning-sideband Suppression in DOR NMR Spectra Using a Magic-angle-turning Technique', *Chem. Phys. Lett.*, **260**, 249–252 (1996).
59. B.Q. Sun, J.H. Baltisberger, Y. Wu, A. Samoson, A. Pines, 'Sidebands in Dynamic Angle Spinning (DAS) and Double Rotation (DOR) NMR', *Solid State NMR*, **1**, 267–295 (1992).
60. E. Cochon, J.P. Amoureux, 'Sideband Analysis in DOR NMR Spectra. 1. 'Infinite' Inner-rotor Speed', *Solid State NMR*, **2**, 205–222 (1993).
61. J.P. Amoureux, E. Cochon, 'Sideband Analysis in DOR NMR Spectra. 2. Real Finite Inner-rotor Speed', *Solid State NMR*, **2**, 223–234 (1993).
62. A. Samoson, A. Pines, 'Double Rotor for Solid-state NMR', *Rev. Sci. Instrum.*, **60**, 3239–3241 (1989).
63. D. Müller, M. Smith, L. Wunsch, 'NMR at More Than One Magic Angle', Bruker Report, Bruker, Karlsruhe, 31–32, 1990.
64. B.F. Chmelka, K.T. Mueller, A. Pines, J. Stebbins, Y. Wu, J.W. Zwanziger, 'Oxygen-17 NMR in Solids by Dynamic-angle Spinning and Double Rotation', *Nature*, **339**, 42–43 (1989).
65. K.T. Mueller, Y. Wu, B.F. Chmelka, J. Stebbins, A. Pines, 'High-resolution Oxygen-17 NMR of Solid Silicates', *J. Am. Chem. Soc.*, **113**, 32–38 (1991).
66. R. Jelinek, B.F. Chmelka, Y. Wu, M.E. Davis, J.G. Ulan, R. Gronsky, A. Pines, 'Adsorption Effects in Aluminophosphate Molecular Sieves Studied by Al-27 Double-rotation NMR', *Catal. Lett.*, **15**, 65–73 (1992).
67. G.J. Ray, A. Samoson, 'Double Rotation and Variable Field Al-27 NMR Study of Dealuminated Y-Zeolites', *Zeolites*, **13**, 410–413 (1993).
68. M. Hunger, G. Engelhardt, H. Koller, J. Weitkamp, 'Characterization of Sodium Cations in Dehydrated Faujasites and Zeolite EMT by Na-23 DOR, 2D-Nutation, and MAS NMR', *Solid State NMR*, **2**, 111–120 (1993).
69. H.A.M. Verhulst, W.J.J. Welters, G. Vorbeck, L.J.M. Vandeven, V.H.J. Debeer, R.A. Vansanten, J.W. Dehaan, 'New Assignment of the Signals in Na-23 DOR NMR to Sodium Sites in Dehydrated NaY Zeolite', *J. Phys. Chem.*, **98**, 7056–7062 (1994).
70. G.W. Haddix, M. Narayana, S.C. Tang, Y. Wu, 'Double-rotation NMR, Magic Angle Spinning NMR, and X-ray Diffraction Study of the Structure of Aluminum Molybdate', *J. Phys. Chem.*, **97**, 4624–4627 (1993).
71. R. Jelinek, S. Özkar, G.A. Ozin, 'Extraframework Sodium Cation Sites in Sodium Zeolite Y Probed by 23-Na Double-rotation NMR', *J. Am. Chem. Soc.*, **114**, 4907–4908 (1992).
72. R. Jelinek, S. Ozkar, G.A. Ozin, 'Intrazeolite Topotaxy – Na-23 Double-rotation NMR Study of Transition-metal Hexacarbonyls and Oxides Encapsulated in Sodium Zeolite-Y', *J. Phys. Chem.*, **96**, 5949–5953 (1992).
73. M. Hunger, G. Engelhardt, J. Weitkamp, 'Solid-state Na-23, La-139, Al-27 and Si-29 NMR Spectroscopic Investigations of Cation Location and Migration in

- Zeolites LaNaY', *Microporous Mater.*, **3**, 497–510 (1995).
74. M. Feuerstein, M. Hunger, G. Engelhardt, J. Amoureux, 'Characterisation of Sodium Cations in Dehydrated Zeolite NaX by Na-23 NMR Spectroscopy', *Solid State NMR*, **7**, 95–103 (1996).
75. H. Koller, E. Meijer, R. Vansanten, 'Al-27 Quadrupole Interaction in Zeolites Loaded with Probe Molecules – A Quantum-chemical Study of Trends in Electric Field Gradients and Chemical Bonds in Clusters', *Solid State NMR*, **9**, 165–175 (1997).
76. Y. Wu, B. Chmelka, A. Pines, M.E. Davis, P.J. Grobet, P.A. Jacobs, 'High-resolution Al-27 NMR Spectroscopy for the Aluminophosphate Molecular Sieve VPI-5', *Nature*, **346**, 550–552 (1990).
77. P.J. Grobet, A. Samoson, H. Geerts, J.A. Martens, P.A. Jacobs, 'Crystallographic Site Discrimination in Aluminophosphate Molecular Sieves by Solid-state NMR – Influence of the Field-dependent Isotropic 2nd-order Quadrupole Shift', *J. Phys. Chem.*, **95**, 9620–9622 (1991).
78. R. Jelinek, B.F. Chmelka, Y. Wu, P.J. Grandinetti, A. Pines, P.J. Barrie, J. Klinowski, 'Study of the Aluminophosphates AlPO₄-21 and AlPO₄-25 by ²⁷Al Double-rotation NMR', *J. Am. Chem. Soc.*, **113**, 4097–4101 (1991).
79. Y. Wu, D. Lewis, J.S. Frye, A.R. Palmer, R.A. Wind, 'Cross-polarization Double-rotation NMR', *J. Magn. Reson.*, **100**, 425–430 (1992).
80. J. Jänchen, M.P.J. Peeters, J.W. Dehaan, L.J.M. Vandeven, J.H.C. Vanhooff, I. Girnus, U. Lohse, 'Adsorption Calorimetric Measurements and Al-27 DOR NMR Studies on the Molecular Sieve AlPO₄-18', *J. Phys. Chem.*, **97**, 12042–12046 (1993).
81. G.J. Kennedy, J.B. Higgins, C.F. Ridenour, H.X. Li, M.E. Davis, 'Multifield MAS and DOR NMR Studies of a Hydrated Aluminophosphate Molecular Sieve – AlPO₄-H₂', *Solid State NMR*, **4**, 173–178 (1995).
82. M. Kovalakova, P. Grobet, 'Double Rotation Al-27 NMR in Molecular Sieves', *Appl. Magn. Reson.*, **10**, 447–476 (1996).
83. C.A. Fyfe, H.M.Z. Altenschildesche, K.C. Wong-Moon, H. Grondey, J.M. Chezeau, '1D and 2D Solid State NMR Investigations of the Framework Structure of As-synthesized AlPO₄-14', *Solid State NMR*, **9**, 97–106 (1997).
84. M. Kovalakova, P. Grobet, 'The Al-27 DOR NMR Characterization of the Molecular Sieve AlPO₄-8', *Solid State NMR*, **9**, 107–113 (1997).
85. L. Bull, A. Cheetham, T. Anupold, A. Reinhold, A. Samoson, J. Sauer, B. Bussemer, Y. Lee, S. Gann, J. Shore, A. Pines, R. Dupree, 'A High-resolution O-17 NMR Study of Siliceous Zeolite Faujasite', *J. Am. Chem. Soc.*, **120**, 3510–3511 (1998).
86. U.T. Pingel, J.P. Amoureux, T. Anupold, F. Bauer, H. Ernst, C. Fernandez, D. Freude, A. Samoson, 'High-field O-17 NMR Studies of the SiOAl Bond in Solids', *Chem. Phys. Lett.*, **194**, 345–350 (1998).
87. C. Rohrig, I. Dierdorf, H. Gies, 'X-ray Powder Diffraction and NMR-spectroscopic Investigations on a Porous Zincosilicate Related to the Zeolite VPI-7 (VSV)', *J. Phys. Chem. Solids.*, **56**, 1369–1376 (1995).
88. R. Jelinek, B.F. Chmelka, A. Stein, G.A. Ozin, 'Multi-nuclear Magic-angle Spinning and Double-rotation NMR Study of the Synthesis and Assembly of a Sodalite Semiconductor Supralattice', *J. Phys. Chem.*, **96**, 6744–6752 (1992).
89. G. Engelhardt, P. Sieger, J. Felsche, 'Multinuclear Solid State NMR of Host–Guest Systems with TO₂ (T = Si, Al) Host-frameworks – A Case Study on Sodalites', *Anal. Chim. Acta*, **283**, 967–985 (1993).
90. T.J. Bastow, J.S. Hall, M.E. Smith, S. Steuernagel, 'Characterisation of Hydrated Aluminas by MAS and DOR Al-27 NMR', *Mater. Lett.*, **18**, 197–200 (1994).
91. D. Massiot, D. Müller, T. Hubert, M. Schneider, A.P.M. Kentgens, B. Cote, J.P. Coutures, W. Gessner, 'Double Rotation and Magic-angle Spinning Nuclear Magnetic Resonance Study of Al-27: Reexamination of the Aluminum Borate 9Al₂O₃·2B₂O₃', *Solid State NMR*, **5**, 175–180 (1995).
92. F. Taulelle, A. Samoson, T. Loiseau, G. Ferey, 'ULM-18, a Fluorinated Gallium Phosphate with Perforated Layers: XRD and NMR, Structure Determination, and HF Localization in a D4R', *J. Phys. Chem. B*, **102**, 8588–8598 (1998).
93. G. Jeschke, 'Spin Locking of $I = \frac{3}{2}$ Nuclei in Static and Spinning Samples – A Description by Abstract Spins and Floquet Formalism', *J. Chem. Phys.*, **108**, 907–917 (1998).
94. J.P. Amoureux, 'Variable-angle Double Rotation Technique: A New Two-dimensional High-resolution Technique for Quadrupole Nuclei', *Solid State NMR*, **4**, 229–239 (1995).
95. A. Llor, J. Virlet, 'Towards High-resolution NMR of More Nuclei in Solids: Sample Spinning with Time-dependent Spinner Axis Angle', *Chem. Phys. Lett.*, **152**, 248–253 (1988).
96. K.T. Mueller, E.W. Wooten, A. Pines, 'Pure-absorption-phase Dynamic-angle Spinning', *J. Magn. Reson.*, **92**, 620–627 (1991).
97. P.J. Grandinetti, J.H. Baltisberger, A. Llor, Y.K. Lee, U. Werner, M.A. Eastman, A. Pines, 'Pure-absorption-mode Lineshapes and Sensitivity in 2-Dimensional Dynamic-angle Spinning NMR', *J. Magn. Reson. A*, **103**, 72–81 (1993).
98. P.J. Grandinetti, Y.K. Lee, J.H. Baltisberger, B.Q. Sun, A. Pines, 'Sideband Patterns in Dynamic-angle-spinning NMR', *J. Magn. Reson. A*, **102**, 195–204 (1993).
99. C.A. Fyfe, K.C. Wongmoon, H. Grondey, K.T. Mueller, 'Increased Efficiency of Coherence Transfer in Cross-polarization NMR from Quadrupole

- Nuclei – Dynamic-angle Cross-polarization’, *J. Phys. Chem.*, **98**, 2139–2142 (1994).
100. T.P. Jarvie, R.M. Wenslow, K.T. Mueller, ‘High-resolution Solid-state Heteronuclear Correlation NMR for Quadrupolar and Spin- $\frac{1}{2}$ Nuclei’, *J. Am. Chem. Soc.*, **117**, 570–571 (1995).
 101. R.M. Wenslow, K.T. Mueller, ‘Cation Sites in Mixed-alkali Phosphate Glasses’, *J. Non-Cryst. Solids*, **231**, 78–88 (1998).
 102. A. Medek, J.R. Sachleben, P. Beverwyk, L. Frydman, ‘Multi-rank Nuclear Magnetic Resonance Studies of Half-integer Quadrupole Nuclei in Solids by Three-dimensional Dynamic-angle Correlation Spectroscopy’, *J. Chem. Phys.*, **104**, 5374–5382 (1996).
 103. C. Fernandez, J.P. Amoureux, ‘Triple-quantum MAS-NMR of Quadrupole Nuclei’, *Solid State NMR*, **5**, 315–321 (1996).
 104. S.P. Brown, S. Wimperis, ‘Two-dimensional Multiple-quantum MAS NMR of Quadrupole Nuclei: A Comparison of Methods’, *J. Magn. Reson.*, **128**, 42–61 (1997).
 105. J.P. Amoureux, C. Fernandez, S. Steuernagel, ‘Z Filtering in MQMAS NMR’, *J. Magn. Reson. A*, **123**, 116–118 (1996).
 106. J.P. Amoureux, C. Fernandez, L. Frydman, ‘Optimized Multiple-quantum Magic-angle Spinning NMR Experiments on Half-integer Quadrupoles’, *Chem. Phys. Lett.*, **259**, 347–355 (1996).
 107. J.P. Amoureux, C. Fernandez, Y. Dumazy, ‘A Useful Tool for the Elaboration of New Solid-state NMR Experiments: PULSAR’, *J. Chim. Phys.*, **92**, 1939–1942 (1995).
 108. J.P. Amoureux, C. Fernandez, ‘Triple, Quintuple and Higher Orders Multiple Quantum MAS NMR of Quadrupole Nuclei’, *Solid State NMR*, **10**, 211–224 (1998).
 109. G. Wu, D. Rovnyak, R.G. Griffin, ‘Quantitative Multiple-quantum Magic-angle-spinning NMR Spectroscopy of Quadrupole Nuclei in Solids’, *J. Am. Chem. Soc.*, **118**, 9326–9332 (1996).
 110. K.H. Lim, C.P. Grey, ‘Analysis of the Anisotropic Dimension in the RIACT (II) Multiple Quantum MAS NMR Experiment for $I = \frac{3}{2}$ Nuclei’, *Solid State NMR*, **13**, 101–112 (1998).
 111. T. Mildner, M.E. Smith, R. Dupree, ‘Rotationally Induced Triple Quantum Coherence Excitation in MAS NMR Spectroscopy of $I = \frac{5}{2}$ Spins’, *Chem. Phys. Lett.*, **301**, 389–394 (1999).
 112. S. Ding, C.A. McDowell, ‘Shaped Pulse Excitation in Multi-quantum Magic-angle Spinning Spectroscopy of Half-integer Quadrupole Spin Systems’, *Chem. Phys. Lett.*, **270**, 81–86 (1997).
 113. S.W. Ding, C.A. McDowell, ‘Multiple-quantum MAS NMR Spectroscopy of Spin- $\frac{3}{2}$ Quadrupole Spin Systems Using Shaped Pulses’, *J. Magn. Reson.*, **135**, 61–69 (1998).
 114. L. Marinelli, A. Medek, L. Frydman, ‘Composite Pulse Excitation Schemes for MQMAS NMR of Half-integer Quadrupole Spins’, *J. Magn. Reson.*, **132**, 88–95 (1998).
 115. A. Goldbourt, P.K. Madhu, L. Frydman, S. Vega, ‘Fast RF Amplitude Modulation in MQMAS NMR Spectroscopy’, in *Abstracts of the 41st Rocky Mountain Conference*, 97–98, 1999.
 116. J. Rocha, ‘Direct Observation of Highly Distorted Hexacoordinated Aluminum in Andalusite by Very Fast Al-27 MAS NMR’, *Chem. Commun.*, 2489 (1998).
 117. D. Massiot, B. Touzo, D. Trumeau, J.P. Coutures, J. Virlet, P. Florian, P.J. Grandinetti, ‘Two-dimensional Magic-angle Spinning Isotropic Reconstruction Sequences for Quadrupole Nuclei’, *Solid State NMR*, **6**, 73–83 (1996).
 118. R.R. Ernst, G. Bodenhausen, A. Wokaun, *Principles of Nuclear Magnetic Resonance in One and Two Dimensions*, Oxford University Press, London, 1987.
 119. C.A. Fyfe, J. Skibsted, H. Grondey, H. Meyer zu Alten-schildesche, ‘Pulsed Field Gradient Multiple-quantum MAS NMR Spectroscopy of Half-integer Spin Quadrupolar Nuclei’, *Chem. Phys. Lett.*, **281**, 44–48 (1997).
 120. S.P. Brown, S.J. Heyes, S. Wimperis, ‘Two-dimensional MAS Multiple-quantum NMR of Quadrupole Nuclei, Removal of Inhomogeneous Second-order Broadening’, *J. Magn. Reson. A*, **119**, 280–284 (1996).
 121. S.P. Brown, S.E. Ashbrook, S. Wimperis, ‘Al-27 Multiple-quantum Magic Angle Spinning NMR Study of the Thermal Transformation Between the Microporous Aluminum Methylphosphonates AlMePO-beta and AlMePO-alpha’, *J. Phys. Chem. B*, **103**, 812–817 (1999).
 122. L. Delevoye, ‘Quantification des Spectres MQMAS et Application a l’Etude des Matériaux Microporeux’, Thesis, Lille, 1988.
 123. P.P. Man, ‘Scaling and Labeling the High-resolution Isotropic Axis of Two-dimensional Multiple-quantum Magic-angle-spinning Spectra of Half-integer Quadrupole Spins’, *Phys. Rev. B*, **58**, 2764 (1998).
 124. G. Wu, R.E. Wasylishen, ‘The Influence of the Heteronuclear Dipolar Interaction on NMR Spectra of Quadrupole Nuclei’, *Mol. Phys.*, **95**, 1177–1183 (1998).
 125. U. Friedrich, I. Schnell, S.P. Brown, A. Lupulescu, D.E. Demco, H.W. Spiess, ‘Spinning-sideband Patterns in Multiple-quantum Magic-angle Spinning NMR Spectroscopy’, *Mol. Phys.*, **95**, 1209–1227 (1998).
 126. L. Marinelli, L. Frydman, ‘On the Origin of Spinning Side Bands in MQMAS NMR Experiments’, *Chem. Phys. Lett.*, **275**, 188–198 (1997).
 127. T. Charpentier, C. Fermon, J. Virlet, ‘Efficient Time Propagation Technique for MAS NMR Simulation – Application to Quadrupole Nuclei’, *J. Magn. Reson.*, **132**, 181–190 (1998).
 128. T. Charpentier, C. Fermon, J. Virlet, ‘Numerical and Theoretical Analysis of Multiquantum Magic-angle

- Spinning Experiments', *J. Chem. Phys.*, **109**, 3116–3130 (1998).
129. J.P. Amoureux, M. Pruski, D.P. Lang, C. Fernandez, 'The Effect of RF Power and Spinning Speed on MQMAS NMR', *J. Magn. Reson.*, **131**, 170–175 (1998).
130. D. Massiot, 'Sensitivity and Lineshape Improvements of MQMAS by Rotor-synchronized Data Acquisition', *J. Magn. Reson. A*, **122**, 240–244 (1996).
131. T. Vosegaard, F.H. Larsen, H.J. Jakobsen, P.D. Ellis, N.C. Nielsen, 'Sensitivity-enhanced Multiple-quantum MAS NMR of Half-integer Quadrupole Nuclei', *J. Am. Chem. Soc.*, **119**, 9055–9056 (1997).
132. G. Wu, D. Rovnyank, B. Sun, R.G. Griffin, 'High-resolution Multiple Quantum MAS NMR Spectroscopy of Half-integer Quadrupole Nuclei', *Chem. Phys. Lett.*, **249**, 210–217 (1996).
133. M. Hanaya, R.K. Harris, 'Effect of ^1H -decoupling in Two-dimensional Multiple-quantum MAS NMR Spectroscopy of Na-23 in a Hydrated Layered Silicate', *Solid State NMR*, **8**, 147–151 (1997).
134. V. Lacassagne, P. Florian, V. Montoullout, C. Gervais, F. Babonneau, D. Massiot, 'Resolution Enhancement in Solid-state MQMAS Experiments Achieved by Composite Decoupling', *Magn. Reson. Chem.*, **36**, 956–959 (1998).
135. S.H. Wang, Z. Xu, J.H. Baltisberger, L.M. Bull, J.F. Stebbins, A. Pines, 'Multiple-quantum Magic-angle Spinning and Dynamic-angle Spinning NMR Spectroscopy of Quadrupolar Nuclei', *Solid State NMR*, **8**, 1–16 (1997).
136. M. Pruski, D.P. Lang, C. Fernandez, J.P. Amoureux, 'Multiple-quantum Magic-angle Spinning NMR with Cross-polarization: Spectral Editing of High-resolution Spectra of Quadrupole Nuclei', *Solid State NMR*, **7**, 327–331 (1997).
137. C. Fernandez, L. Delevoye, J.P. Amoureux, $^{27}\text{Al}\{^1\text{H}\}$ Cross Polarization Triple Quantum Magic Angle Spinning NMR', *J. Am. Chem. Soc.*, **119**, 6858–6862 (1997).
138. S.H. Wang, S.M. De Paul, L.M. Bull, 'High-resolution Heteronuclear Correlation Between Quadrupole and Spin- $\frac{1}{2}$ Nuclei Using Multiple-quantum Magic-angle Spinning', *J. Magn. Reson.*, **125**, 364–368 (1997).
139. C. Magnenet, D. Massiot, I. Klur, J.P. Coutures, 'Characterization of TiO_2 pigments by Al-27 NMR', *J. Chim. Phys.*, **95**, 310–316 (1998).
140. C. Fernandez, D.P. Lang, J.P. Amoureux, M. Pruski, 'Measurement of Heteronuclear Dipolar Interactions Between Quadrupole and Spin- $\frac{1}{2}$ Nuclei in Solids by Multiple-quantum REDOR NMR', *J. Am. Chem. Soc.*, **120**, 2672–2673 (1998).
141. M. Pruski, C. Fernandez, D.P. Lang, J.P. Amoureux, 'Measurement of Interatomic Connectivities in Molecular Sieves Using MQMAS-based Methods', *Catal. Today*, **10**, 401–409 (1999).
142. S. Steuernagel, 'A New Sequence for the MQMAS/HETCOR Experiment', *Solid State NMR*, **11**, 197–201 (1998).
143. A. Samoson, 'Two-dimensional Isotropic NMR of Quadrupole Nuclei in Solids', *J. Magn. Reson.*, **121**, 209–211 (1996).
144. T. Anupold, A. Reinhold, P. Sarv, A. Samoson, 'A Comparison of Double Rotation and Multi-quantum Magic Angle Spinning Spectra', *Solid State NMR*, **13**, 87–91 (1998).
145. S.R. Jansen, H.T. Hintzen, R. Metselaar, J.W. de Haan, L.J.M. van de Ven, A.P.M. Kentgens, G.H. Nachttegaal, 'Multiple Quantum Al-27 Magic-angle-spinning Nuclear Magnetic Resonance Spectroscopic Study of $\text{SrAl}_{12}\text{O}_{19}$: Identification of an Al-27 Resonance from a Well-defined AlO_5 Site', *J. Phys. Chem.*, **102**, 5969–5976 (1998).
146. M. Hunger, P. Sarv, A. Samoson, 'Two-dimensional Triple-quantum Na-23 MAS NMR Spectroscopy of Sodium Cations in Dehydrated Zeolites', *Solid State NMR*, **9**, 115–120 (1997).
147. C. Jäger, P. Hartmann, G. Kunath-Fandrei, O. Hirsch, P. Rehak, J. Vogel, M. Feike, H.W. Spiess, K. Herzog, B. Thomas, 'Novel Opportunities of Structural Investigations of Glasses by 2D NMR', *Ber. Bunsenges. Phys. Chem.*, **100**, 1560–1562 (1996).
148. L. Zuchner, J.C.C. Chan, W. Müller-Warmuth, H. Eckert, 'Short-range Order and Site Connectivities in Sodium Aluminoborate Glasses: I. Quantification of Local Environments by High-resolution B-11, Na-23, and Al-27 Solid-state NMR', *J. Phys. Chem. B*, **102**, 4495 (1998).
149. H.C. Torrey, 'Transient Nutations in NMR', *Phys. Rev.*, **76**, 1059–1068 (1949).
150. A. Samoson, E. Lippmaa, 'Excitation Phenomena and Line Intensities in High-resolution NMR Spectra of Half-integer Quadrupole Nuclei', *Phys. Rev. B*, **28**, 6567 (1983).
151. A. Samoson, E. Lippmaa, 'Central Transition NMR Excitation Spectra of Half-integer Quadrupole Nuclei', *Chem. Phys. Lett.*, **100**, 205–208 (1983).
152. D. Fenzke, D. Freude, T. Fröhlich, J. Haase, 'NMR Intensity Measurements of Half-integer Quadrupole Nuclei', *Chem. Phys. Lett.*, **111**, 171–175 (1984).
153. A. Wokaun, R.R. Ernst, 'Selective Excitation and Detection in Multilevel Spin Systems: Application of Single Transition Operators', *J. Chem. Phys.*, **67**, 1752 (1977).
154. L. Pandey, S. Towta, D.G. Hughes, 'NMR Pulse Response and Measurement of the Quadrupole of $I = \frac{3}{2}$ Nuclei', *J. Chem. Phys.*, **85**, 6923–6927 (1986).
155. P.P. Man, 'Investigation of the Central Line of Mn-55 in KMnO_4 by a Two-dimensional NMR Method', *J. Magn. Reson.*, **67**, 78–90 (1986).
156. R. Janssen, W.S. Veeman, 'Quadrupole Nutation NMR in Solids', *J. Chem. Soc., Faraday Trans.*, **184**, 3747–3759 (1988).

157. J.A.M.v.d. Mijden, R. Janssen, W.S. Veeman, 'Analytical Description of the $I = \frac{5}{2}$ Quadrupole Nutation Experiment', *Mol. Phys.*, **69**, 53–64 (1990).
158. P.P. Man, 'Analytical Expression for the Spin- $\frac{5}{2}$ Line Intensities', *Mol. Phys.*, **78**, 307–318 (1993).
159. P.P. Man, P. Tougne, 'Exact Expression for the Spin- $\frac{7}{2}$ Line Intensities: Application to Solid State Co-59(III) NMR', *Mol. Phys.*, **83**, 997–1009 (1994).
160. S.Z. Ageev, B.C. Sanctuary, 'Analytical Solutions for Spin- $\frac{7}{2}$ Line Intensities in Solid State NMR', *Mol. Phys.*, **84**, 835–844 (1995).
161. A.P.M. Kentgens, J.J.M. Lemmens, F.M.M. Geurts, W.S. Veeman, 'Two-dimensional Solid-state Nutation NMR of Half-integer Quadrupole Nuclei', *J. Magn. Reson.*, **71**, 62–74 (1987).
162. A.P.M. Kentgens, 'Off-resonance Nutation NMR Spectroscopy of Half-integer Quadrupole Nuclei', *Prog. Nucl. Magn. Reson. Spectrosc.*, **32**, 141–164 (1998).
163. S.W. Ding, C.A. McDowell, 'Nutation Magic-angle Spinning Spectra of Half-integer Quadrupole Spin Systems', *J. Magn. Reson. A*, **112**, 36–42 (1995).
164. A.P.M. Kentgens, 'Off-resonance Nutation NMR Spectroscopy of Half-integer Quadrupole Nuclei', *J. Magn. Reson. A*, **114**, 302–309 (1993).
165. E.L. Hahn, 'Spin Echoes', *Phys. Rev.*, **80**, 580–594 (1950).
166. J. Haase, E. Oldfield, 'Spin-echo Behavior of Non-integral Spin Quadrupole Nuclei in Inorganic Solids', *J. Magn. Reson. A*, **101**, 30–40 (1993).
167. I. Furo, B. Halle, 'Multiple Quantum NMR Spectroscopy on $I > 1$ Nuclei in Anisotropic Systems', *Mol. Phys.*, **76**, 1169–1197 (1992).
168. I. Furo, B. Halle, '2-D Quadrupole-echo Spectroscopy with Coherence Selection and Optimized Pulse Angle', *J. Magn. Reson.*, **98**, 388–407 (1992).
169. U. Eliav, G. Navon, 'A Study of Dipolar Interactions and Dynamic Processes of Water Molecules in Tendon by H-1 and H-2 Homonuclear and Heteronuclear Multiple-quantum-filtered NMR Spectroscopy', *J. Magn. Reson.*, **137**, 295–310 (1999).
170. U. Eliav, G. Navon, 'Corrections and Additions To "Quadrupole-echo Techniques in Multiple-quantum-filtered NMR Spectroscopy of Heterogeneous Systems"', *JMR 1995*, *J. Magn. Reson.*, **128**, 98 (1997).
171. U. Eliav, G. Navon, 'Quadrupole-echo Techniques in Multiple-quantum-filtered NMR Spectroscopy of Heterogeneous Systems', *J. Magn. Reson. A*, **115**, 241–253 (1995).
172. U. Eliav, T. Kushnir, T. Knubovets, Y. Itzchak, G. Navon, 'The Effect of Magnetic Field Inhomogeneity on the Transverse Relaxation of Quadrupole Nuclei Measured by Multiple Quantum Filtered NMR', *J. Magn. Reson.*, **128**, 82–86 (1997).
173. K.D. Schmitt, J. Haase, E. Oldfield, 'Spectral Editing: A Quantitative Application of Spin-echo-nuclear Magnetic Resonance Spectroscopy to the Study of Zeolite Catalysts', *Zeolites*, **14**, 89 (1994).
174. Y. Dumazy, J.P. Amoureux, C. Fernandez, 'Theoretical and Experimental Study of Quadrupole Echoes in Solid State NMR', *Mol. Phys.*, **90**, 959–970 (1997).
175. P. Man, 'Second-order Quadrupole Effects on Hahn Echoes in Fast-rotating Solids at the Magic Angle [Review]', *Phys. Rev. B*, **55**, 8406–8424 (1997).
176. P. Man, 'Numerical Analysis of Solomon Echo Amplitudes in Static Solids', *J. Chem. Phys.*, **105**, 3908–3919 (1997).
177. S.Z. Ageev, P.P. Man, J. Fraissard, B.C. Sanctuary, 'Determination of Quadrupole Spin Coupling for Spin- $\frac{7}{2}$ Using Two Pulse Sequences', *Mol. Phys.*, **91**, 75–80 (1997).
178. H.Y. Carr, E.M. Purcell, 'Effects of Diffusion on Free Precession in Nuclear Magnetic Resonance Experiments', *Phys. Rev.*, **80**, 630–638 (1954).
179. S. Meiboom, D. Gill, 'Modified Spin-echo Method for Measuring Nuclear Relaxation Times', *Rev. Sci. Instrum.*, **29**, 688–691 (1958).
180. F.H. Larsen, H.J. Jakobsen, P.D. Ellis, N.C. Nielsen, 'Sensitivity-enhanced Quadrupole-echo NMR of Half-integer Quadrupole Nuclei. Magnitudes and Relative Orientation of Chemical Shielding and Quadrupole Coupling Tensors', *J. Phys. Chem.*, **101**, 8597–8606 (1997).
181. F.H. Larsen, H.J. Jakobsen, P.D. Ellis, N.C. Nielsen, 'High-field QCPMG-MAS NMR of Half-integer Quadrupolar Nuclei with Large Quadrupole Couplings', *Mol. Phys.*, **95**, 1185–1195 (1998).
182. G.E. Pake, 'Nuclear Resonance Adsorption in Hydrated Crystals: Fine Structure of the Proton Line', *J. Chem. Phys.*, **16**, 327–336 (1948).
183. G. Hoatson, 'Broadband Composite Excitation Sequences for Creating Quadrupole Order in H-2 NMR', *J. Magn. Reson.*, **94**, 152–159 (1991).
184. G.L. Hoatson, B. Blümich, 'Deuteron Hadamard NMR of Solids and Liquid Crystals', *J. Magn. Reson.*, **95**, 446–451 (1991).
185. B. Blümich, 'Wideline ^2H -NMR Spectroscopy and Imaging of Solids', *Z. Naturforsch., Teil A*, **49**, 19–26 (1994).
186. D.-K. Yang, J.E. Atkins, C.C. Lester, D.B. Zax, 'New Developments in NMR Using Noise Spectroscopy', *Mol. Phys.*, **95**, 747–757 (1998).
187. D.-K. Yang, D.B. Zax, 'Bandwidth Extension in Noise Spectroscopy', *J. Magn. Reson.*, **135**, 267–270 (1998).
188. S. Habot, D.L. Lu, N.J. Tagg, G.R. Gall, D.J. Siminovich, 'Time Symmetry – An Application to Shaped Pulse Excitation of Spin-1 Systems', *Solid State NMR*, **10**, 137–150 (1998).
189. M.A. McCoy, W.S. Warren, 'Pulse Shaping in Quadrupole-echo NMR', *J. Magn. Reson.*, **98**, 24–35 (1992).
190. A.E. Aliev, K.D.M. Harris, D.C. Apperley, 'Natural Abundance High-resolution Solid State H-2 NMR Spectroscopy', *Chem. Phys. Lett.*, **226**, 193–198 (1994).

191. R. Poupko, Z. Olender, D. Reichert, Z. Luz, 'Deuterium MAS NMR in Natural Abundance', *J. Magn. Reson. A*, **106**, 113–115 (1994).
192. S. Vega, T.W. Shattuck, A. Pines, 'Double-quantum Cross-polarization NMR in Solids', *Phys. Rev. A*, **22**, 638–661 (1980).
193. Y. Ba, C.I. Ratcliffe, J.A. Ripmeester, 'Quadrupole Echo Double Resonance (QEDOR) and Solid Echo Double Resonance (SOLEDOR) NMR', *Chem. Phys. Lett.*, **299**, 201–206 (1999).
194. D. Marks, N. Zumbulyadis, S. Vega, 'Deuterium Cross-polarization Magic-angle Spinning', *J. Magn. Reson. A*, **122**, 16–36 (1996).
195. Z. Gan, P. Robyr, 'Deuterium Polarization Transfer in Rotating Solids and Its Application in Structural Investigation', *Mol. Phys.*, **95**, 1143–1152 (1998).
196. J.H. Kristensen, H. Bildsoe, H.J. Jakobsen, N.C. Nielsen, 'Deuterium Quadrupole Couplings from Least-squares Computer Simulations of ^2H MAS NMR Spectra', *J. Magn. Reson.*, **92**, 443–453 (1991).
197. B. Blümich, P. Blümli, J. Jansen, 'Presentation of Sideband Envelopes by Two-dimensional One Pulse (TOP) Spectroscopy', *Solid State NMR*, **1**, 111–113 (1992).
198. H. Ernst, D. Freude, I. Wolf, 'Multinuclear Solid-state NMR Studies of Brønsted Sites in Zeolites', *Chem. Phys. Lett.*, **212**, 588–596 (1993).
199. T.P. Spaniol, A. Kubo, T. Terao, 'Two-dimensional Deuterium MAS NMR of Paramagnetic Compounds – Separation of Paramagnetic and Quadrupole Interactions', *J. Chem. Phys.*, **106**, 5393–5405 (1997).
200. S. Vega, A. Pines, 'Operator Formalism for Double Quantum NMR', *J. Chem. Phys.*, **66**, 5624–5644 (1977).
201. R. Eckman, L. Mueller, A. Pines, 'Deuterium Double-quantum NMR with MAS', *Chem. Phys. Lett.*, **74**, 376–378 (1980).
202. Y. Yang, M. Schuster, B. Blümich, H.W. Spiess, 'Dynamic Magic-angle Spinning NMR Spectroscopy: Exchange Induced Sidebands', *Chem. Phys. Lett.*, **139**, 239–243 (1987).
203. N. Chandrakumar, G.v. Fircks, H. Günther, 'The 2-D Quadshift Experiment. Separation of Deuterium Chemical Shifts and Quadrupole Couplings by Two-dimensional Solid-state MAS NMR Spectroscopy', *Magn. Reson. Chem.*, **32**, 433–435 (1994).
204. A. Detken, H. Zimmermann, U. Haerberlen, Z. Luz, 'Dynamic Hydrogen Disorder in Solid Tropolone. A Single-crystal NMR Study of Hydroxyl Deuterons', *J. Magn. Reson.*, **126**, 95–102 (1997).
205. P. Speier, H. Zimmermann, U. Haerberlen, Z. Luz, 'Dynamic Disorder in 2,3-Dimethylnaphthalene: A Single Crystal Deuteron Nuclear Magnetic Resonance Study', *Mol. Phys.*, **95**, 1153–1167 (1998).
206. P. Freude, D. Michel, J. Totz, K.A., 'Ordering Behavior at the Antiferrodistortive Phase Transition in Betaine Phosphate and Betaine Phosphite', *Ferroelectrics*, **208**, 93–103 (1998).
207. A. Kubo, A. Yogo, F. Imashiro, T. Terao, 'Deuterium NMR Study of the Glassy Crystal Pentachlorotoluene – Hadamard Quadrupole-order Exchange NMR', *J. Phys. Chem.*, **100**, 15933–15941 (1996).
208. N. Bloembergen, E.M. Purcell, R.V. Pound, 'Relaxation Effects in NMR Absorption', *Phys. Rev.*, **102**, 679–712 (1948).
209. A. Schleicher, K. Müller, G. Kothe, '2-D NMR Relaxation Spectroscopy of Solids', *J. Chem. Phys.*, **92**, 6432 (1990).
210. K. Müller, R. Poupko, Z. Luz, '2-D Presentation of the Quadrupole-echo Modulation in Chemically Exchanging Systems of Spin $I = 1$ ', *J. Magn. Reson.*, **93**, 291–298 (1991).
211. R.R. Vold, R.L. Vold, 'Deuterium Relaxation in Molecular Solids', *Adv. Magn. Opt. Reson.*, **16**, 85–171 (1991).
212. F.H. Larsen, H.J. Jakobsen, P.D. Ellis, N.C. Nielsen, 'Molecular Dynamics from H-2 Quadrupole Carr–Purcell–Meiboom–Gill Solid-state NMR Spectroscopy', *Chem. Phys. Lett.*, **292**, 467–473 (1998).
213. O. Weintraub, S. Vega, 'Dynamic H-2 NMR of Rotating Solids', *Solid State NMR*, **4**, 341–351 (1995).
214. J.H. Kristensen, G.L. Hoatson, R.L. Vold, 'Investigation of Multiaxial Molecular Dynamics by H-2 MAS NMR Spectroscopy', *Solid State NMR*, **13**, 1–37 (1998).
215. J.H. Kristensen, G.L. Hoatson, R.L. Vold, 'Effect of Restricted Rotational Diffusion on H-2 MAS NMR Spectra', *J. Chem. Phys.*, **110**, 4533–4553 (1999).
216. Y.J. Lee, F. Wang, C.P. Grey, 'Li-6 and Li-7 MAS NMR Studies of Lithium Manganate Cathode Materials', *J. Am. Chem. Soc.*, **120**, 12601–12613 (1998).
217. N.C. Nielsen, H. Bildsoe, H.J. Jakobsen, P. Norby, 'Li-7, Na-23, and Al-27 Quadrupole Interactions in Some Aluminosilicate Sodalites from MAS NMR Spectra of Satellite Transitions', *Zeolites*, **11**, 622–633 (1991).
218. J. Skibsted, P. Norby, H. Bildsoe, H.J. Jakobsen, 'Line Shapes and Widths of MAS Sidebands for Al-27 Satellite Transitions – Multinuclear MAS NMR of Tugtupite $\text{Na}_8\text{Al}_2\text{Be}_2\text{Si}_8\text{O}_{24}\text{Cl}_2$ ', *Solid State NMR*, **5**, 239–255 (1995).
219. P.J. Bray, S.J. Gravina, P.E. Stallworth, S.P. Szu, J. Zhong, 'NMR Studies of the Structure of Glasses', *Exp. Tech. Phys.*, **36**, 397–413 (1988).
220. W. Müller-Warmuth, 'The Structure of Glasses Studied by MAS-NMR Spectroscopy of Quadrupole Nuclei', *Z. Naturforsch., Teil A*, **51**, 585–590 (1996).
221. S.J. Hwang, C. Fernandez, J.P. Amoureux, J. Cho, S.W. Martin, M. Pruski, 'Quantitative Study of the Short Range Order in B_2O_3 and B_2S_3 by MAS and Two-dimensional Triple-quantum MAS ^{11}B NMR', *Solid State NMR*, **8**, 109–121 (1997).
222. T.J. Bastow, D. Massiot, J.P. Coutures, 'N-14 NMR in AlN and BN', *Solid State Nucl. Magn. Reson.*, **10**, 241–245 (1998).

223. K.J.D. Mackenzie, R.H. Meinhold, 'MAS NMR Study of Pentacoordinated Magnesium in Grandierite', *Am. Mineral.*, **82**, 479–482 (1997).
224. T.J. Bastow, S.N. Stuart, 'NMR Study of the Zinc Chalcogenides (ZnX, X = 0, S, Se, Te)', *Phys. Status Solidi B*, **145**, 719–728 (1988).
225. W.A. Daunch, P.L. Rinaldi, 'Natural-abundance Solid-state S-33 NMR with High-speed Magic-angle Spinning', *J. Magn. Reson. A*, **123**, 219–221 (1996).
226. M.A. Fedotov, O.L. Malkina, V.G. Malkin, 'Cl-35/37 NMR Chemical Shifts and Nuclear Quadrupole Couplings for Some Small Chlorine Compounds – Experimental and Theoretical Study of Chemical Shifts and Nuclear Quadrupole Couplings for Some Small Chlorine Compounds', *Chem. Phys. Lett.*, **258**, 330–335 (1996).
227. T.J. Bastow, S.L. Segel, K.R. Jeffrey, 'Antiferroelectric Transition in KOH(D) – A H-2 and K-39 NMR Study', *Solid State Commun.*, **78**, 565–568 (1991).
228. R. Blinc, J. Dolinsek, T. Apih, W. Schranz, A. Fuith, H. Warhanek, '2D K-39 NMR Study of the Phase Transition in KSCN', *Solid State Commun.*, **93**, 609–611 (1995).
229. P.V. Bellot, A. Trokiner, Y. Zhdanov, A. Yakubovskii, 'Ca-43 NMR in Solid State', *J. Chim. Phys.*, **95**, 280–288 (1998).
230. R. Dupree, A.P. Howes, S.C. Kohn, 'Natural Abundance Solid State Ca-43 NMR', *Chem. Phys. Lett.*, **276**, 399–404 (1997).
231. R.G. Bryant, S. Ganapathy, S.D. Kennedy, 'High-resolution Ca-43 NMR in Solids', *J. Magn. Reson.*, **72**, 376–378 (1987).
232. A.R. Thompson, E. Oldfield, 'Solid-state Scandium-45, Yttrium-89, and Lanthanum-139 NMR Spectroscopy', *J. Chem. Soc., Chem. Commun.*, 27–29 (1987).
233. A. Labouriau, W.L. Earl, 'Titanium Solid-state NMR in Anatase, Brookite and Rutile', *Chem. Phys. Lett.*, **270**, 278–284 (1997).
234. S.F. Dec, M.F. Davis, G.E. Maciel, C.E. Bronnimann, J.J. Fitzgerald, S.S. Han, 'Solid-state Multinuclear NMR Studies of Ferroelectric, Piezoelectric, and Related Materials', *Inorg. Chem.*, **32**, 955–959 (1993).
235. J. Skibsted, N.C. Nielsen, H. Bildsoe, H.J. Jakobsen, 'Magnitudes and Relative Orientation of V-51 Quadrupole Coupling and Anisotropic Shielding Tensors in Metavanadates and KV₃O₈ from V-51 MAS NMR Spectra – Na-23', *J. Am. Chem. Soc.*, **115**, 7351–7362 (1993).
236. S. Hayashi, 'V-51 and CO-59 Off-MAS NMR Spectra – Determination of Quadrupole Coupling, Chemical Shift Anisotropy and Their Relative Orientation', *Magn. Reson. Chem.*, **34**, 791–798 (1996).
237. G.N. Abelyashev, V.N. Berzhanskii, S.N. Polulyah, N.A. Sergeev, 'Peculiarities of the Formation of a Two Pulse Echo in Spin- $\frac{3}{2}$ Systems', *Fiz. Tverd. Tela*, **34**, 676–678 (1992) (in Russian).
238. F.H. Larsen, H.J. Jakobsen, P.D. Ellis, N.C. Nielsen, 'QCPMG-MAS NMR of Half-integer Quadrupole Nuclei', *J. Magn. Reson.*, **131**, 144–147 (1998).
239. T. Charpentier, J. Virlet, 'Triple Quantum MQMAS Spectroscopy of Co-59 ($I = \frac{7}{2}$) in Na₃Co(NO₂)₆ and trans-Co[(en₂)(NO₂)₂]NO₃ Interplay Between the Quadrupole Coupling and Anisotropic Shielding Tensors', *Solid State NMR*, **12**, 227–242 (1998).
240. S.L. Hu, J.A. Reimer, A.T. Bell, 'Cu-65 NMR Spectroscopy of Cu-exchanged ZSM-5 Catalysts', *J. Phys. Chem. B*, **101**, 1869–1871 (1997).
241. G. Wu, 'Zinc-67 NMR Spectroscopy of Solids', *Chem. Phys. Lett.*, **298**, 375–380 (1998).
242. T.J. Bastow, 'Zn-67 NMR in Zinc Metal', *J. Phys. Condens. Matter*, **8**, 11309–11315 (1996).
243. D. Massiot, V. Montouillout, F. Fayon, F.P.C. Bessada, 'QPASS – Towards Higher Resolution in NMR of Half Integer Quadrupole Nuclei with High Quadrupole Couplings', *J. Chim. Phys.*, **95**, 270–279 (1998).
244. T. Vosegaard, D. Massiot, N. Gautier, H.J. Jakobsen, 'Ga-71 Chemical Shielding and Quadrupole Coupling Tensors of the Garnet Y₃Ga₅O₁₂ from Single-crystal Ga-71 NMR', *Inorg. Chem.*, **36**, 2446–2450 (1997).
245. R. Klik, V. Bosacek, L. Kubelkova, D. Freude, D. Michel, 'Coordination State of Gallium in MFI Structures Prepared by Direct Synthesis and by Postsynthetic Modification of Boralites', *Zeolites*, **19**, 343–348 (1997).
246. R. Jelinek, A. Stein, G.A. Ozin, 'Br-81 and Cl-35 NMR Investigation of Sodium, Silver, Halo Sodalite Semiconductor Supralattices', *J. Am. Chem. Soc.*, **115**, 2390–2396 (1993).
247. T. Vosegaard, J. Skibsted, H. Bildsoe, H.J. Jakobsen, 'Combined Effect of Second-order Quadrupole Coupling and Chemical Shielding Anisotropy on the Central Transition in MAS NMR of Quadrupole Nuclei. Rb-87 MAS NMR', *J. Phys. Chem.*, **99**, 10731–10735 (1995).
248. T. Vosegaard, I.P. Byriel, H.J. Jakobsen, T. Vosegaard, I.P. Byriel, H.J. Jakobsen, 'Characterization of the Two Rubidium Sites in Rb₂CrO₄ by Rb-87 Single-crystal NMR', *J. Phys. Chem. B*, **101**, 8955–8958 (1997).
249. T.J. Bastow, 'Materials Characterisation by Nuclear Quadrupole Interaction', *Z. Naturforsch., Teil A*, **49**, 320–328 (1994).
250. V.M. Mastikhin, O.B. Lapina, R.I. Maximovskaya, 'Mo-95 Solid-state NMR Spectra of Molybdates', *Chem. Phys. Lett.*, **148**, 413–416 (1988).
251. O.H. Han, H.K.C. Timken, E. Oldfield, 'Solid-state MAS NMR Spectroscopic Study of Group III–V Semiconductors', *J. Chem. Phys.*, **89**, 6046–6052 (1988).
252. T. Ueda, N. Nakamura, 'Sb-121 NMR and SCF-MS-X-alpha Studies of Quadrupole Interaction and the Electronic Structure of Mixed-valence Compound, Cs₂SbC₁₆', *Z. Naturforsch., Teil A*, **51**, 672–676 (1996).
253. N. Lee, B.C. Sanctuary, T.K. Halstead, 'I-127 NMR Study of Quadrupole Echoes in KI', *J. Magn. Reson.*, **98**, 534–555 (1992).

254. G. Hinze, R. Bohmer, B. Zalar, R. Blinc, 'The Orientational Glass $(\text{KI})_{(0.56)}(\text{NH}_4\text{I})_{(0.44)}$ studied by I-127 NMR', *J. Phys. Condens. Matter*, **9**, 117–125 (1997).
255. S. Kroeker, K. Eichele, R. Wasylshen, J. Britten, 'Cesium-133 NMR Study of $\text{CsCD}(\text{SCN})(3)$ – Relative Orientation of the Chemical Shift and Electric Field Gradient Tensors', *J. Phys. Chem. B*, **101**, 3727–3733 (1997).
256. J. Skibsted, T. Vosegaard, H. Bildsoe, H.J. Jakobsen, 'Cs-133 Chemical Shielding Anisotropies and Quadrupole Couplings from MAS NMR of Cesium Salts', *J. Phys. Chem.*, **100**, 14872–14881 (1996).
257. K. Kumagai, Y.V. Piskunov, A.Y. Yakubovskii, S.V. Verkhovskii, A.P. Gerashenko, Y.I. Zhdanov, K.N. Mikhalev, I.V. Sagaradze, E.Y. Medvedev, S.M. Cheshnitskii, R.N. Pletnev, 'Local Distortions in the BiO_6 -octahedra Sublattice $\text{BaPb}_x\text{Bi}_{1-x}\text{O}_3$ as seen by Ba-137 NMR/NQR', *Physica C*, **247**, 209–220 (1997).
258. T.J. Bastow, 'An NMR Study of Ba-137 and Ti-47, 49 in Ferroelectric BaTiO_3 ', *J. Phys. Condens. Matter*, **1**, 4985–4991 (1989).
259. T.J. Bastow, 'La-139 Nuclear Magnetic Resonance Characterisation of La_2O_3 and $\text{La}_{1-x}\text{Sr}_x\text{MO}_3$ Where M = Cr, Mn or Co', *Solid State NMR*, **3**, 17–22 (1994).
260. P.J. Chu, B.C. Gerstein, H.D. Tang, R.N. Shelton, 'Studies of the Electronic Phase Transition in $\text{Lu}_5\text{Ir}_4\text{Si}_{10}$ and $\text{Lu}_5\text{Rh}_4\text{Si}_{10}$ by Lu-175 NMR', *Phys. Rev. B*, **37**, 1796–1806 (1988).
261. D. Müller, W. Gessner, A. Samoson, E. Lippmaa, G. Scheler, 'Solid-state Al-27 NMR Studies on Polycrystalline Aluminates of the Systems $\text{CaO}\cdot\text{Al}_2\text{O}_3$ ', *Polyhedron*, **5**, 779 (1986).
262. W.S. Veeman, 'Quadrupole Nutation NMR in Solids', *Z. Naturforsch., Teil A*, **47**, 353–360 (1992).
263. D. Müller, W. Gessner, A. Samoson, E. Lippmaa, G. Scheler, 'Solid-state Aluminum-27 Nuclear Magnetic Resonance Chemical Shift and Quadrupole Coupling Data for Condensed AlO_4 Tetrahedra', *J. Chem. Soc., Dalton Trans*, 1277–1281 (1986).
264. J. Skibsted, H. Bildsoe, H.J. Jakobsen, 'High-speed Spinning Versus High Magnetic Field in MAS NMR of Quadrupole Nuclei. Al-27 MAS NMR of $3\text{Ca Al}_2\text{O}_3$ ', *J. Magn. Reson.*, **92**, 669–676 (1991).
265. D. Müller, W. Gessner, G. Scheler, 'Chemical Shift and Quadrupole Coupling of the Al-27 NMR Spectra of LiAlO_2 Polymorphs', *Polyhedron*, **2**, 1195–1200 (1984).
266. J. Skibsted, N.C. Nielsen, H. Bildsøe, H.J. Jacobsen, 'Satellite Transitions in MAS NMR Spectra of Quadrupolar Nuclei', *J. Magn. Reson.*, **95**, 88–117 (1991).
267. T. Vosegaard, H.J. Jakobsen, 'Al-27 Chemical Shielding Anisotropy', *J. Magn. Reson.*, **128**, 135–137 (1997).
268. H. Kraus, R. Prins, A.P.M. Kentgens, 'A Al-27 MQMAS and Off-resonance Nutation NMR Investigation of Mo-P/gamma- Al_2O_3 Hydrotreating Catalyst Precursors', *J. Phys. Chem.*, **100**, 16336–16345 (1996).
269. H. Kraus, M. Muller, R. Prins, A.P.M. Kentgens, 'Comments on the Al-27 NMR Visibility of Aluminas', *J. Phys. Chem. B*, **102**, 3862–3865 (1998).
270. D. Coster, A.L. Blumenfeld, J.J. Fripiat, 'Lewis Acid Sites and Surface Aluminum in Aluminas and Zeolites: A High-resolution NMR Study', *J. Phys. Chem.*, **98**, 6201–6211 (1994).
271. B. Ollivier, R. Retoux, P. Lacorre, D. Massiot, G. Ferey, 'Crystal Structure of kappa-Alumina – An X-ray Powder Diffraction, TEM and NMR Study', *J. Mater. Chem.*, **7**, 1049–1056 (1997).
272. G. Kunathfandrei, T.J. Bastow, J.S. Hall, C. Jäger, M.E. Smith, 'Quantification of Aluminum Coordinations in Amorphous Aluminas by Combined Central and Satellite Transition Magic Angle Spinning NMR Spectroscopy', *J. Phys. Chem.*, **99**, 15138–15141 (1995).
273. M.T. Weller, M.E. Brenchley, D.C. Apperley, N.A. Davies, 'Correlations Between Al-27 MAS NMR Spectra and the Coordination Geometry of Framework Aluminates', *Solid State NMR*, **3**, 103–106 (1994).
274. D. Müller, E. Jahn, G. Ladwig, U. Haubenreisser, 'High-resolution Solid-state 27-Al and 31P NMR: Correlation Between Chemical Shift and Mean Al–O–P angle in AlPO_4 Polymorphs', *Chem. Phys. Lett.*, **109**, 332–336 (1984).
275. W.F. Bleam, S.F. Dec, J.S. Frye, 'Al-27 Solid-state NMR Study of Five-coordinate Aluminum in Augelite and Senegalite', *Phys. Chem. Miner.*, **16**, 817–820 (1989).
276. D. Müller, I. Grunze, E. Hallas, G. Ladwig, 'Hochfeld-Al-27-NMR-Untersuchungen zur Aluminiumkoordination in kristallinen Aluminiumphosphaten', *Z. Anorg. Allg. Chem.*, **500**, 80–88 (1983).
277. C. Fernandez, J.P. Amoureux, J.M. Chezeau, L. Delmotte, H. Kessler, 'Al-27 MAS NMR Characterization of AlPO_4 -14. Enhanced Resolution and Information by MQMAS', *Microporous Mater.*, **6**, 331–340 (1996).
278. E. Lippmaa, A. Samoson, M. Mägi, 'High-resolution Al-27 NMR of Aluminosilicates', *J. Am. Chem. Soc.*, **108**, 1730–1735 (1986).
279. L.B. Alemany, D. Massiot, B.L. Sheriff, M.E. Smith, F. Taulelle, 'Observation and Accurate Quantification of Al-27 MAS NMR Spectra of Some Al_2SiO_5 Polymorphs Containing Sites with Large Quadrupole Interactions', *Chem. Phys. Lett.*, **177**, 301–306 (1991).
280. L.B. Alemany, S. Steuernagel, J.P. Amoureux, R.L. Callender, A.R. Barron, 'Very Fast MAS and MQMAS NMR Studies of the Spectroscopically Challenging Minerals Kyanite and Andalusite on 400, 500, 800 MHz Spectrometers', *Solid State NMR*, **14**, 1–18 (1999).
281. G. Kunathfandrei, P. Rehak, S. Steuernagel, H. Schneider, C. Jäger, 'Quantitative Structural Analysis of Mullite by Al-27 Nuclear Magnetic Resonance Satellite Transition Spectroscopy', *Solid State NMR*, **3**, 241–248 (1994).
282. J.H. Baltisberger, Z. Xu, J.F. Stebbins, S.H. Wang, A. Pines, 'Triple-quantum Two-dimensional Al-27 MAS

- NMR Spectroscopic Study of Aluminosilicate and Aluminate Crystals and Glasses', *J. Am. Chem. Soc.*, **118**, 7209–7214 (1996).
283. R.J. Kirkpatrick, R.A. Kinsey, K.A. Smith, D.M. Henderson, E. Oldfield, 'High Resolution Solid-state Sodium-23, Aluminum-27, and Silicon-29 Nuclear Magnetic Resonance Spectroscopic Reconnaissance of Alkali and Plagioclase Feldspars', *Am. Mineral.*, **70**, 106–123 (1985).
284. M.E. Smith, S. Steuernagel, 'A Multinuclear Magnetic Resonance Examination of the Mineral Grandidierite', *Solid State NMR*, **1**, 175–183 (1992).
285. D. Freude, H. Ernst, I. Wolf, 'Solid-state NMR Studies of Acid Sites in Zeolites', *Solid State NMR*, **3**, 271–286 (1994).
286. M. Hunger, T. Horvath, 'Multi-nuclear Solid-state NMR Study of the Local Structure of SiOHAl Groups and Their Interaction with Probe-molecules in Dehydrated Faujasite, Mordenite and Zeolite ZSM-5', *Ber. Bunsenges. Phys. Chem.*, **99**, 1316–1320 (1995).
287. C.P. Grey, A.J. Vega, 'Determination of the Quadrupole of the Invisible Aluminum Spins in Zeolite HY with H-1/Al-27 TRAPDOR NMR', *J. Am. Chem. Soc.*, **117**, 8232–8242 (1995).
288. H. Kosslick, G. Lischke, G. Walther, W. Storek, A. Martin, R. Fricke, 'Physico-chemical and Catalytic Properties of Al-, Ga- and Fe-substituted Mesoporous Materials Related to MCM-41', *Microporous Mater.*, **9**, 13–33 (1997).
289. D. Müller, U. Bentrup, 'Al-27 NMR Studies on Alkali Fluoroaluminates', *Z. Anorg. Allg. Chem.*, **575**, 17–25 (1989).
290. R.W. Schurko, R.E. Wasylshen, H. Foerster, 'Characterization of Anisotropic Aluminum Magnetic Shielding Tensors. Distorted Octahedral Complexes and Linear Molecules', *J. Phys. Chem. A*, **102**, 9750–9760 (1998).
291. D. Müller, personal communication, 1992.
292. R.W. Schurko, R.E. Wasylshen, A.D. Phillips, 'A Definitive Example of Aluminum-27 Chemical Shielding Anisotropy', *J. Magn. Reson.*, **133**, 388–394 (1998).
293. D. Massiot, A. Kahn-Harari, D. Michel, D. Müller, F. Taulelle, 'Aluminum-27 MAS NMR of Al₂Ge₂O₇ and LaAlGe₂O₇: Two Pentacoordinated Aluminum Environments', *Magn. Reson. Chem.*, **28**, 82–88 (1990).
294. M. Feuerstein, G. Engelhardt, P.L. McDaniel, J.E. MacDougall, T.R. Gaffney, 'Solid-state Nuclear Magnetic Resonance Investigation of Cation Siting in LiNaLSX Zeolites', *Microporous Mater.*, **16**, 27–35 (1998).
295. A.M. George, J.F. Stebbins, 'High-temperature Na-23 MAS NMR Data for Albite – Comparison to Chemical-shift Models', *Am. Mineral.*, **80**, 878–884 (1995).
296. L. Delevoye, S.X. Liu, M.D. Welch, C. Fernandez, J.P. Amoureux, J. Klinowski, 'Triple-quantum Al-27 and Na-23 MAS NMR Study of Amphiboles', *J. Chem. Soc., Faraday Trans.*, **93**, 2591–2595 (1997).
297. R. Janssen, G.A.H. Tjink, W.S. Veeman, T.L.M. Maesen, J.F.v. Lent, 'High-temperature NMR Study of Zeolite Na-A: Detection of a Phase Transition', *J. Phys. Chem.*, **93**, 899–904 (1989).
298. G. Engelhardt, H. Koller, 'A Simple Procedure for the Determination of the Quadrupole Interaction Parameters and Isotropic Chemical Shifts from MAS NMR Spectra of Half-integer Spins in Solids', *Magn. Reson. Chem.*, **29**, 941–945 (1991).
299. T.H. Walter, E. Oldfield, 'Magic-angle Spinning Oxygen-17 NMR of Aluminum Oxides and Hydroxides', *J. Phys. Chem.*, **93**, 6744–6751 (1989).
300. A.R. Thompson, A.C. Kunwar, H.S. Gutowsky, E. Oldfield, 'Oxygen-17 and Aluminum-27 NMR Spectroscopic Investigations of Aluminum(III) Hydrolysis Products', *J. Chem. Soc., Dalton Trans.*, 2317–2322 (1987).
301. H.K.C. Timken, N. James, G.L. Turner, S.L. Lambert, L.B. Welsh, E. Oldfield, 'Solid-state Oxygen-17 NMR Spectroscopic Studies of Zeolites and Related Systems. Part 2', *J. Am. Chem. Soc.*, **108**, 7236–7241 (1986).
302. H.K.C. Timken, G.L. Turner, J.P. Gilson, L.B. Welsh, E. Oldfield, 'Solid-state Oxygen-17 NMR Spectroscopic Studies of Zeolites and Related Systems. Part 1', *J. Am. Chem. Soc.*, **108**, 7231–7235 (1986).
303. Z. Xu, J.F. Stebbins, 'Oxygen Sites in the Zeolite Stilbite: A Comparison of Static, MAS, VAS, DAS and Triple Quantum MAS NMR Techniques', *Solid State NMR*, **11**, 243–251 (1998).
304. D.R. Spearing, I. Farnan, J.F. Stebbins, 'Dynamics of the Alpha–Beta Phase Transitions in Quartz and Cristobalite as Observed by In Situ High Temperature Si-29 NMR and O-17 NMR', *Phys. Chem. Miner.*, **19**, 307–321 (1992).
305. T.H. Walter, G.L. Turner, E. Oldfield, 'Oxygen-17 Cross-polarization NMR Spectroscopy of Inorganic Solids', *J. Magn. Reson.*, **76**, 106–120 (1988).
306. X. Xue, J.F. Stebbins, M. Kanzaki, 'Correlations Between O-17 NMR Parameters and Local Structure Around Oxygen in High-pressure Silicates: Implications for the Structure of Silicate Melts at High Pressure', *Am. Mineral.*, **79**, 31–42 (1994).
307. P.J. Grandinetti, J.H. Baltisberger, I. Farnan, J.F. Stebbins, U. Werner, A. Pines, 'Solid-state O-17 Magic-angle and Dynamic-angle Spinning NMR Study of the SiO₂ Polymorph Coesite', *J. Phys. Chem.*, **99**, 12 341–12 348 (1995).
308. S. Schramm, E. Oldfield, 'High-resolution Oxygen-17 NMR of Solids', *J. Am. Chem. Soc.*, **106**, 2502–2506 (1984).
309. K.T. Mueller, J.H. Baltisberger, E.W. Woote, A. Pines., 'Isotropic Chemical Shifts and Quadrupole Parameters for Oxygen-17 Using Dynamic-angle Spinning NMR', *J. Phys. Chem.*, **96**, 7001–7004 (1992).
310. H.K.C. Timken, S.E. Schramm, R.J. Kirkpatrick, E. Oldfield, 'Solid-state Oxygen-17 NMR Spectroscopic Studies of Alkaline Earth Metasilicates', *J. Phys. Chem.*, **91**, 1054–1058 (1987).

311. H. Maekawa, P. Florian, D. Massiot, H. Kiyono, M. Nakamura, 'Effect of Alkali Metal Oxide on O-17 NMR Parameters and Si-O-Si Angles of Alkali Metal Disilicate', *J. Phys. Chem.*, **100**, 5525–5532 (1996).
312. U. Pingel, 'O-17 NMR of Porous Solids', Thesis, Universität Leipzig, 1999.
313. T. Schaller, J.F. Stebbins, 'The Structural Role of Lanthanum and Yttrium in Aluminosilicate Glasses: A Al-27 and O-17 MAS NMR Study', *J. Phys. Chem. B*, **102**, 10690–10697 (1998).
314. P.J. Dirken, S.C. Kohn, M.E. Smith, E.R.H. van Eck, 'Complete Resolution of Si-O-Si and Si-O-Al Fragments in an Aluminosilicate Glass by O-17 Multiple Quantum Magic Angle Spinning NMR Spectroscopy', *Chem. Phys. Lett.*, **266**, 568–574 (1997).
315. H. Maekawa, T. Saito, T. Yokokawa, 'Water in Silicate Glass: O-17 NMR of Hydrous Silica, Albite, and Na₂Si₄O₉ Glasses', *J. Phys. Chem. B*, **102**, 7523–7529 (1998).
316. Z. Xu, H. Maekawa, J.V. Oglesby, J.F. Stebbins, 'Oxygen Speciation in Hydrous Silicate Glasses: An Oxygen-17 NMR Study', *J. Am. Chem. Soc.*, **120**, 9894 (1998).
317. J.F. Stebbins, J.V. Oglesby, Z. Xu, 'Disorder Among Network-modifier Cations in Silicate Glasses – New Constraints from Triple-quantum O-17 NMR', *Am. Mineral.*, **82**, 1116–1124 (1997).
318. X. Cong, R.J. Kirkpatrick, 'O-17 MAS NMR Investigation of the Structure of Calcium Silicate Hydrate Gel', *J. Am. Ceram. Soc.*, **79**, 1585–1592 (1996).
319. R. Hussin, D. Holland, R. Dupree, 'Does Six-coordinate Germanium Exist in Na₂O–GeO₂ glasses – O-17 NMR Measurements', *J. Non-cryst. Solids*, **234**, 440–445 (1998).
320. T.J. Bastow, M.E. Smith, H.J. Whitfield, 'O-17 NMR Investigation of Hafnia and Ternary Hafnium Oxides', *J. Mater. Chem.*, **6**, 1951–1955 (1996).
321. E.R.H. Van Eck, M.E. Smith, 'Orientation of the Quadrupole and Dipole Tensors of Hydroxyl Groups by O-17 Quadrupole Separated Local Field NMR', *J. Chem. Phys.*, **108**, 5904–5912 (1998).
322. G. Wu, D. Rovnyak, P.C. Huang, R.G. Griffin, 'High-resolution Oxygen-17 NMR Spectroscopy of Solids by Multiple-quantum Magic-angle-spinning', *Chem. Phys. Lett.*, **277**, 79–83 (1997).
323. M.E. Smith, S. Steuernagel, H.J. Whitfield, 'O-17 Magic-angle Spinning Nuclear Magnetic Resonance of CaCO₃', *Solid State NMR*, **4**, 313–316 (1995).